FOREWORD

This report, written in four parts, presents the results of a portion of the experimental program for the investigation of hypersonic flow separation and control characteristics being conducted by the Research Department of Grumman Aircraft Engineering Corporation, Bethpage, New York. Messrs. Donald E. Hoak and Wilfred J. Klotzback, of the Flight Control Division. Air Force Flight Dynamics Laboratory, Research and Technology Division , located at Wright-Patterson Air Force Base, Ohio, are the Air Force Project Engineers for the program, which is being supported primarily under Contract AF33(616)8130, Air Force Task 821902.

The author wishes to express his appreciation to the staff of the von Karman Facility for their helpfulness in conducting the tests and particularly to Messrs. Sivells, Burchfield and Hube for providing the machine plotted graphs of the experimental data included in this report. Ozalid reproducible copies of the tabulated data are available on loan from the Flight Control Division of the Air Force Flight Dynamics Laboratory.
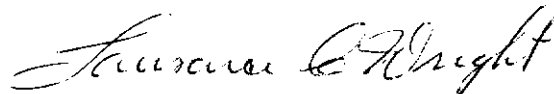
The parts of this report are:

  Part I: Pressure Data for Delta Wing Surface

  Part II: Pressure Data for Dihedral Surfaces

  Part III: Heat Transfer Data for Delta Wing Surface

  Part IV: Heat Transfer Data for Dihedral Surfaces

ABSTRACT

Pressure and heat transfer data were obtained for Mach 8 flows
over a blunt pyramidal configuration composed of a 70 degree sweep-
back delta wing surface and two dihedral surfaces. Trailing edge
flap deflections were varied up to 40 degrees on all surfaces, and
the model was tested with and without canards and ventral fins.
The model was pitched at angles of attack between ± 54 degrees and
was tested at sideslip angles of 0 and 12 degrees for free
stream Reynolds numbers, based on model length, of 1.5 and 4.5
million.

This technical documentary report has been reviewed and is approved.

Lawrence C. Wright

LAWRENCE C. WRIGHT, Lt/Col, USAF
Chief, Flight Control Division
Air Force Flight Dynamics Laboratory

iii

TABLE OF CONTENTS

ILLUSTRATIONS

[*]See Table II, p. 14, for figure numbers corresponding to
particular test conditions.

a,b,c   properties of model skin material (see Data Reduction and Accuracy)

C_p pressure coefficient, $C_p \equiv (p - p_\infty)/q_\infty$

h   heat transfer coefficient (BTU/ft^2 sec °R), $h \equiv \dot{q}_w/(T_O - T_w)$

k   thermal conductivity of air (BTU/ft sec °R)

M_∞ free stream Mach number

Nu   Nusselt number, $Nu \equiv hx/k$

p   pressure (psia)

P_O stagnation pressure (psia)

P_∞ free stream static pressure (psia)

$\dot{q}_w$ aerodynamic heating rate (BTU/ft^2 sec)

q_∞ free stream dynamic pressure (psia)

Re_x Reynolds number based on x, $Re_x \equiv \rho_\infty U_\infty x/\mu_\infty$

Re_∞/ft Reynolds number per foot, $Re_\infty/ft \equiv \rho_\infty U_\infty/\mu_\infty$

t   time (sec)

T_O stagnation temperature (°R)

T_w wall temperature (°R)

T_∞ free stream static temperature (°R)

U_∞ free stream velocity (ft/sec)

x   streamwise distance from virtual apex to planform projection of thermocouple, $x \equiv \dfrac{16.650 \text{ in.}}{12 \text{ in./ft.}} X'$ (see Fig. 3)

X' nondimensional streamwise distance from virtual apex to planform projection (see Fig. 3)

Y' nondimensional spanwise distance measured outboard from the model centerline

α angle of attack (degrees), positive for nose up

β sideslip angle (degrees), positive for nose left

ζ correction factor for aerodynamic heating rate

μ_∞ viscosity of air in the free stream (slugs/ft sec)

ρ_∞ density of air in the free stream (slugs/ft^3)

INTRODUCTION

The experimental data generated for an investigation of hypersonic flow separation and aerodynamic control characteristics are to be presented in a series of reports, of which this is one. Pressure, heat transfer and force data are to be obtained for hypersonic flows over "basic geometries," such as a wedge mounted on a flat plate, and for "typical" hypersonic flight configurations with aerodynamic control surfaces. The experimental portion of the program requires a total of 11 models (see Fig. 1, p. 19); 8 for tests in the von Karman Facility of the Arnold Engineering Development Center and 3 for tests in the Grumman Hypersonic Shock Tunnel (Refs. 1 and 2). Data obtained from AEDC tests of one of the models are given in this four part report (see Foreword).

This report (Part IV) presents heat transfer data obtained in the AEDC 50-inch Mach 8 tunnel (Ref. 3) on the upper surfaces of a blunt pyramidal configuration having remotely controlled trailing edge flaps. Heat transfer data obtained on the lower surface of the model are presented in Part III, and pressure data obtained on the model are presented in Parts I and II. The same model was tested in the AEDC 40-inch Supersonic Tunnel to obtain pressure distributions for Mach 5 flows (Ref. 4). A geometrically similar force model was tested at the same Mach numbers and at the same model length Reynolds numbers in both the 40-inch and 50-inch tunnels. A third geometrically similar model, with limited pressure and heat transfer instrumentation, is to be tested in the Grumman Hypersonic Shock Tunnel (see Fig. 1).
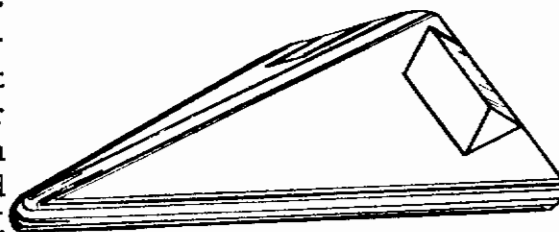
MODEL

Photographs of the model installed in the 50-inch Mach 8 tunnel are shown in Fig. 2. The lower surface of the model is a blunt delta wing with 70 degree sweepback. The planar portions of the

---

1

dihedral surfaces are right triangles and are connected by a cylindrical segment which forms the model's "ridge line." The three cylindrical leading edges and the spherical nose have the same radius (also the same as for Configuration "C" shown in Fig. 1). The cross-sectional shape is the same as one of the ASD — General Applied Sciences Laboratory pyramidal models tested in the AEDC Hotshot 2 hypervelocity facility (Ref. 5).

The model has four, remotely controlled, trailing edge flaps, one on each dihedral surface (both of which are deflected in Fig. 2), and two on the lower surface of the model. The two lower surface flaps are actuated as a pair and are always set at equal deflections. As shown in Fig. 3, the flaps have rectangular planforms, and their hinge lines are parallel to the base of the model (perpendicular to the ridge line). The chords of the remotely controlled flaps are 15 per cent of the virtual length of the model. The flaps are deflectable at angles between 0 and 40 degrees, measured in the planes normal to the flap hinge lines. In addition to the remotely controlled flaps, one pair of instrumented flaps having a set deflection of 20 degrees and a chord equal to 25 per cent of the model reference length are attachable to the lower surface of the model (see Fig. 3).

As indicated in Fig. 3, there are also attachable canards and a ventral fin for the model. The canards, shown attached to the model in Fig. 2, have cylindrical leading edges and 45 degree sweepback. They are geometrically similar to the force model canards and have a planform area equal to that of the basic model from the nose to the trailing edge of the canards. The ventral fin is attachable in either of two positions on the lower surface of the model between the trailing edge flaps. The fin is wedge shaped (total wedge angle of 30 degrees), has a cylindrical leading edge, and is geometrically similar to the instrumented fin of Configuration "B" shown in Fig. 1. As indicated in Fig. 3, the fin can be set at fin (or rudder) deflection angles of 0 or +15 degrees (trailing edge left), and has a chord equal to 15 per cent of the model reference length.

Pressure tap and thermocouple locations are shown in Fig. 3. There are 5 streamwise lines of pressure taps on the lower surface; 8 taps are on the centerline of the lower surface and 10 taps are positioned along a streamwise line coincident with the flap centerline and extending forward to the leading edge of the model. There are four streamwise lines of thermocouples on the lower surface of the model. As indicated in Fig. 3, the attachable extended-chord flaps also are instrumented for pressure and temperature measurements. The upper surface of the model has a similar array of

2

pressure taps and thermocouples in lines parallel to the ridge line of the model. Eight pressure taps are on the ridge line; 10 taps are positioned along a line coincident with the flap centerline and extending forward to the leading edge of the model.

The planar portions of the model, in the regions instrumented for heat transfer measurements, are fabricated of stainless steel honeycomb sandwich panels. The panels are composed of 1/4 inch thick honeycomb, having 3/8 inch cells, sandwiched between 0.020 inch thick stainless steel sheets. The thermocouples are spot welded to the inner surface of the outer wall of the honeycomb sandwich in the middle of individual honeycomb cells. Conduction effects are further minimized by keeping all supporting structures of the model at least 3/8 inch away from all thermocouple locations (Ref. 6 and 7).

Remote Control System for Flaps

The trailing edge flaps are actuated by bell cranks and push-pull rods connected to drive screws and 28 volt dc motors housed in a water cooled jacket mounted to the base of the model. The water cooled actuator housing contains three each: motors, drive screws, and potentiometers required to actuate the flaps and to determine the flap deflection angles (see Fig. 4). For the model discussed herein one motor is used to actuate the pair of flaps on the lower surface of the model and the other motors are used to actuate the flaps on the left and right dihedral surfaces. The same actuator housing is used for the other pressure and heat transfer models having remotely controlled flaps (Configurations "A", "C" and "D", Fig. 1).

The electrical circuits for the flaps are shown in Fig. 5. As indicated in the diagram, the flaps are driven by the 28 volt dc motors and the potentiometer readings, used to position the flaps, appear on Leeds and Northrup indicators. A "limit light" circuit is also shown in Fig. 5. Microswitches at both ends of each drive screw are calibrated to close when any flap is in a limiting position (either 0 or 40 degree deflection for the model considered herein). When in this limiting position, a limit lamp lights in the control room. Finally, the actuator housing also contains thermocouples used to monitor temperatures at three locations in the housing.

The temperature and potentiometer indicators are shown in Fig. 6. Also shown in Fig. 6, from left to right, are the limit lamp box, variable resistors used in calibrating the potentiometer

3

readings, the flap motor control box, and an ammeter used to indicate the motor loads. Any excess motor loads, due, for example, to binding in the flap control linkage, would be apparent immediately by a high ammeter reading, and the motor could be stopped before causing further damage.

TEST CONDITIONS

The heat transfer data presented herein were obtained from tests in the AEDC 50-inch Mach 8 tunnel made during the latter part of July 1963. The model was pitched from 45 degrees nose down to 54 degrees nose up for various flap settings and for free stream Reynolds numbers per foot of 1.1 and 3.3 million. Data were also obtained for selected flap settings for +12 degree sideslip and for changes in the basic geometry of the configuration (longer chord flaps on the lower surface, canards, and ventral fin). The test conditions for the heat transfer data are shown in Tables I and II. Flap deflection angles are considered positive when the flap trailing edge is deflected downward. Thus, the flaps on the lower surface were deflected at positive angles and the flaps on the upper, dihedral, surfaces were deflected at negative angles. The 15 degree ventral fin (rudder) setting is indicated in Fig. 3 and is set to trim at positive sideslip angle (nose left).

Flap deflections were set using Leeds and Northrup indicator readings of the potentiometers connected to the drive screws in the water cooled actuator housing. The potentiometer readings for the desired flap settings were calibrated using hand held templates. Flap settings were checked frequently while the tunnel was running by using a flood lamp and a surveyor's transit focused on scribe lines on the trailing edges of the flaps.

In order to minimize model cooling time, heat transfer data were obtained for a set of test conditions before obtaining pressure data for the same conditions. The flaps were set at the desired deflections and the model was pitched to the desired angle of attack while inside the tunnel cooling shoes (shown retracted in Fig. 2). The cooling shoes were rapidly retracted (full retraction within 3/4 sec) and temperature readings recorded for every thermocouple every 0.05 seconds for 4.00 seconds. The shoes were then closed quickly, the model cooled to approximately 500°R and pitched to the next desired angle of attack. In this manner, the heat transfer data were obtained for a given configuration and value of Re_∞/ft for the various angles of attack and flap settings while limiting the amount of heat absorbed by the model. The shoes were then left retracted while the pressure data, which require several minutes to stabilize for each set of test conditions, were obtained.

4

As noted in Tables I and II, the tunnel flow choked when the cooling shoes were retracted for maximum model angle of attack and maximum deflection of the upper surface flaps. The tunnel flow also choked when the cooling shoes were "popped" open for all flap deflections for a model angle of attack of -54 degrees. In these cases, the frontal area of the model combined with that of the partially retracted cooling shoes and blocked the tunnel flow; causing the tunnel shock to move upstream into the test section. Although heat transfer data could not be obtained for these test conditions, pressure data were obtained (cooling shoes fully retracted) and are presented in the first two parts of this report.

DATA REDUCTION AND ACCURACY

The thin wall, transient temperature, method was used to obtain the heat transfer rates from the wall temperatures, T_W, measured by the thermocouples during the initial heating of the model immediately after the cooling shoes opened (Ref. 8). Thus, the aerodynamic heating rates, $\dot{q}_W$, were obtained from

$$\dot{q}_W = \zeta abc \frac{dT_W}{dt}$$

where a (lbm/ft^3) is the density of the stainless steel skin, b (ft) is the skin thickness, c (BTU/lbm) is the specific heat of the steel, and ζ is the correction factor for conduction effects and relates the measured heat transfer rates to the aerodynamic heating rates. Because of the thinness of the wall and the absence of heat sinks near the thermocouple locations, made possible by the honeycomb sandwich construction used in the model, the inside wall temperatures responded very quickly to the aerodynamic heating rates. This made possible reducing the data at t = 1.25 seconds after the start of the retraction of the cooling shoes. At this comparatively short time, conduction effects were negligible and the value of ζ, to within experimental accuracy, was 1.00.

The aerodynamic heating rates were nondimensionalized in the form

$$\frac{Nu}{\sqrt{Re_x}} = \left(\frac{\dot{q}_W}{T_o - T_W}\right)\left(\frac{x}{k}\right) \Bigg/ \sqrt{\frac{\rho_\infty U_\infty x}{\mu_\infty}}$$

5

where Nu is the Nusselt number; T_O is the tunnel stagnation temperature; k is the thermal conductivity of the gas flow in the tunnel; ρ_∞, U_∞ and μ_∞ are the density, velocity and viscosity of the free stream flow; and x is the streamwise distance from the virtual apex to the planform projection of the thermocouple (x/ft = 1.3875X'). Values of x are tabulated for each thermocouple location in Table III.

Too many parameters affect the heat transfer measurements to successfully assess the inaccuracies of the plotted values of $Nu/\sqrt{Re_x}$. The accuracy of the data may best be ascertained by comparing the repeatability of the data (see Table II). The automatic plotting machines, used in presenting the data herein, introduce the possibility of completely misplotting a point. Each graph has been inspected and questionable points compared with the tabulated values. Finally, the remotely controlled flap settings were estimated to be accurate to well within half a degree.

RESULTS

Table II summarizes the Mach 8 heat transfer data obtained on the upper, dihedral, surfaces of the model and indicates the corresponding figure numbers where the sets of data are presented herein. The AEDC group number is presented in the last column of the Table. This number indicates the order in which the data were obtained and is to be used when referring to the tabulated data.

Streamwise and spanwise distributions of the aerodynamic heating rates, in coefficient form, are presented in Figs. 7 through 82. The first part of each figure presents streamwise distributions of the heating rates at four spanwise stations and the second part of each figure presents spanwise distributions at five X' stations. An outline of the model, showing the position of the streamwise and spanwise lines of thermocouples, appears on each full-page figure. As indicated in the figures, X' is the nondimensional streamwise distance from the planform virtual apex to the projection of a thermocouple on the planform, and Y' is the nondimensional spanwise distance of the planform projection of the thermocouple measured outboard from the centerline (see Fig. 3 and Table III).

Thermocouple number 639 (see Fig. 3) broke after AEDC group number 42 and thermocouple 649 broke after group 53. The erroneous Nusselt number values have been omitted from the graphs presented herein.

6

Although the accuracy of the plotted data should suffice for engineering purposes, ozalid reproducible copies of the tabulated data are available on loan (see "Foreword"). The plotted data can be read accurately using standard 20/inch grid, tracing graph paper overlays. Minor distortions in the paper size can be overcome by slightly shifting the tracing paper so that a $\frac{1}{2}$ inch square of the tracing paper is centered over the graph square containing the particular point of interest. For the automatic plotting of the data, the graph origin was used as the reference alignment point to minimize percentage errors in Nu, X' and Y' values due to minor distortions (less than 1%) in the size of the preprinted graph paper.

1. Kaufman, Louis G. II, et al., <u>A Review of Hypersonic Flow Separation and Control Characteristics</u>, ASD-TDR-62-168, March 1962.

2. Evans, W.J., and Kaufman, L.G. II, <u>Pretest Report on Hypersonic Flow Separation and Control Models for AEDC Tunnels A, B, Hotshot 2 and Grumman Hypersonic Shock Tunnel</u>, Grumman Research Department Memorandum RM-209, July 1962.

3. Arnold Center, <u>Test Facilities Handbook</u>, Arnold Air Force Station, Tennessee, January 1961.

4. Kaufman, Louis G. II, <u>Pressure Measurements for Mach Five Flows over a Blunt Pyramidal Configuration with Aerodynamic Controls</u>, to be published as a RTD Technical Documentary Report.

5. Wallace, A.R., and Swain, W.N., <u>Pressure Distribution Tests on a 60° and 70° Delta Wing at Mach Numbers 20 to 22</u>, AEDC-TN-61-14, February 1961, CONFIDENTIAL REPORT.

6. Kaufman, L.G. II, Meckler, L.H., Weiss, D., and White, R.F., <u>Feasibility of Using Honeycomb Sandwich Construction for Aerodynamic Heat-Transfer Models</u>, Grumman Research Department Memorandum RM-208, July 1962.

7. <u>Honeycomb Wind Tunnel Models Give Fast Thermal Response</u>, "Space/Aeronautics," Vol. 40, No. 5, p. 130, October 1963.

8. Eber, G.R., and Cady, W.M., <u>Temperature Measurements</u>, "High Speed Aerodynamics and Jet Propulsion," Volume IX, Section D, Princeton University Press, Princeton, 1954.

9. Kaufman, L.G. II, <u>Pressure and Heat Transfer Measurements for Hypersonic Flows Over Expansion Corners and Ahead of Ramps</u>, ASD-TDR-63-679, Part I: Mach 5 and 8 Data for Expansion Corner Flows, September 1963, Part II: Mach 5 Pressure Data for Flows Ahead of Ramps, September 1963, Part III: Mach 8 Pressure Data for Flows Ahead of Ramps, November 1963, Part IV: Mach 8 Heat Transfer Data for Flows Ahead of Ramps, to be published.

10. Baer, A.L., <u>An Investigation of Separated Flows on Two-Dimensional Models at Mach Numbers 5 and 8</u>, AEDC-TDR-63-200, October 1963.

11.   Kaufman, L.G. II, <u>Pressure Measurements for Mach 8 Flows Over</u>
       <u>Expansion Corners and Ramps on an Internally Cooled Model</u>,
       RTD-TDR-63-4044, Part I: Expansion Corner Flows, November 1963,
       Part II: Flows Over a Flat Plate with and without a Partial
       Span Ramp, December 1963, Part III: Flows Over Full Span Ramps
       Mounted on a Flat Plate, to be published.

12.   Kaufman, L.G. II, and Meckler, L.H., <u>Pressure and Heat Transfer</u>
       <u>Measurements at Mach 5 and 8 for a Fin - Flat Plate Model</u>,
       ASD-TDR-63-235, April 1963.

13.   Kaufman, L.G. II, <u>Pressure Distributions and Oil Film Photo-</u>
       <u>graphs for Mach 5 Flows Past Fins Mounted on a Flat Plate</u>,
       ASD-TDR-63-755, September 1963.

14.   Kaufman, L.G. II, <u>Pressure Measurements for Mach 5 Flows Over</u>
       <u>Winged Re-entry Configurations with Aerodynamic Controls</u>,
       RTD-TDR-63-4179, to be published.

15.   Hartofilis, S.A., <u>Pressure Measurements at Mach 19 for a</u>
       <u>Winged Re-entry Configuration</u>, ASD-TDR-63-319, May 1963.

16.   Lacey, J.J. Jr., <u>Pressure Tests on a Blunt Delta Wing Vehicle</u>
       <u>at M = 19</u>, AEDC-TDR-63-32, February 1963.

17.   Meckler, L.H., <u>Static Aerodynamic Characteristics at Mach 5</u>
       <u>and 8 for an Aerodynamically Controllable Winged Re-entry</u>
       <u>Configuration</u>, to be published as a RTD Technical Documentary
       Report.

TABLE I

TEST CONDITIONS

(Sheet 1 of 4)

Tunnel Conditions		
$Re_\infty/10^6 ft$	3.26*	1.09*
M_∞	8.09	8.04
p_∞ (psia)	0.0736	0.0250
q_∞ (psia)	3.37	1.13
p_o (psia)	773	254
T_o (°R)	1,345	1,340

*The corresponding free stream Reynolds numbers, based on the model reference length, are 4.5 and 1.5 million.

TABLE I

TEST CONDITIONS

(Sheet 2 of 4)

BASIC PYRAMIDAL CONFIGURATION (without canards, without ventral fin, and with shorter chord (15% ref. length) flaps on lower surface) AT ZERO SIDESLIP ($\beta = 0$) AND FOR $Re_\infty/10^6 ft = 3.3$									
Flap Settings (deg)			**Angles of Attack (deg)**						
Bottom	Left	Right							
0	-40	-40	-45	0	+14.3*		+45		
				-33	+7		+33		+54†
0	-30	-30		0	+14.3				
0	-20	-20	-45	0	+14.3				
0	-10	-10		0	+14.3				
0	0	0	-45	0	+14.3		+45		
				-33			+33		
+10	0	0		0	+14.3				
+20	0	0		0	+14.3		+45		
							+33		+54
+30	0	0		0	+14.3				
+40	0	0	-45	0	+14.3		+45		
				+7			+33		+54
0	-20	0		0	+14.3				
0	-40	0		0	+14.3				
0	0	-20		0	+14.3				
0	0	-40		0	+14.3				

*Dihedral surfaces parallel to free stream flow at $\alpha = 14.3°$.
†Tunnel flow choked for this one set of test conditions (maximum upper surface flap deflections and maximum angle of attack).

11

TABLE I

TEST CONDITIONS

(Sheet 3 of 4)

BASIC PYRAMIDAL CONFIGURATION					
Flap Settings (deg)			Angles of Attack (deg) at zero sideslip		$\dfrac{Re_\infty}{10^6 ft}$
Bottom	Left	Right			
0	-40	-40	0	+14.3*	1.1
0	-20	-20	0	+14.3	1.1
0	0	0	0	+14.3	1.1
+20	0	0	0	+14.3	1.1
+40	0	0	0	+14.3	1.1
			Sideslip Angles (deg) at $\alpha = 0$		
0	0	0	+12**		3.3
+20	0	0	+12		3.3

BASIC + LONGER CHORD BOTTOM FLAPS (without canards, without ventral fin, and with longer chord (25% ref. length) flaps on lower surface)					
Flap Settings (deg)			Angles of Attack (deg) at zero sideslip		$\dfrac{Re_\infty}{10^6 ft}$
Bottom	Left	Right			
+20	0	0	0	+14.3	3.3
+20	0	0	0	+14.3	1.1

*Dihedral surfaces parallel to free stream flow at $\alpha = 14.3°$.

**Nose left.

TABLE I

TEST CONDITIONS

(Sheet 4 of 4)

BASIC + CANARDS (without ventral fin and with shorter chord (15% ref. length) flaps on lower surface) FOR $Re_\infty/10^6$ ft = 3.3				
Flap Settings (deg)			**Angles of Attack (deg) at zero sideslip**	
Bottom	Left	Right		
0	-40	-40	0	+14.3*
0	-20	-20	0	+14.3
0	0	0	0	+14.3
+20	0	0	0	+14.3
+40	0	0	0	+14.3

BASIC + VENTRAL FIN (without canards and with shorter chord (15% ref. length) flaps on lower surface) FOR $Re_\infty/10^6$ ft = 3.3					
Flap Settings (deg)			**Fin (Rudder) Setting (deg)**	**Sideslip Angles (deg) at $\alpha = 0$**	
Bottom	Left	Right			
0	0	0	0	0	+12**
+20	0	0	0	0	
0	0	0	+15***	0	+12

*Dihedral surfaces parallel to free stream flow at $\alpha = 14.3°$.
**Nose left.
***Fin trailing edge left.

13

TABLE II

TEST DATA FIGURE NUMBERS

(Sheet 1 of 4)

Configuration*	Flap Settings (deg)			α* (deg)	β* (deg)	$\frac{Re_\infty}{10^6\,ft}$	Figure Number	AEDC Group Number
	Bottom	Left	Right					
Basic	0	-40	-40	-45	0	3.3	7	76
	0	-20	-20	-45	0	3.3	8	74
	0	0	0	-45	0	3.3	9	73
	+40	0	0	-45	0	3.3	10	77
	0	-40	-40	-33	0	3.3	11	75
	0	0	0	-33	0	3.3	12	72
	0	-40	-40	0	0	1.1	13	43
	0	-40	-40	0	0	3.3	14	32
	0	-40	0	0	0	3.3	15	35
	0	0	-40	0	0	3.3	16	41
+ Canards	0	-40	-40	0	0	3.3	17	9
Basic	0	-30	-30	0	0	3.3	18	31
	0	-20	-20	0	0	1.1	19	45
	0	-20	-20	0	0	3.3	20	28
	0	-20	0	0	0	3.3	21	37
	0	0	-20	0	0	3.3	22	39
+ Canards	0	-20	-20	0	0	3.3	23	7
Basic	0	-10	-10	0	0	3.3	24	27
	0	0	0	0	0	1.1	25	51
	0	0	0	0	0	3.3	26	15
+ Canards	0	0	0	0	0	3.3	27	5
+ Fin ($\delta = 0$)	0	0	0	0	0	3.3	28	56
+ Fin ($\delta = 15°$)	0	0	0	0	0	3.3	29	53

*See last sheet of Table for notes.

14

TABLE II

TEST DATA FIGURE NUMBERS

(Sheet 2 of 4)

Configuration*	Flap Settings (deg)			α* (deg)	β* (deg)	$\frac{Re_\infty}{10^6 ft}$	Figure Number	AEDC Group Number
	Bottom	Left	Right					
Basic	+10	0	0	0	0	3.3	30	18
	+20	0	0	0	0	1.1	31	47
	+20	0	0	0	0	3.3	32	19
+ Canards	+20	0	0	0	0	3.3	33	11
+ Fin (δ = 0)	+20	0	0	0	0	3.3	34	57
+ Longer Chord Flaps	+20	0	0	0	0	1.1	35	3
	+20	0	0	0	0	3.3	36	1
Basic	+30	0	0	0	0	3.3	37	22
	+40	0	0	0	0	1.1	38	49
	+40	0	0	0	0	3.3	39	23
+ Canards	+40	0	0	0	0	3.3	40	13
Basic	0	0	0	0	+12	3.3	41	58
	+20	0	0	0	+12	3.3	42	59
+ Fin (δ = 0)	0	0	0	0	+12	3.3	43	55
+ Fin (δ = 15°)	0	0	0	0	+12	3.3	44	54
Basic	0	-40	-40	+7	0	3.3	45	34
	+40	0	0	+7	0	3.3	46	24
	0	-40	-40	+14.3	0	1.1	47	44
	0	-40	-40	+14.3	0	3.3	48	33
	0	-40	0	+14.3	0	3.3	49	36
	0	0	-40	+14.3	0	3.3	50	42
+ Canards	0	-40	-40	+14.3	0	3.3	51	10

*See last sheet of Table for notes.

15

TABLE II

TEST DATA FIGURE NUMBERS

(Sheet 3 of 4)

Configuration*	Flap Settings (deg)			α^* (deg)	β^* (deg)	$\frac{Re_\infty}{10^6 ft}$	Figure Number	AEDC Group Number
	Bottom	Left	Right					
Basic	0	-30	-30	+14.3	0	3.3	52	30
	0	-20	-20	+14.3	0	1.1	53	46
	0	-20	-20	+14.3	0	3.3	54	29
	0	-20	0	+14.3	0	3.3	55	38
	0	0	-20	+14.3	0	3.3	56	40
+ Canards	0	-20	-20	+14.3	0	3.3	57	8
Basic	0	-10	-10	+14.3	0	3.3	58	26
	0	0	0	+14.3	0	1.1	59	52
	0	0	0	+14.3	0	3.3	60	16
+ Canards	0	0	0	+14.3	0	3.3	61	6
Basic	+10	0	0	+14.3	0	3.3	62	17
	+20	0	0	+14.3	0	1.1	63	48
	+20	0	0	+14.3	0	3.3	64	20
+ Canards	+20	0	0	+14.3	0	3.3	65	12
+ Longer Chord Flaps	+20	0	0	+14.3	0	1.1	66	4
	+20	0	0	+14.3	0	3.3	67	2
Basic	+30	0	0	+14.3	0	3.3	68	21
	+40	0	0	+14.3	0	1.1	69	50
	+40	0	0	+14.3	0	3.3	70	25
+ Canards	+40	0	0	+14.3	0	3.3	71	14

*See last sheet of Table for notes.

16

TABLE II

TEST DATA FIGURE NUMBERS

(Sheet 4 of 4)

Configuration*	Flap Settings (deg)			α^* (deg)	β^* (deg)	$\frac{Re_\infty}{10^6}$ ft	Figure Number	AEDC Group Number
	Bottom	Left	Right					
Basic	0	-40	-40	+33	0	3.3	72	71
	0	0	0	+33	0	3.3	73	60
	+20	0	0	+33	0	3.3	74	65
	+40	0	0	+33	0	3.3	75	66
	0	-40	-40	+45	0	3.3	76	70
	0	0	0	+45	0	3.3	77	61
	+20	0	0	+45	0	3.3	78	64
	+40	0	0	+45	0	3.3	79	67
	0	-40	-40	+54	0	?	80	69**
	+20	0	0	+54	0	3.3	81	63
	+40	0	0	+54	0	3.3	82	68

*Notes: Basic configuration is without canards, without ventral fin, and with shorter chord (15% ref. length) flaps on the lower surface.
+ Canards is the basic configuration with canards.
+ Longer chord flaps is the basic configuration with the longer chord (25% ref. length) flaps on the lower surface.
+ Fin (δ = 0) is the basic configuration with the ventral fin undeflected (zero rudder angle).
+ Fin (δ = 15°) is the basic configuration with the ventral fin deflected 15 degrees (fin trailing edge left).

Flap settings are measured in planes normal to the flap hinge lines; the bottom flaps always act as a pair and have equal settings.

At α = 14.3° the dihedral surfaces are parallel to the free stream flow.

Positive sideslip angle (β = + 12°) is nose left.

**The tunnel flow choked (shock moved upstream into the test section) when the tunnel cooling shoes were popped open for this set of conditions. See note on Fig. 80.

TABLE III

STREAMWISE DISTANCES FROM VIRTUAL APEX AND
NONDIMENSIONAL COORDINATES OF THERMOCOUPLES

Thermo-couples	x (in feet)	X'	Y'
625	1.0718	0.7725	0.1618
626	1.1364	0.8190	0.1618
627	1.2189	0.8785	0.1618
628	1.2834	0.9250	0.1618
635	1.0718	0.7725	0.3170
637	1.2189	0.8785	0.3170
638	1.2834	0.9250	0.3170
639	1.3480	0.9715	0.3170
642	0.8784	0.6331	0.4722
643	0.9429	0.6796	0.4722
644	1.0073	0.7260	0.4722
645	1.0718	0.7725	0.4722
646	1.1364	0.8190	0.4722
647	1.2189	0.8785	0.4722
648	1.2834	0.9250	0.4722
649	1.3480	0.9715	0.4722
657	1.2189	0.8785	0.6273
658	1.2834	0.9250	0.6273
659	1.3480	0.9715	0.6273

Values of x used in reducing $\dot{q}_w$ to $Nu/\sqrt{Re_x}$.

(x and X' constant in planes parallel to model base, see Fig. 3).
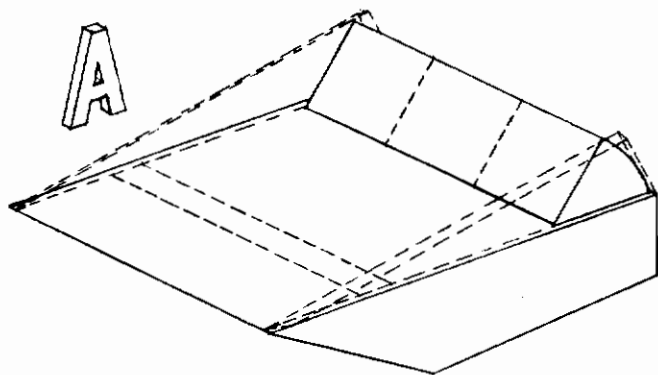
Separated Flows ahead of a Ramp
  Fore and aft flaps, end plates
  3 separate models:

1) Pressure and heat transfer, AEDC Tunnels
   A & B, M = 5 & 8, results in Refs. 9 and 10.

2) Controlled wall temperature, pressure,
   AEDC Tunnel B, M = 8, results in Refs. 10 and 11.

3) Pressure and heat transfer, Grumman Shock
   Tunnel, M ≈ 13 & 19, results not available yet.
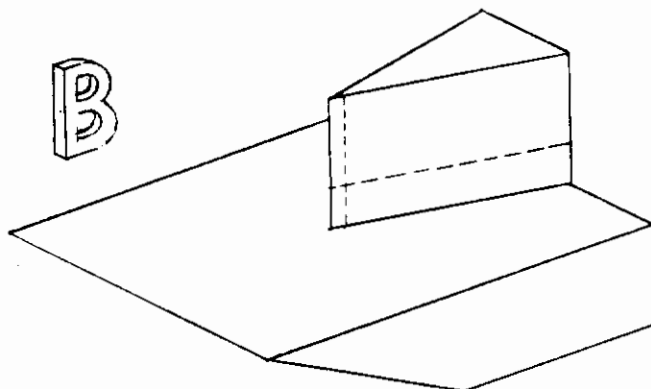
Wedge - Plate Interaction
  Small and large fins with sharp
  and blunt leading edges
  2 separate models:

1) Pressure and heat transfer, AEDC Tunnels
   A & B, M = 5 & 8, results in Refs. 10, 12 and 13.

2) Pressure and heat transfer, Grumman Shock
   Tunnel, M ≈ 13 & 19, results not available yet.
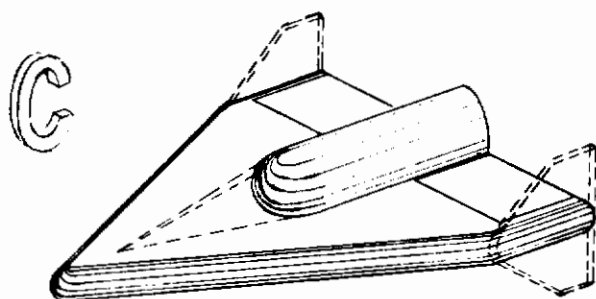
Clipped Delta, Blunt L.E.
  Center body, T.E. flaps, drooped nose,
  spoiler, tip fins
  3 separate models:

1) Pressure and heat transfer, AEDC Tunnels
   A & B, M = 5 & 8, results in Ref. 14.

2) Pressure, AEDC Hotshot 2,
   M ≈ 19, results in Refs. 15 and 16.

3) Six component force, AEDC Tunnels
   A & B, M = 5 & 8, results in Ref. 17.
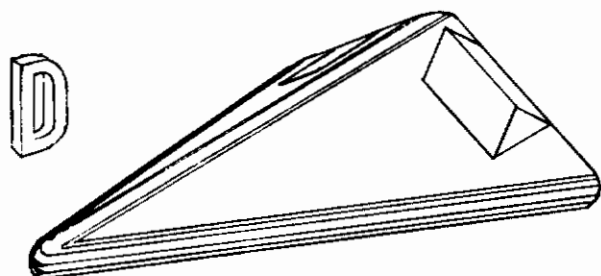
Delta, Blunt L.E., Dihedral
  T.E. flaps, canard, ventral fin
  3 separate models:

1) Pressure and heat transfer, AEDC Tunnels
   A & B, M = 5 & 8, results in Ref. 4 and herein.

2) Pressure and heat transfer, Grumman Shock
   Tunnel, M ≈ 19, results not available yet.

3) Six component force, AEDC Tunnels
   A & B, M = 5 & 8, results not available yet.

Fig. 1 General Outline of Models and Remarks for Over-all Program
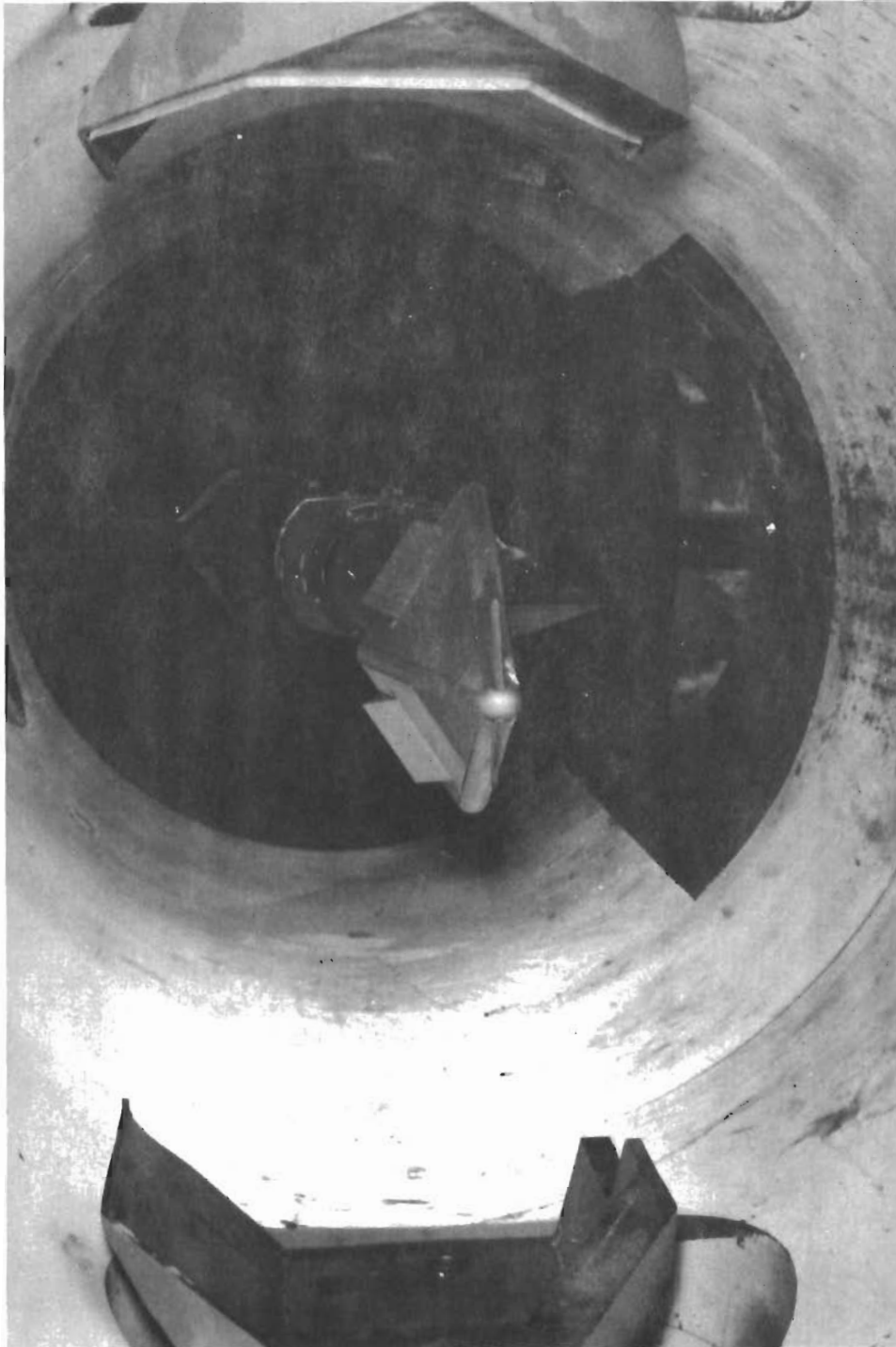
Fig. 2a   Photograph of Model, with Canards and Upper (Dihedral) Flaps Deflected, Installed in the AEDC 50-inch Mach 8 Tunnel

20

Fig. 2b Photograph of Model, with Canards and Upper (Dihedral) Flaps Deflected, Installed in the AEDC 50-inch Mach 8 Tunnel

21

TANGENCY

TANGENCY

642 643 644 645 646

657 658 659

635

647 648 649

625 626

637 638 639

627 628

TOP STARBOARD VIEW

TANGENCY 107   109   111   113   115 116 117 118

TANGENCY

TOP ℄ VIEW

END VIEW

6.000

12.000

2.420

1.198

3.571

6.415

127 128

14.133 REF.

125 126

137 138 139

135

147 148 149

157 158 159

141 142 143 144 145 146

TANGENCY

TANGENCY

140
(REF.)

TOP PORT VIEW
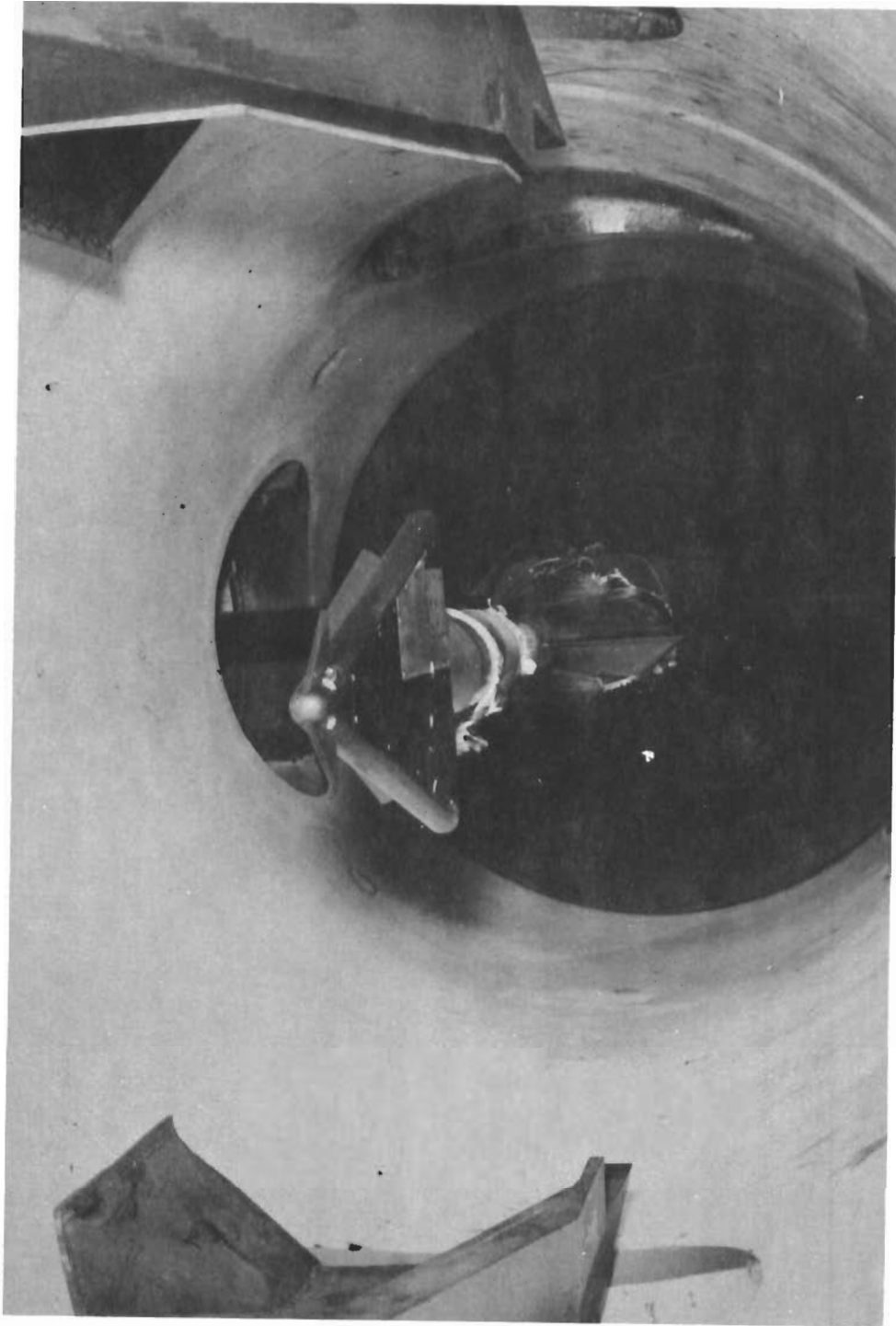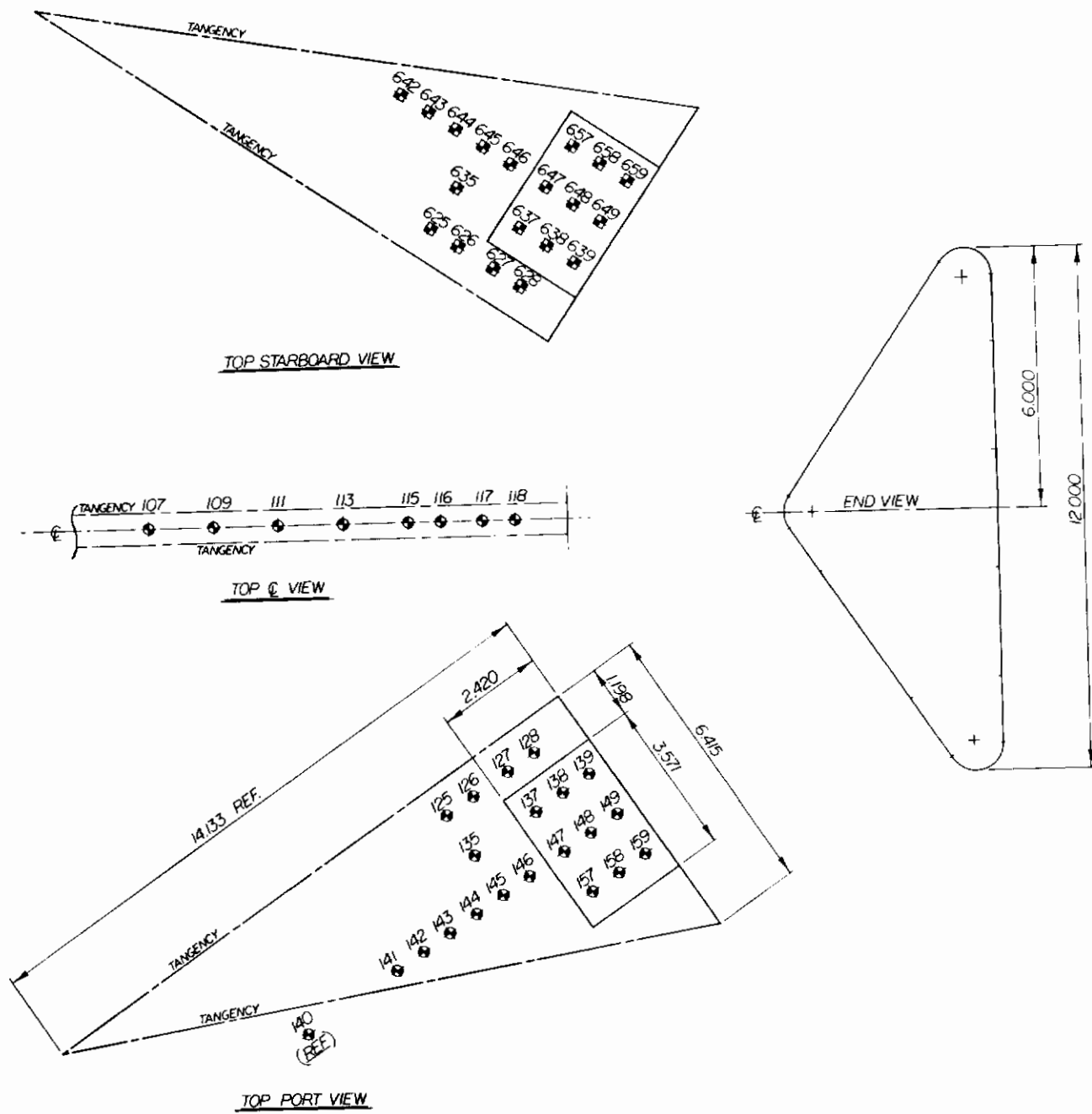
Fig. 3a Model Instrumentation (Sheet 1 of 3)
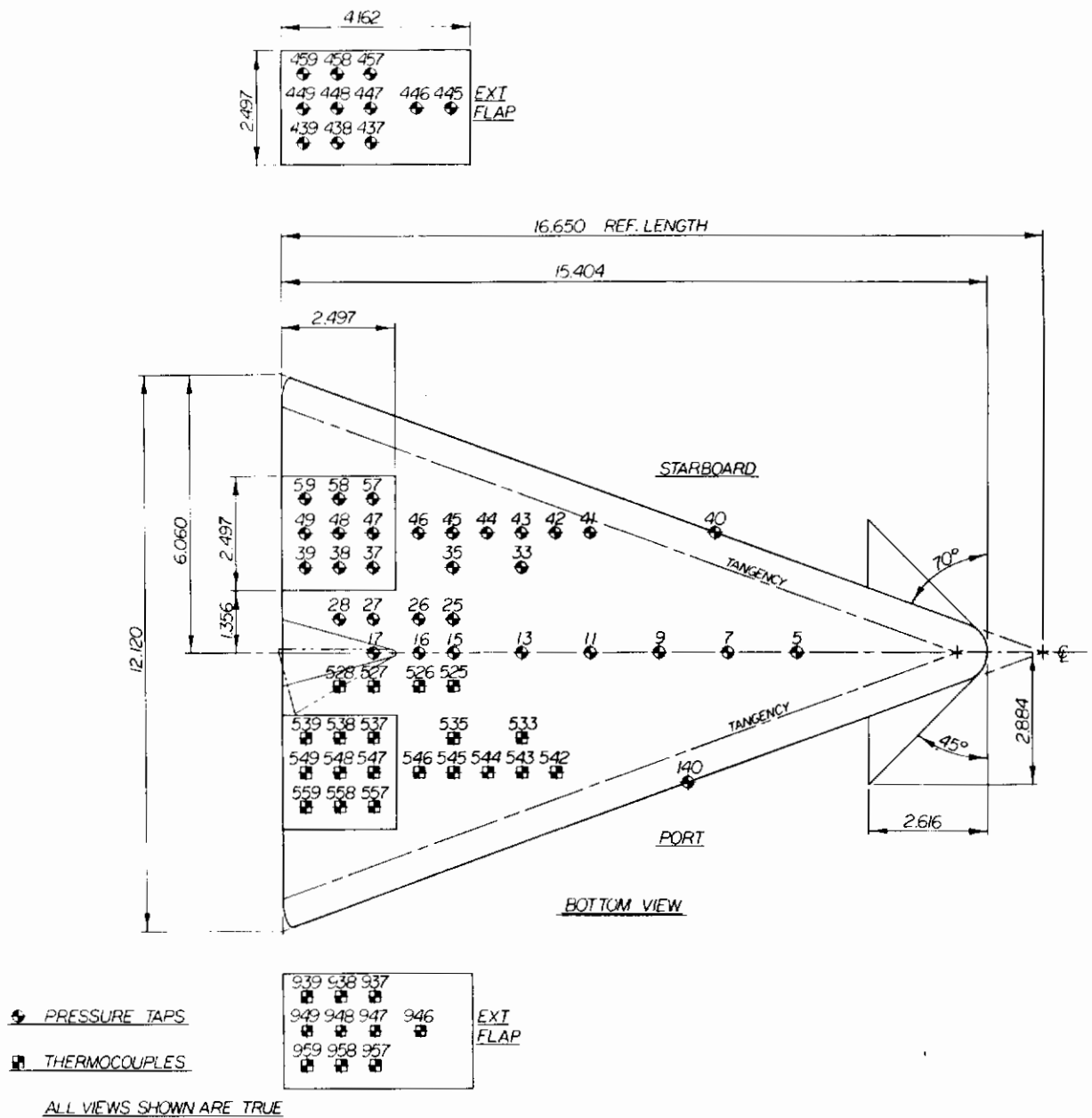
Fig. 3b Model Instrumentation (Sheet 2 of 3)

23
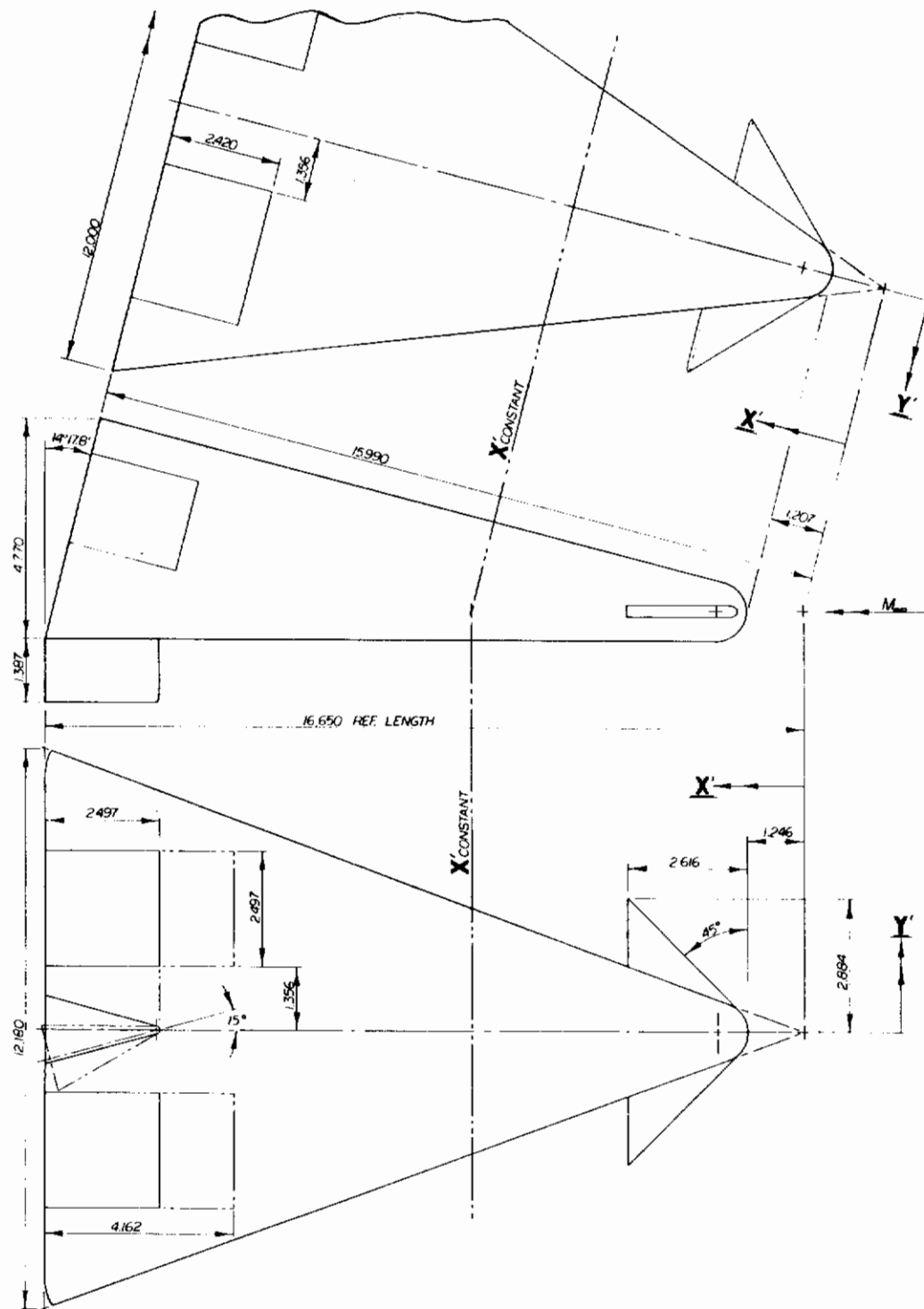
Fig. 3c   Model Instrumentation   (Sheet 3 of 3)

24
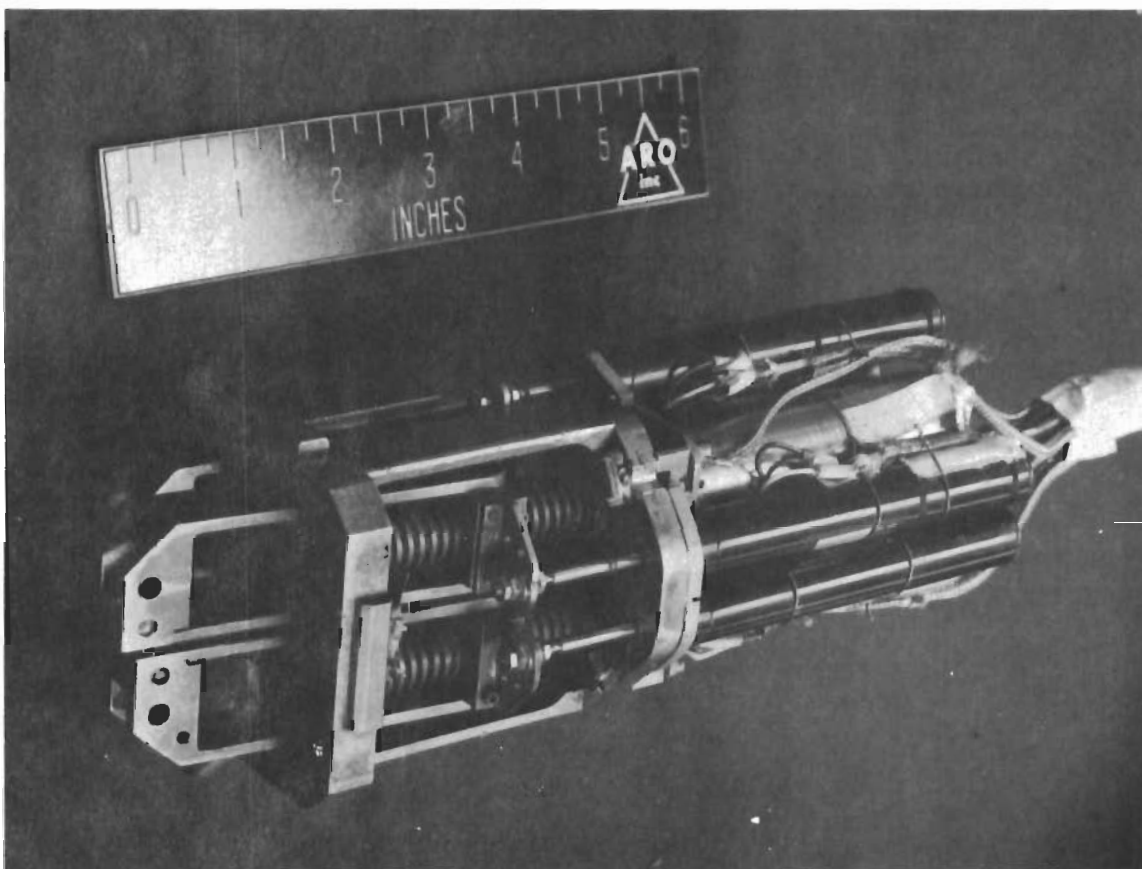
Fig. 4 Actuators for Remotely Controlled Flaps

FLAP MEASURING CIRCUITRY
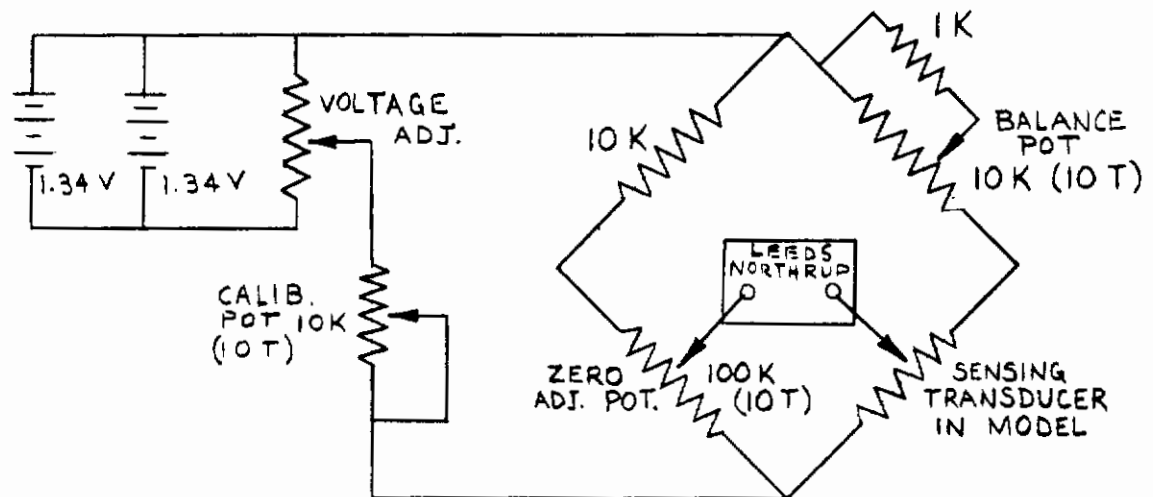
FLAP CONTROL CIRCUITRY
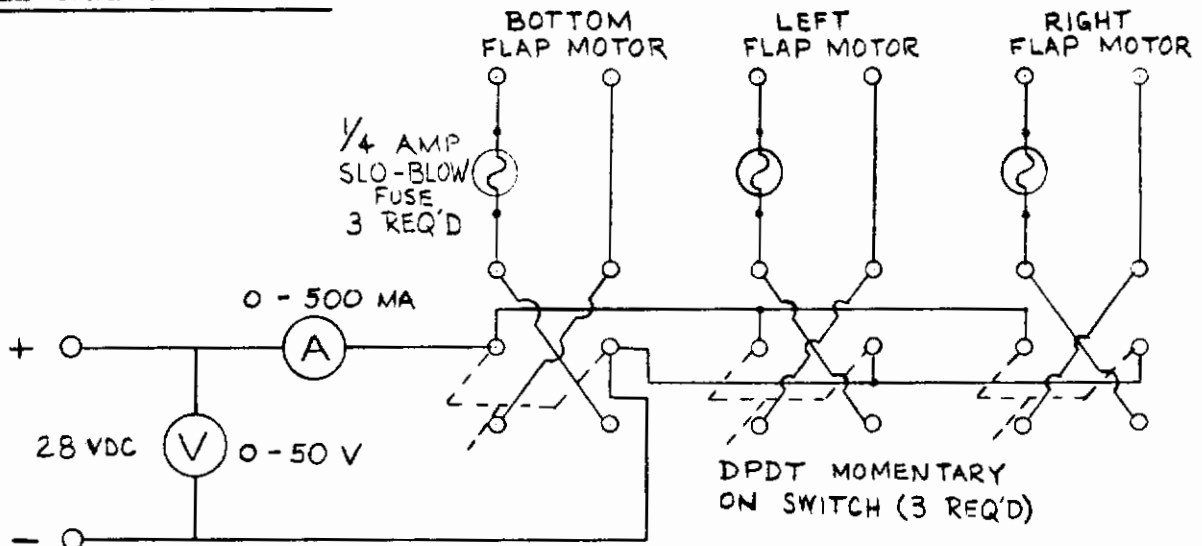
FLAP LIMIT LIGHT CIRCUITRY
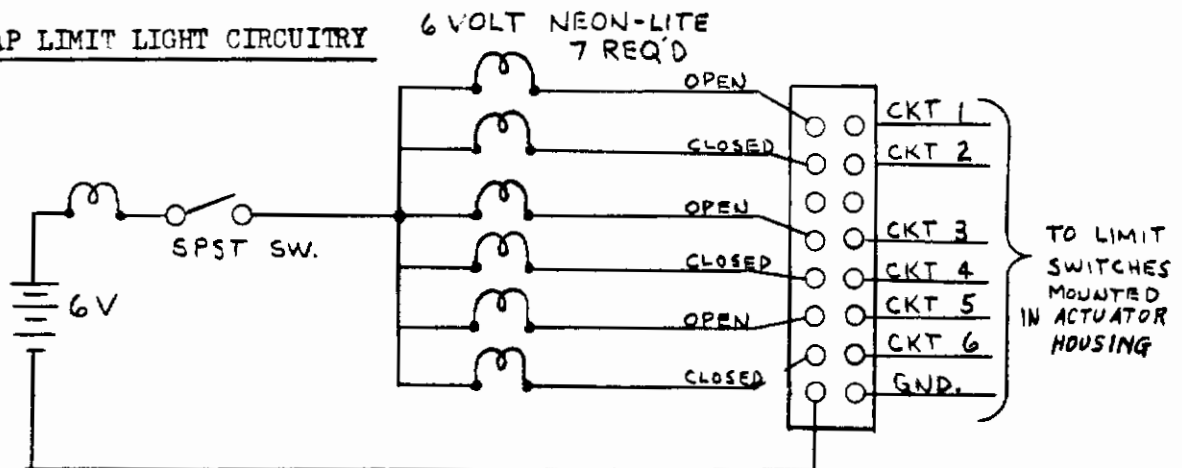
Fig. 5 Electrical Circuits for Remotely Controlled Flaps

26

Fig. 6 Photograph of Flap Control and Indicator Panels

27

Upper Surface

Y'	SYMBOL
0.1618	○
0.3170	□
0.4722	▷
0.6273	◇

$\frac{Nu}{\sqrt{Re_x}}$

X'

(NONDIMENSIONAL STREAMWISE DISTANCE FROM VIRTUAL APEX)
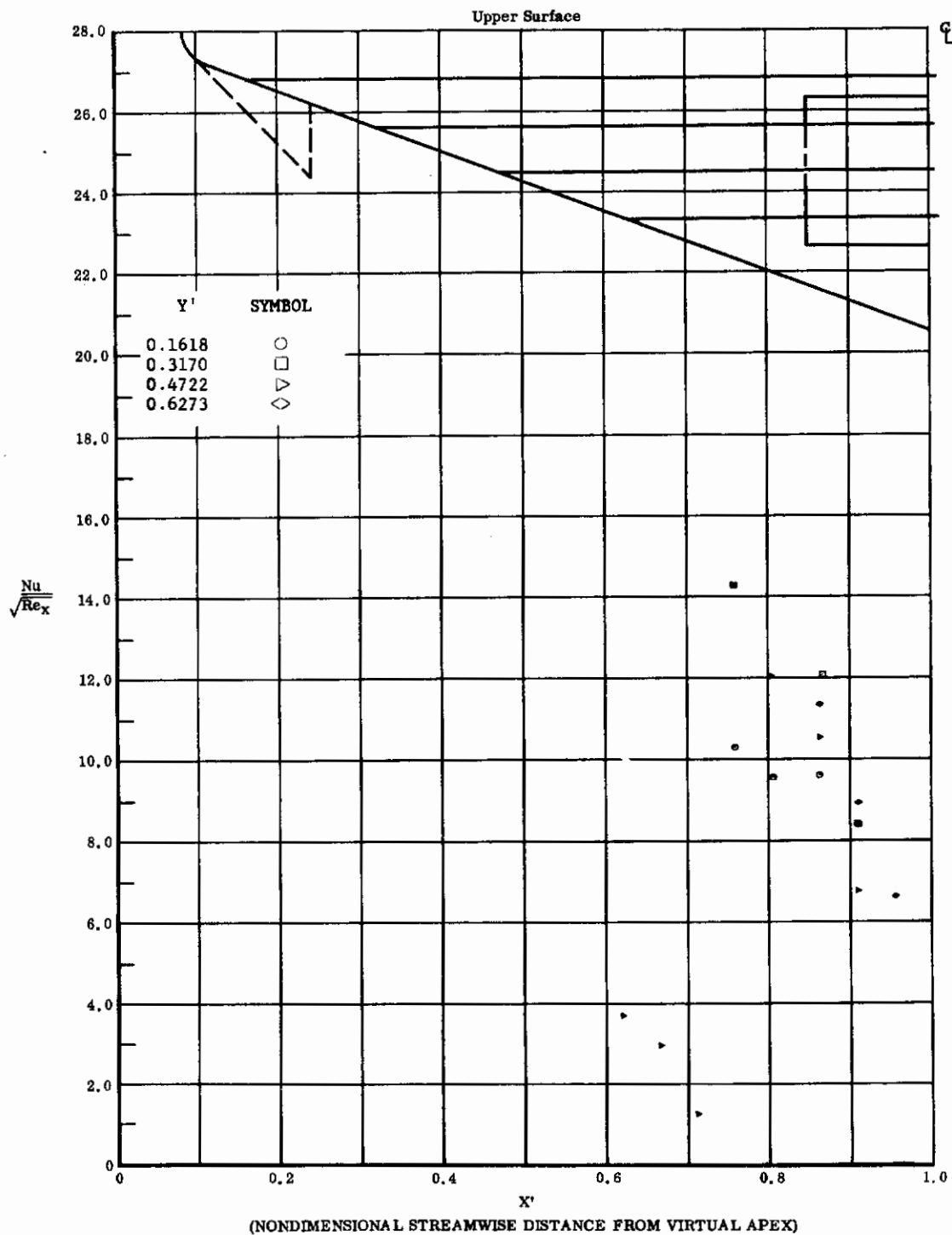
Fig. 7 Streamwise Distributions of Aerodynamic Heating Rates; Basic Configuration, Left and Right (Upper) Flaps Deflected -40°, $\alpha = -45°$, $\beta = 0°$, $Re_\infty/ft = 3,300,000.$
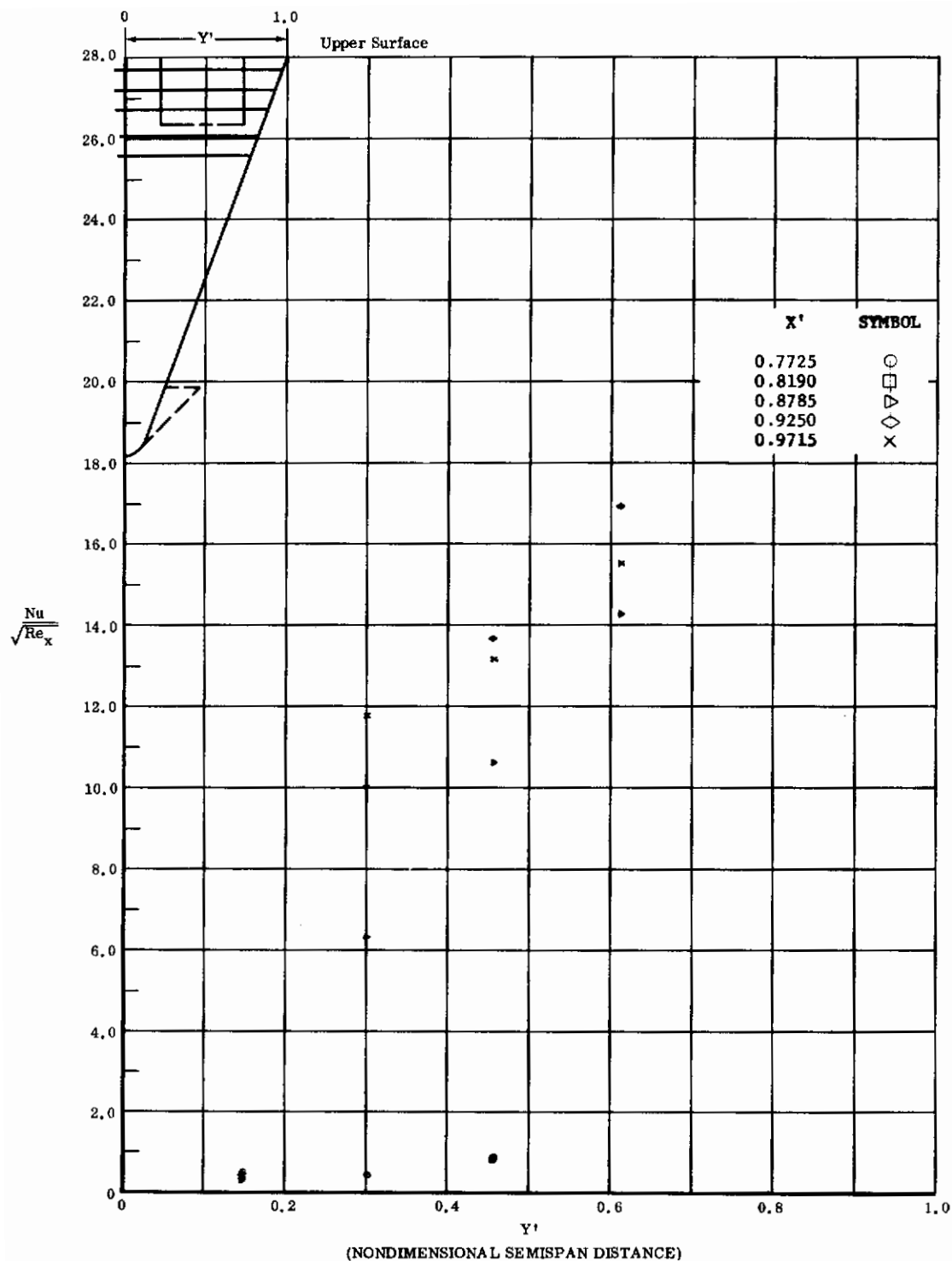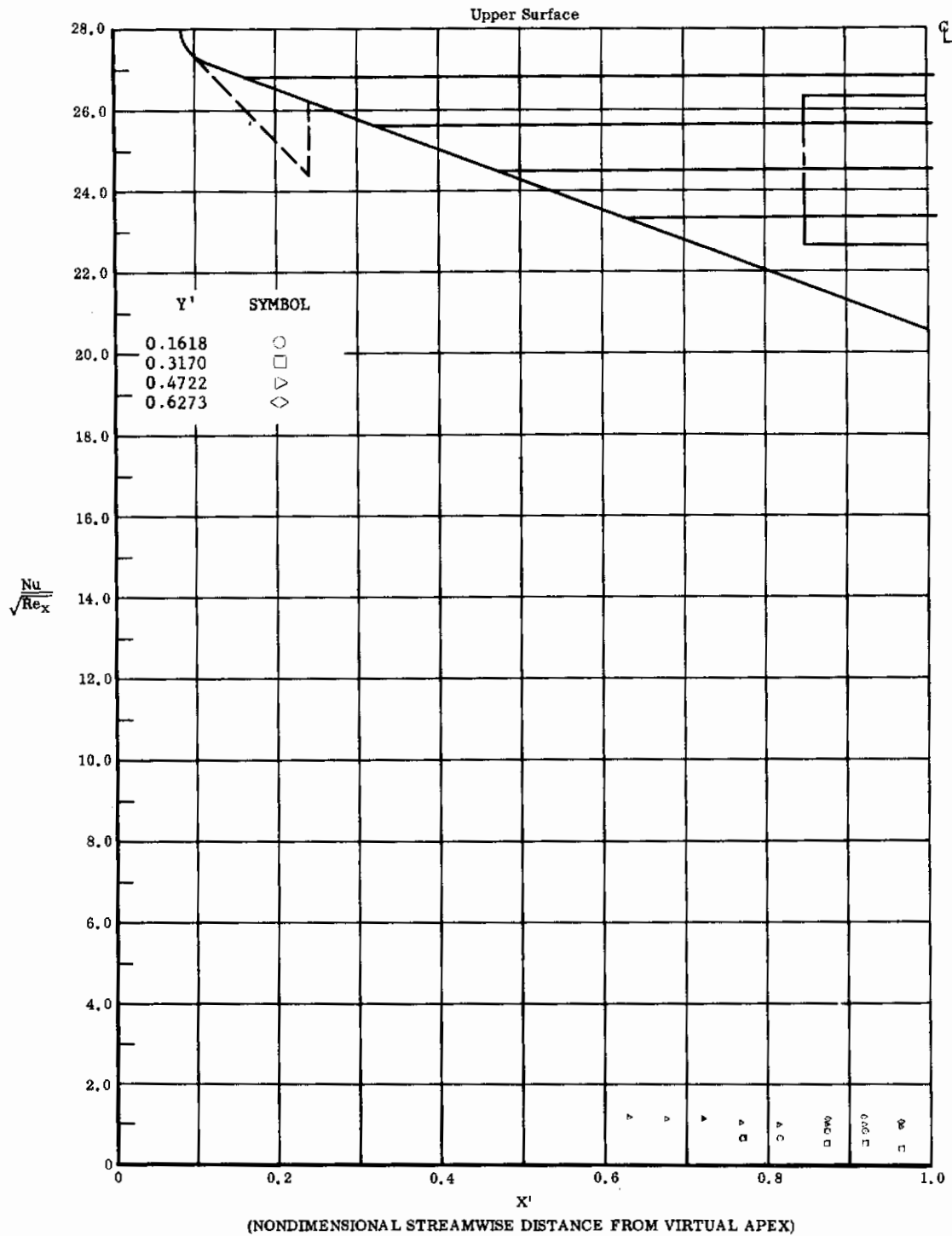
28
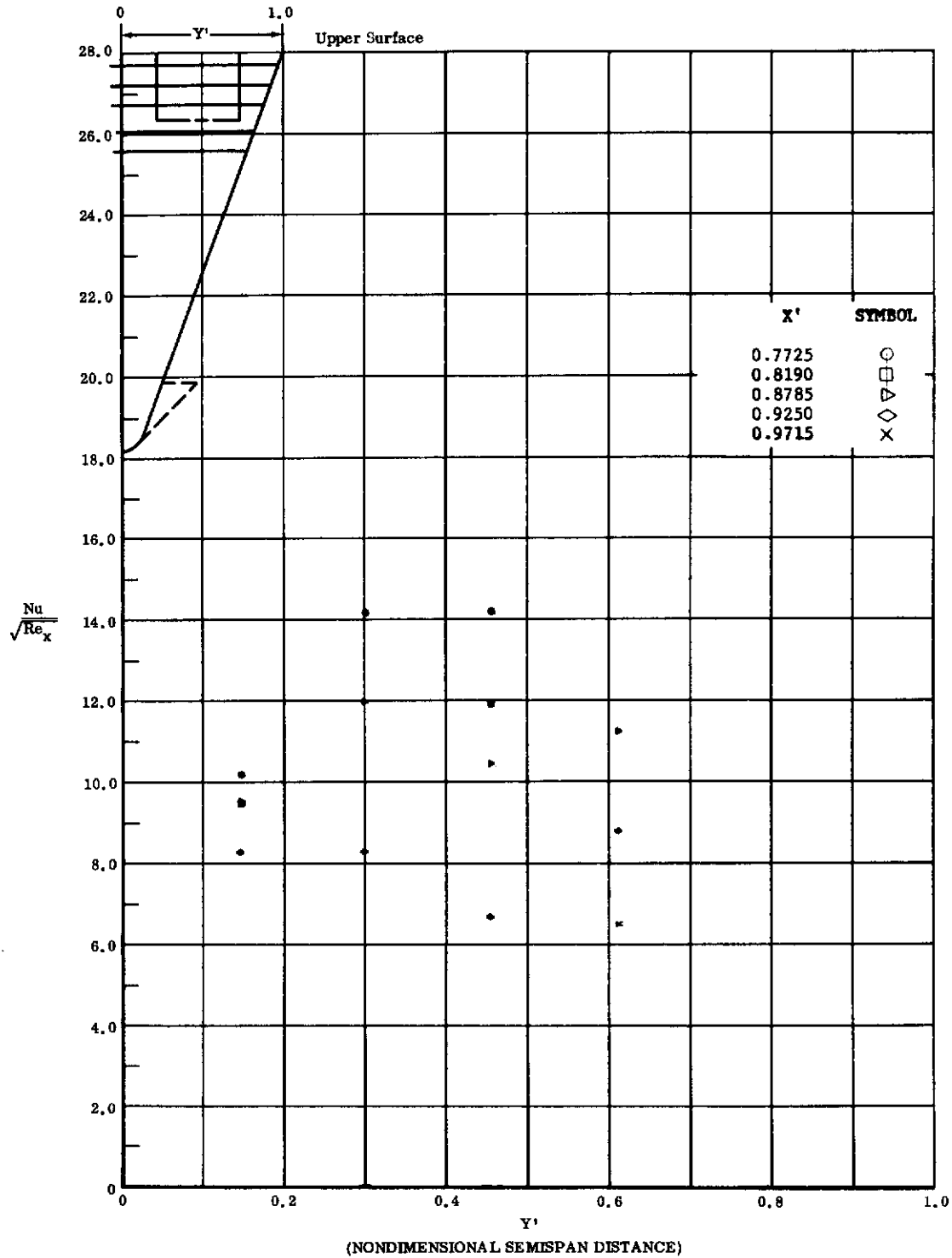
Fig. 7 Spanwise Distributions of Aerodynamic Heating Rates; Basic Configuration, Left and Right (Upper) Flaps Deflected -40°, α = -45°, β = 0°, Re_α/ft = 3,300,000.

29

Upper Surface
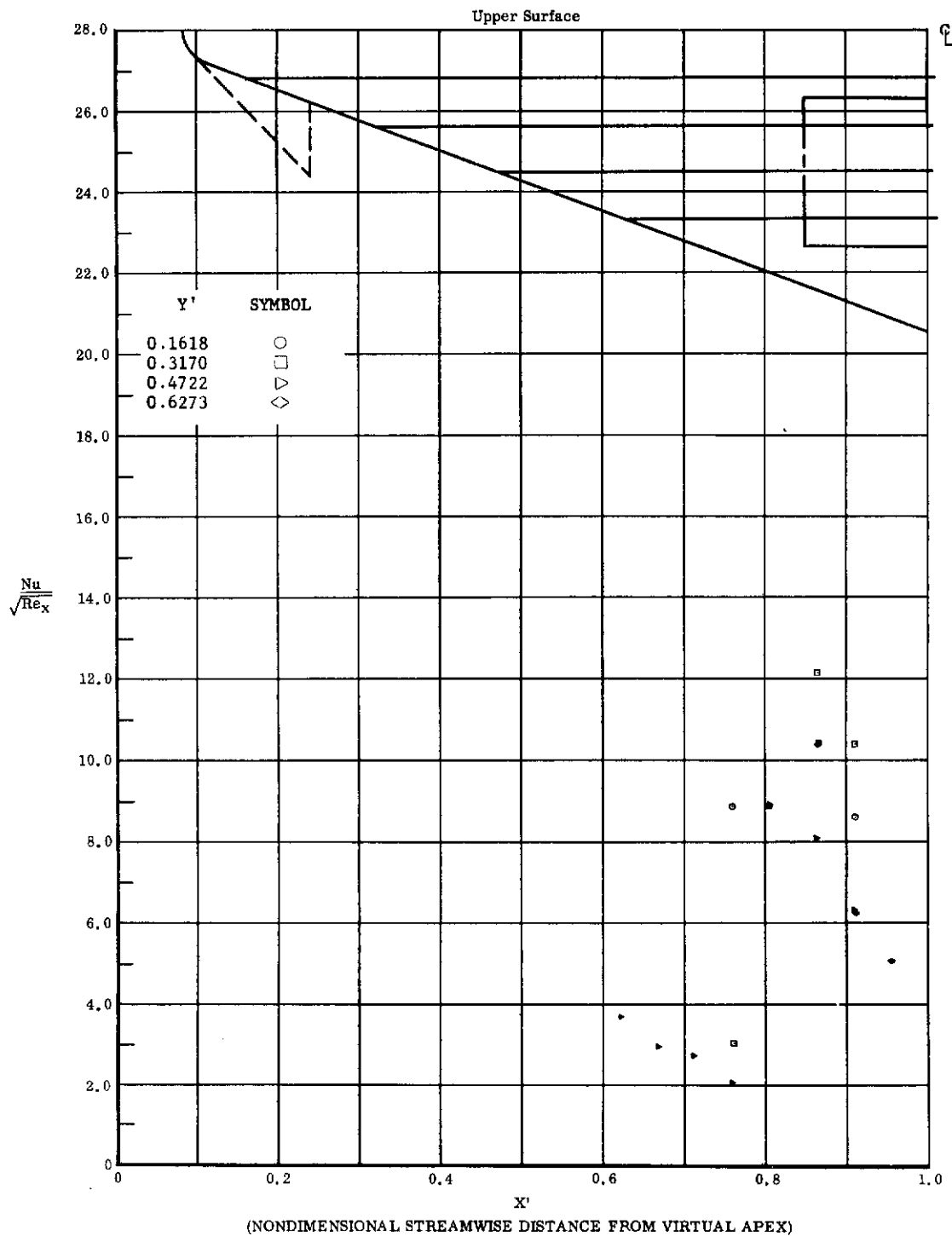
Fig. 8 Streamwise Distributions of Aerodynamic Heating Rates; Basic Configuration, Left and Right (Upper) Flaps Deflected -20°, $\alpha = -45°$, $\beta = 0°$, $Re_\infty/ft = 3,300,000$.
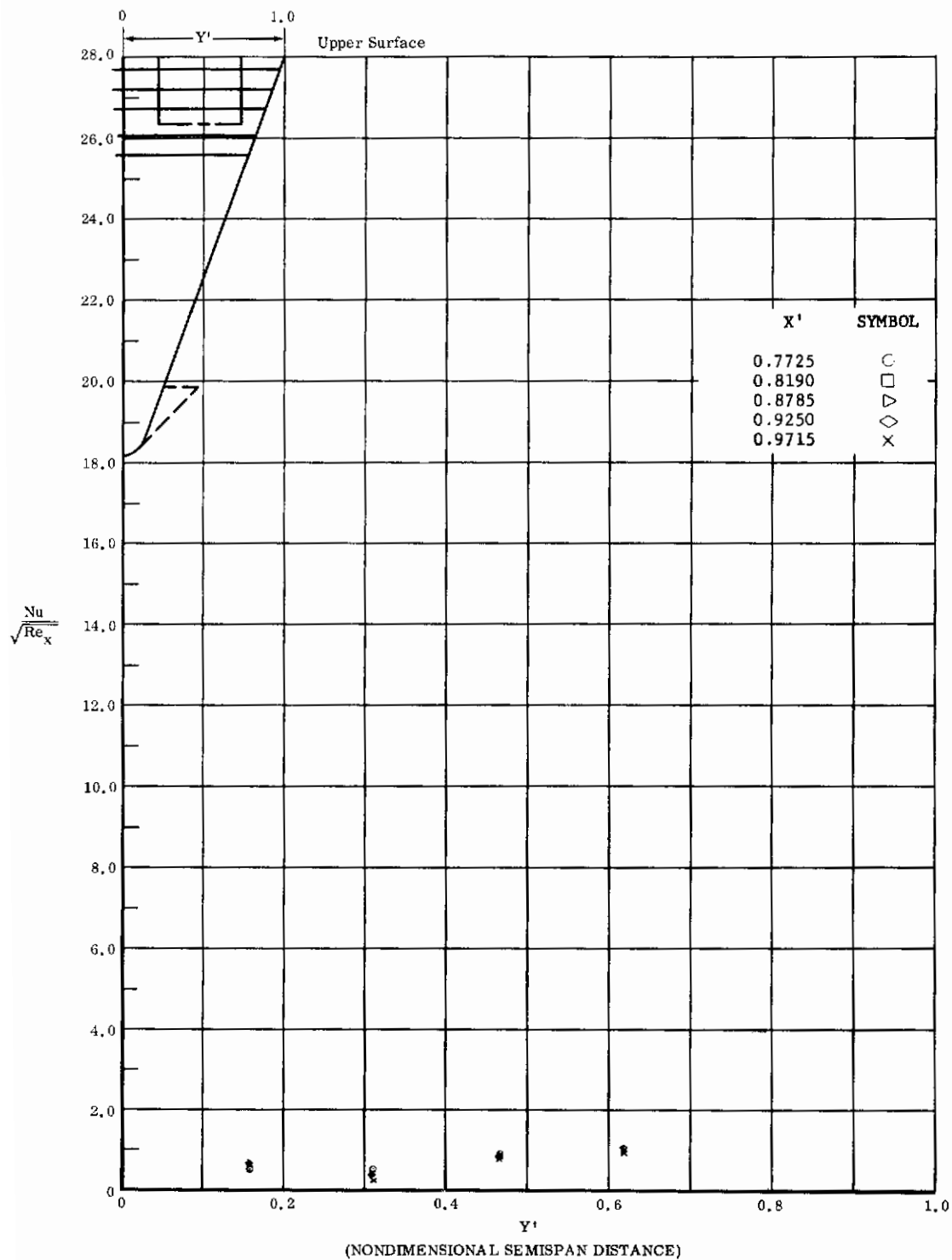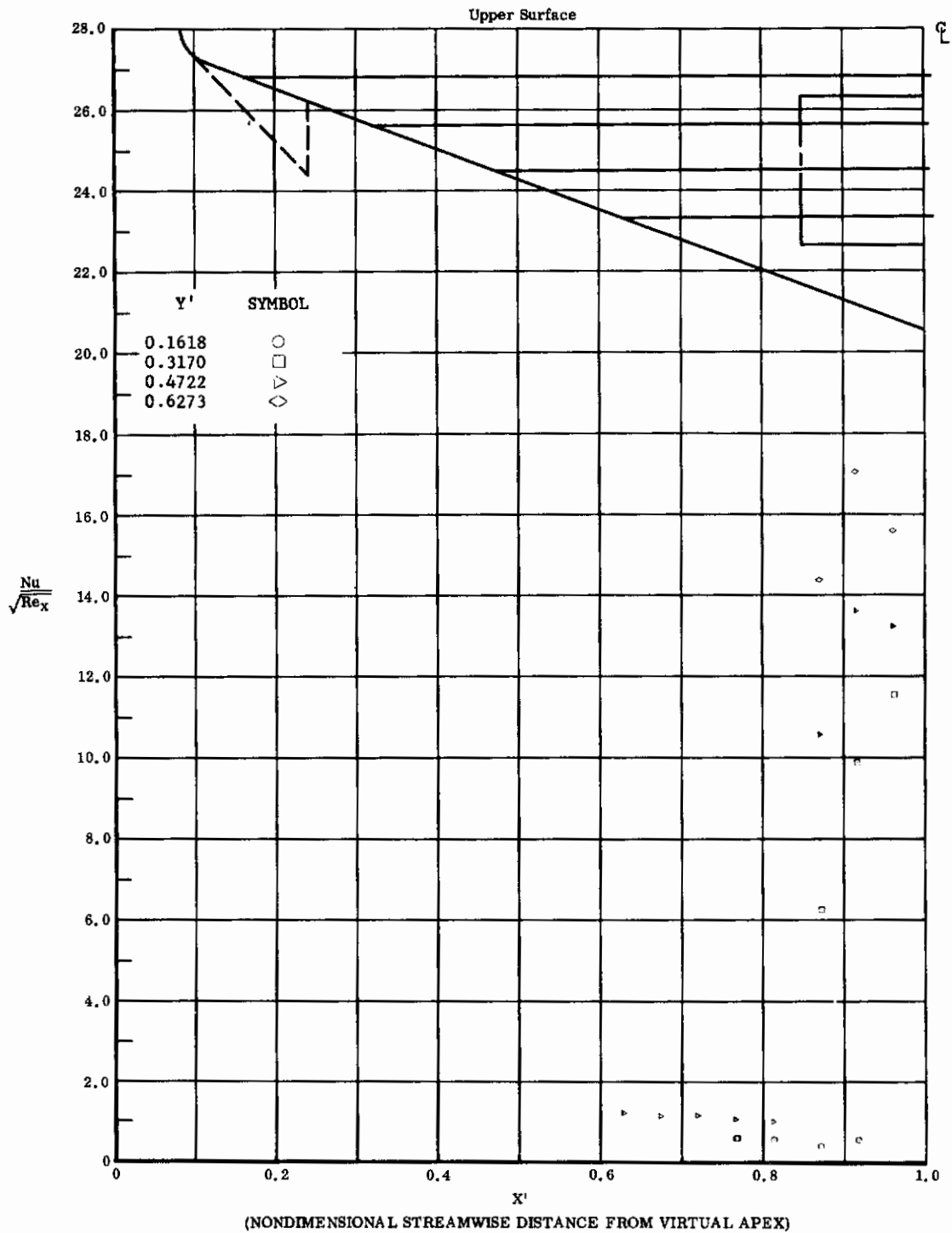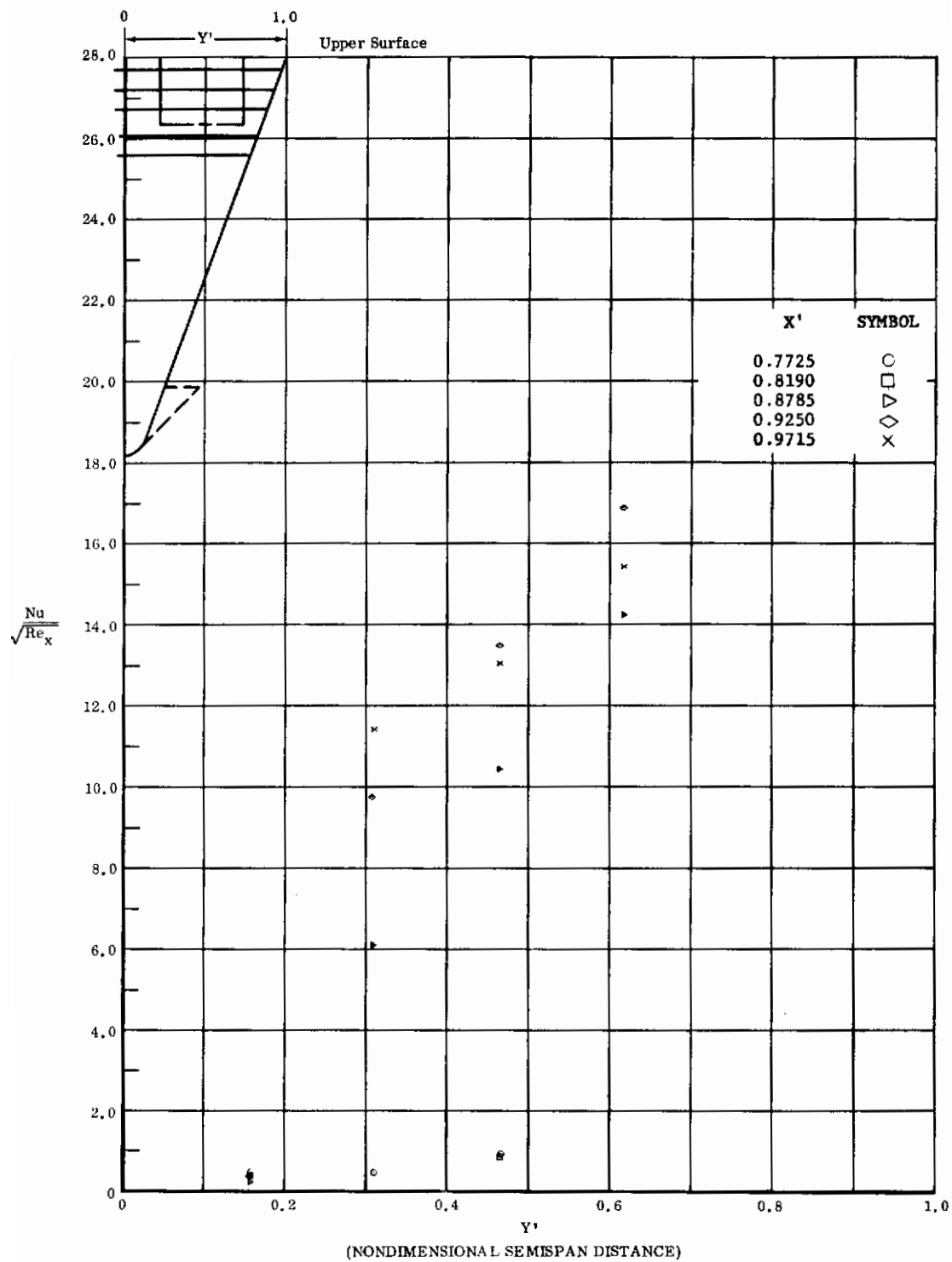
30
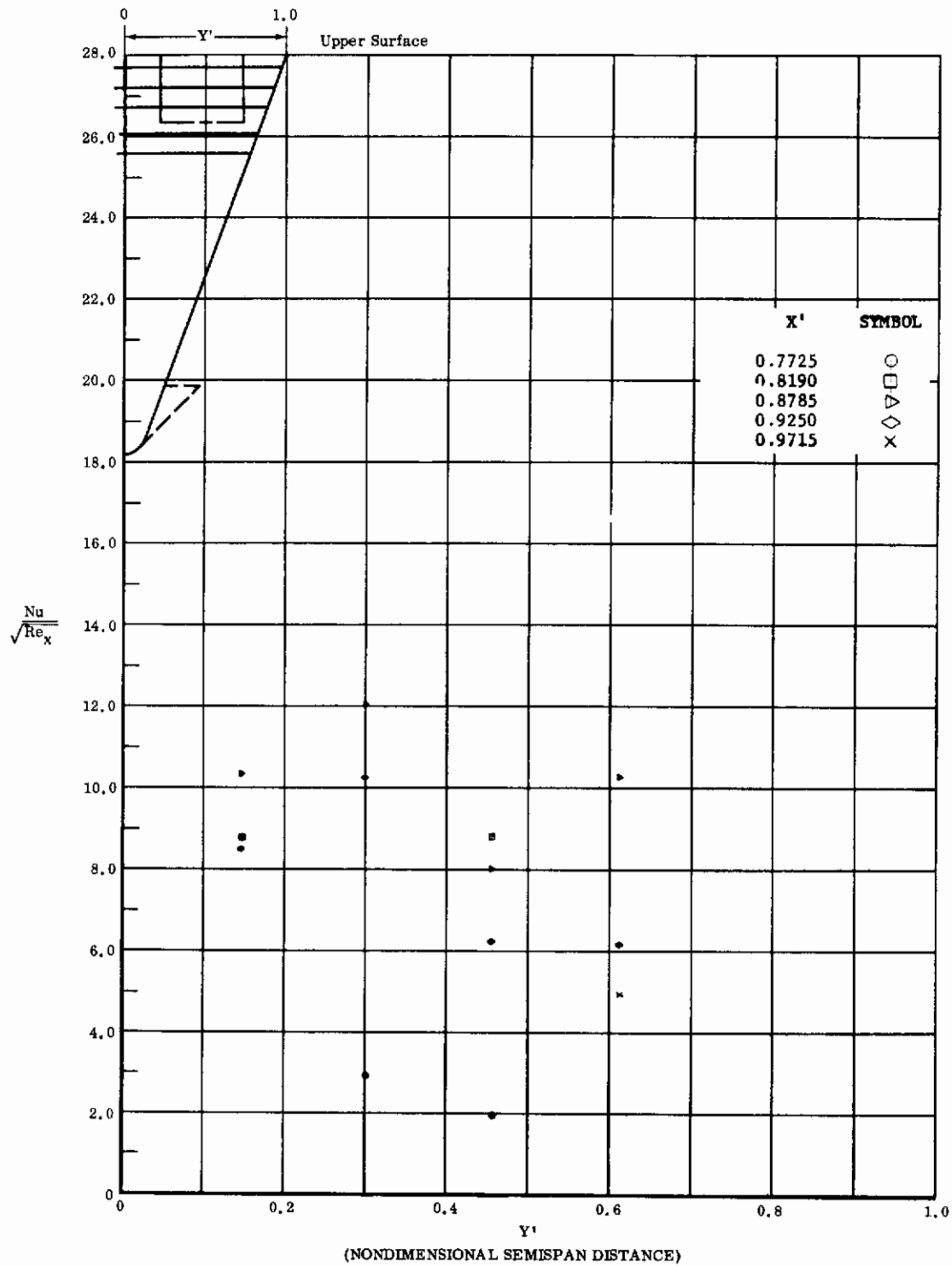
Fig. 8 Spanwise Distributions of Aerodynamic Heating Rates; Basic Configuration, Left and Right (Upper) Flaps Deflected -20°, α = -45°, β = 0°, Re_∞/ft = 3,300,000.

31
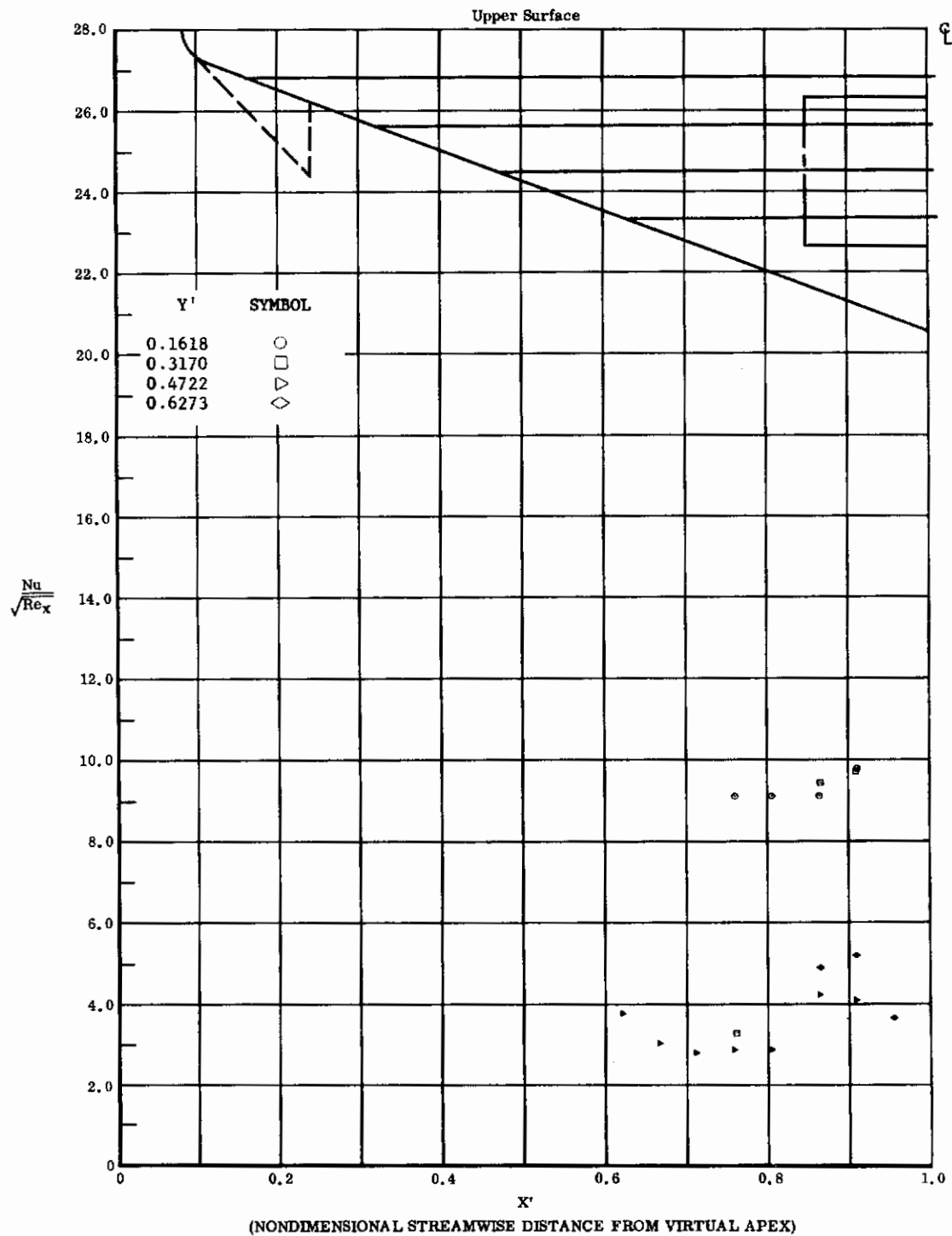
Fig. 9 Streamwise Distributions of Aerodynamic Heating Rates; Basic Configuration, No Flap Deflections, $\alpha = -45°$, $\beta = 0°$, $Re_\infty/ft = 3,300,000$.

32
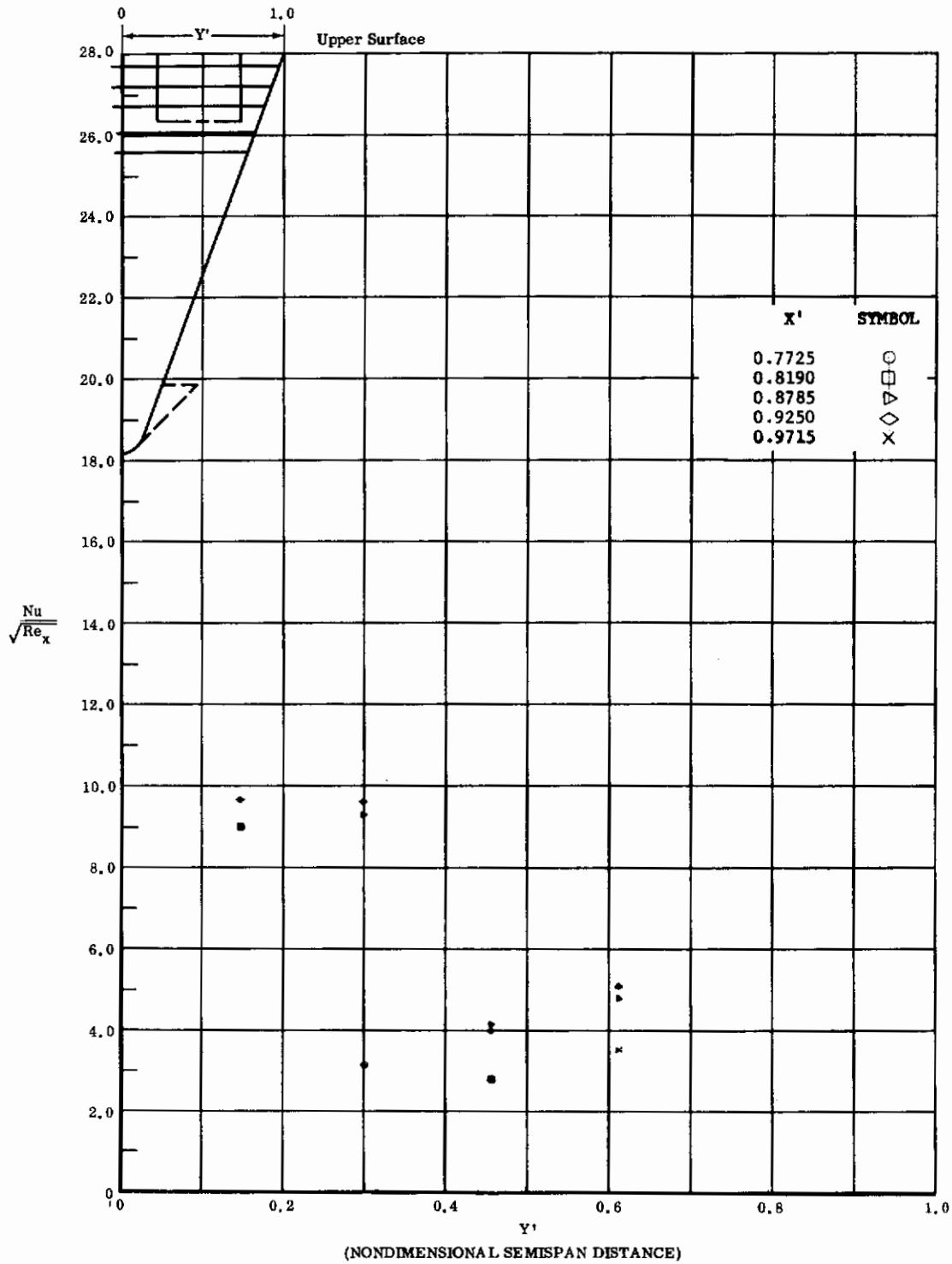
Fig. 9 Spanwise Distributions of Aerodynamic Heating Rates; Basic Configuration, No Flap Deflections, $\alpha = -45°$, $\beta = 0°$, $Re_\infty/ft = 3,300,000$.
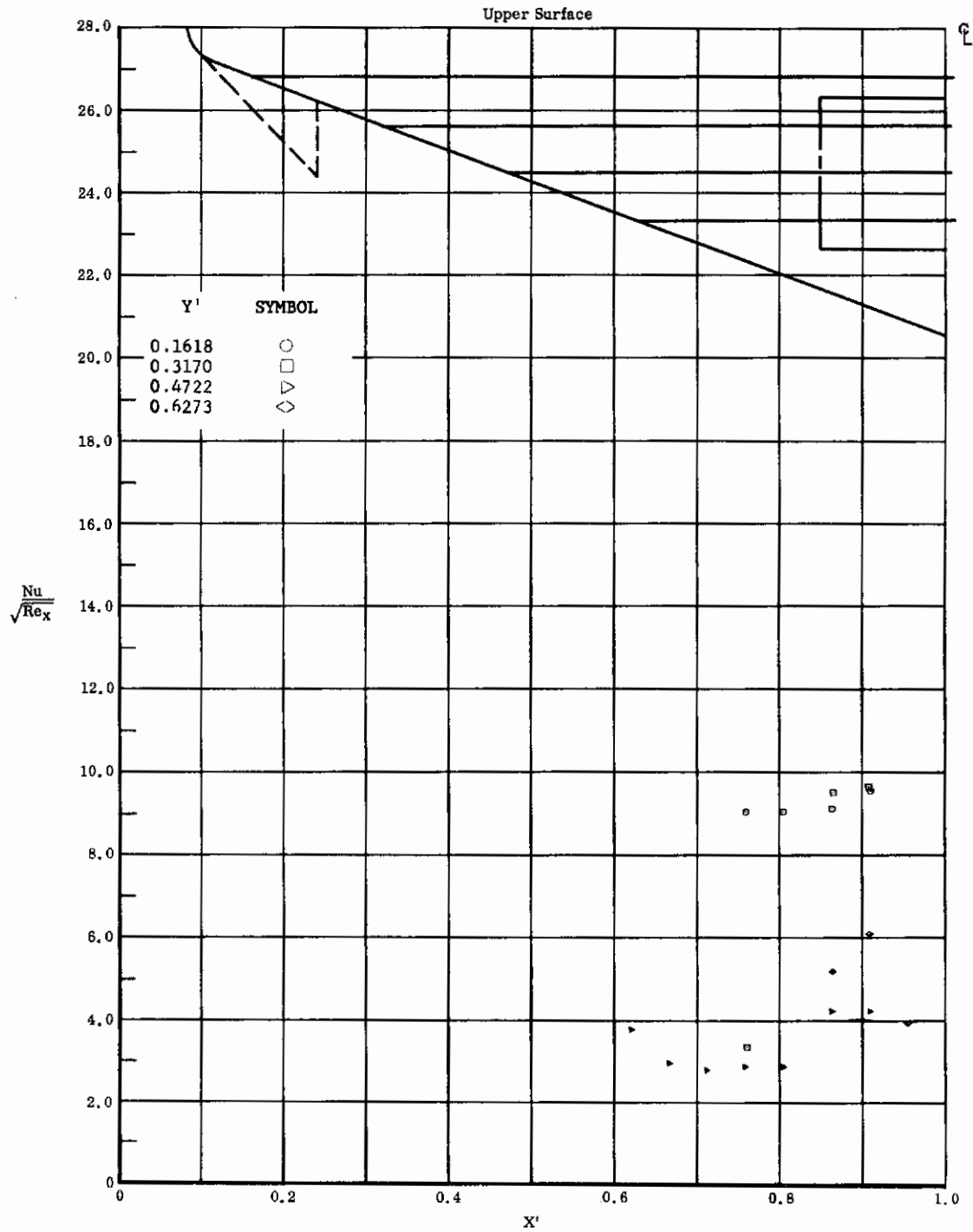
Fig. 10   Streamwise Distributions of Aerodynamic Heating Rates; Basic Configuration, Bottom Flaps Deflected +40°, $\alpha = -45°$, $\beta = 0°$, $Re_\infty/ft = 3,300,000$.
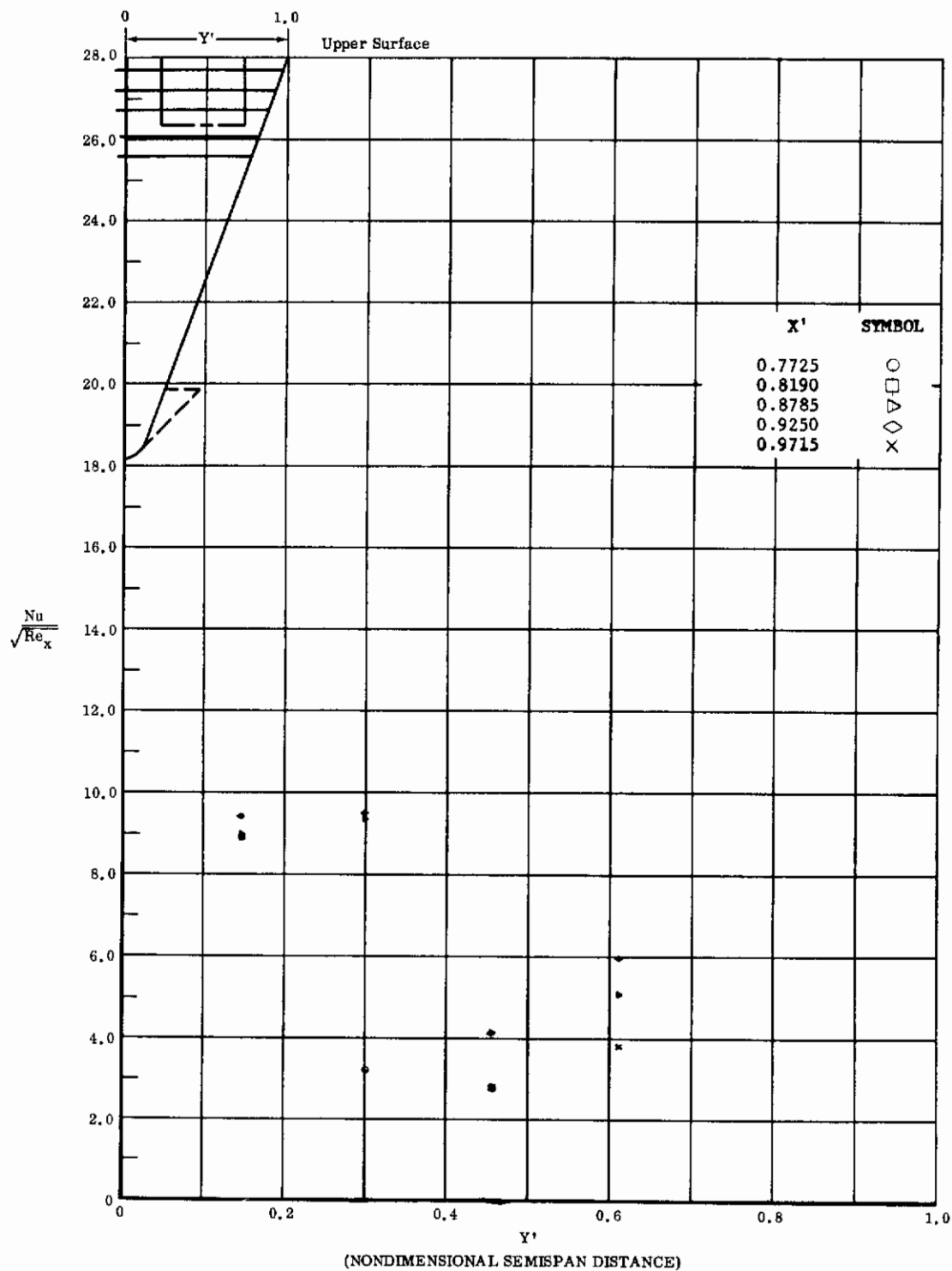
Fig. 10 Spanwise Distributions of Aerodynamic Heating Rates; Basic Configuration, Bottom Flaps Deflected +40°, $\alpha = -45°$, $\beta = 0°$, $Re_\infty/ft = 3,300,000$.

35
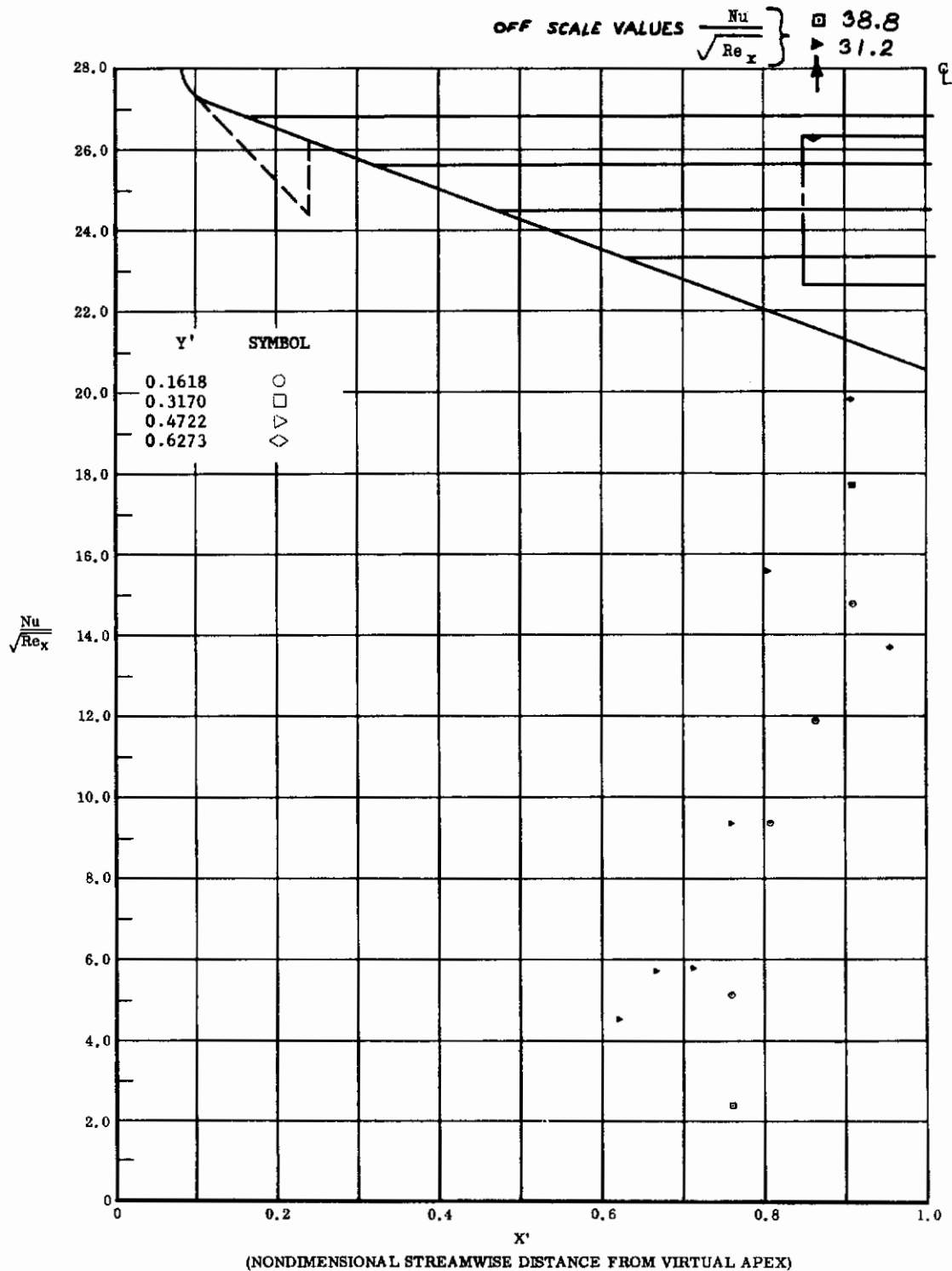
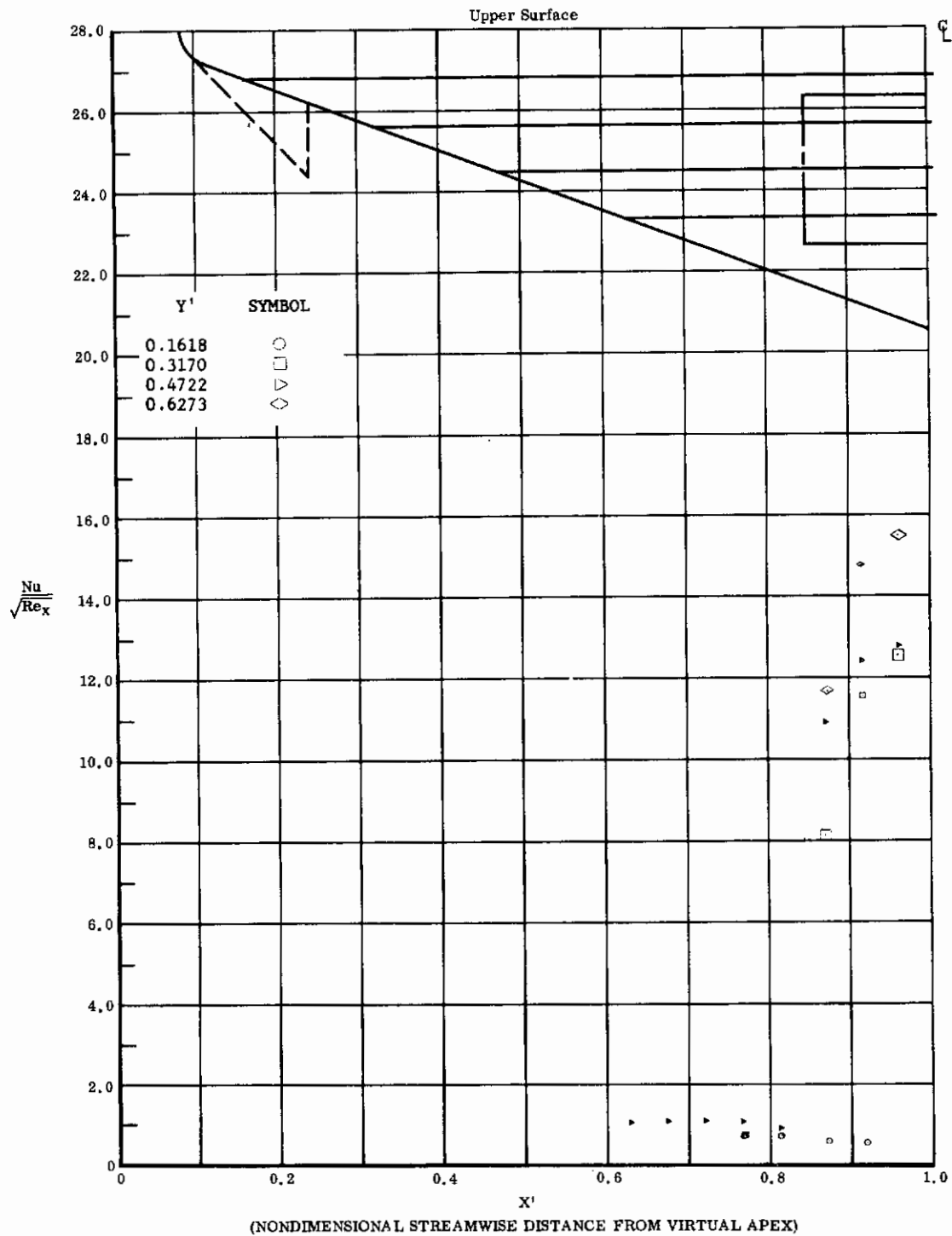Fig. 11 Streamwise Distributions of Aerodynamic Heating Rates; Basic Configuration,
Left and Right (Upper) Flaps Deflected -40°, α = -33°, β = 0°,
Re$_\infty$/ft = 3,300,000.

36
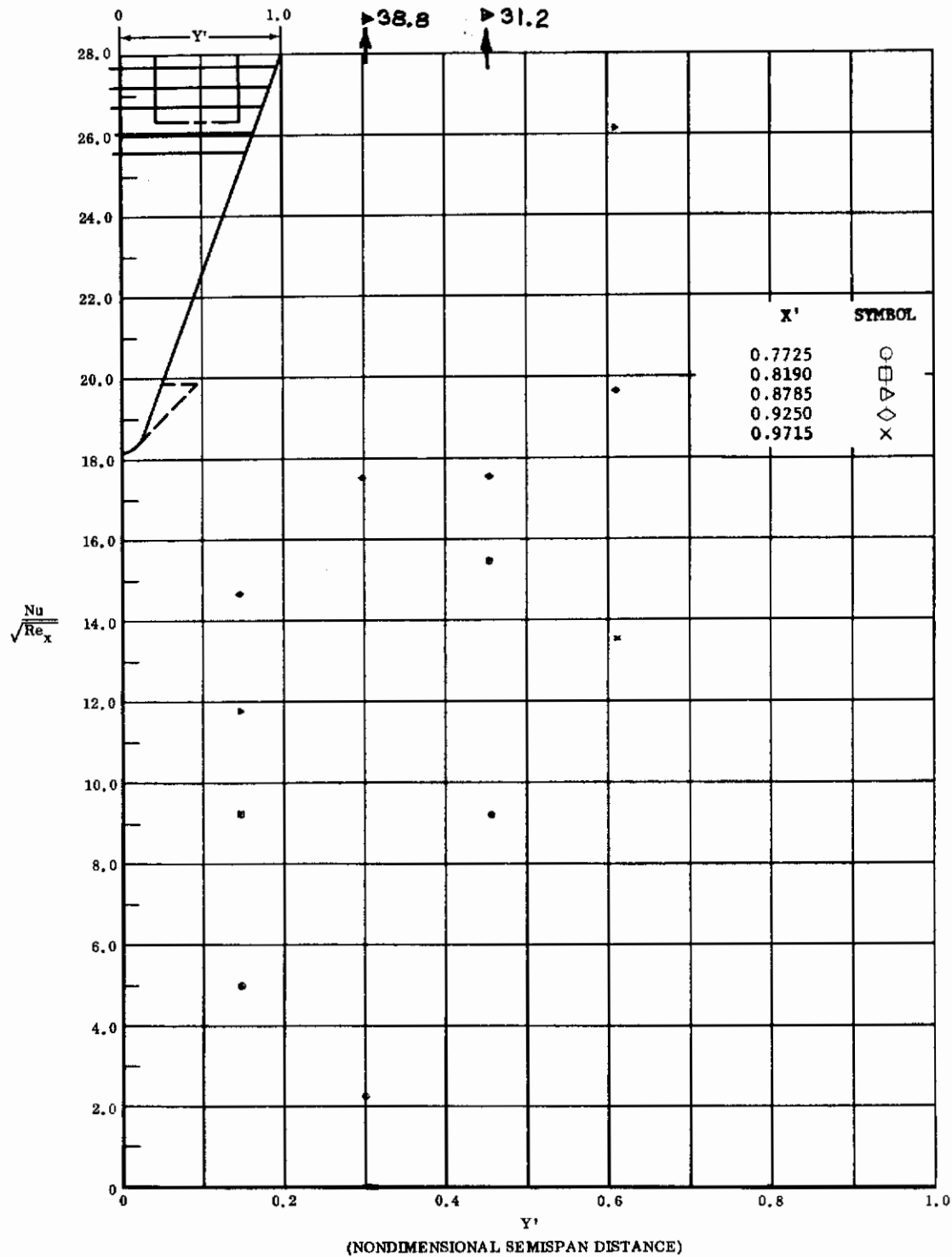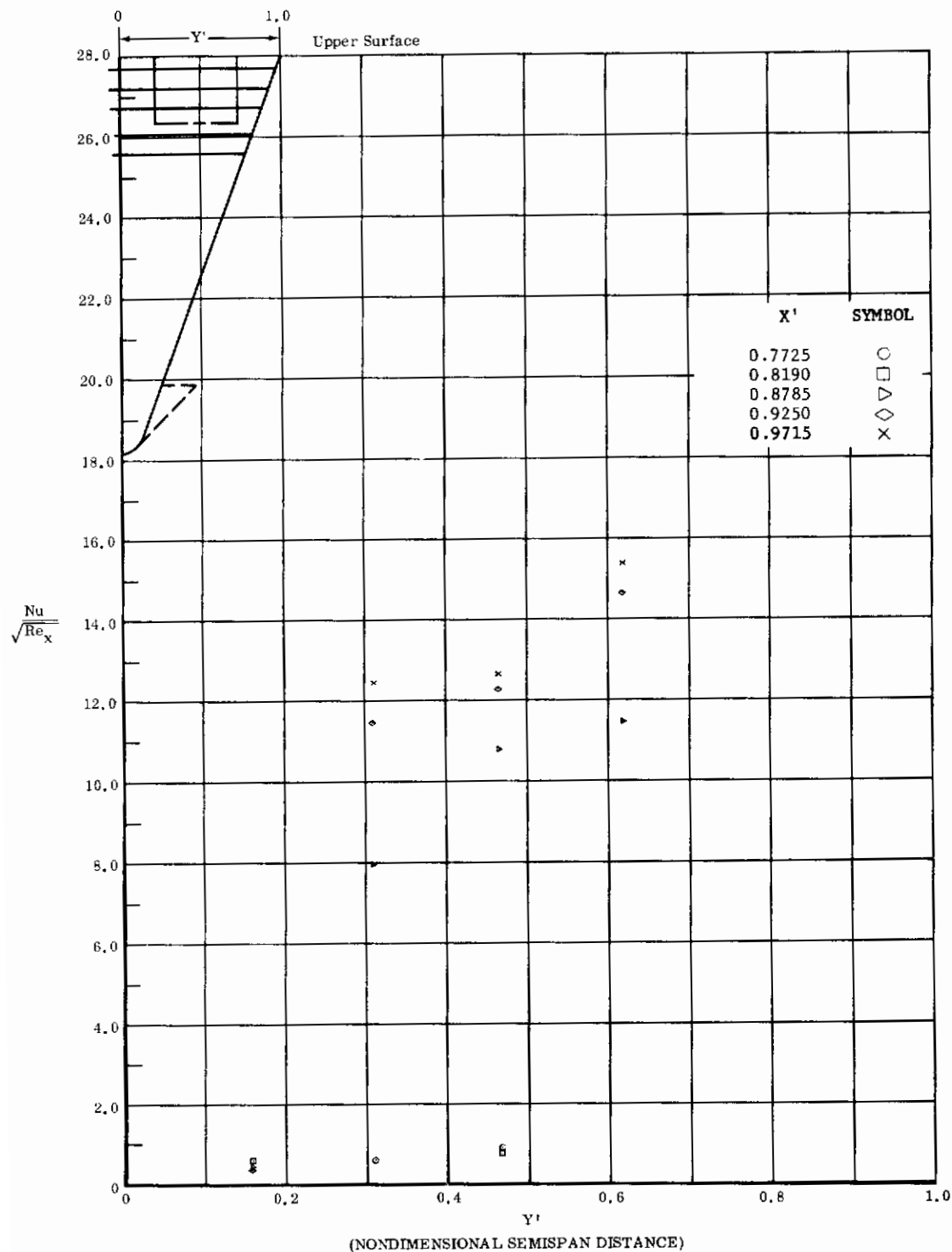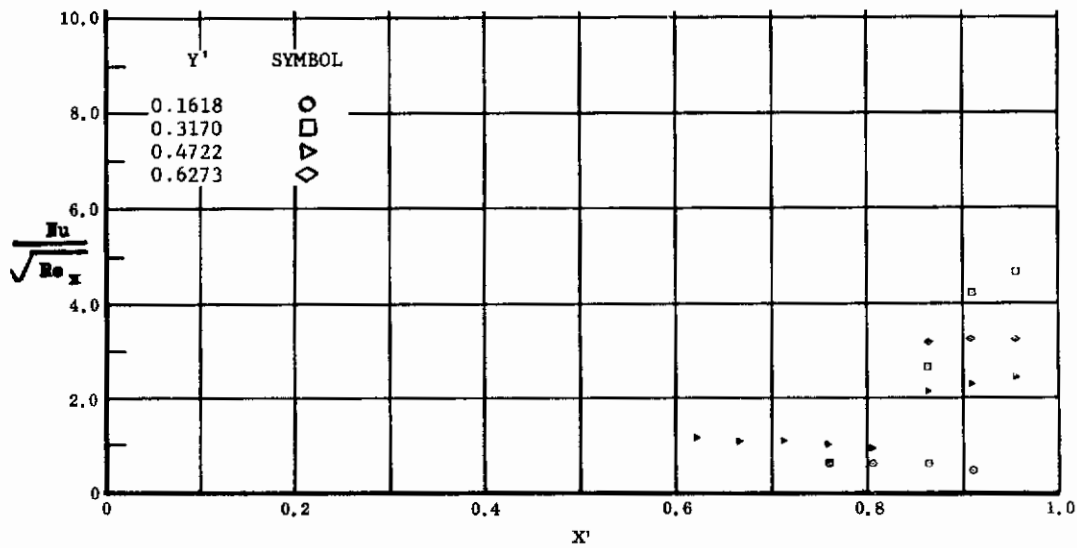
Fig. 11 Spanwise Distributions of Aerodynamic Heating Rates; Basic Configuration,
Left and Right (Upper) Flaps Deflected -40°, α = -33°, β = 0°,
Re∞/ft = 3,300,000.

37

Fig. 12 Streamwise Distributions of Aerodynamic Heating Rates; Basic Configuration, No Flap Deflections, $\alpha = -33°$, $\beta = 0°$, $Re_\infty/ft = 3,300,000$.

0   1.0   Upper Surface

28.0

26.0

24.0

22.0

X'	SYMBOL
0.7725	○
0.8190	□
0.8785	△
0.9250	◇
0.9715	×

20.0

18.0

16.0

$\frac{Nu}{\sqrt{Re_x}}$ 14.0

12.0

10.0

8.0

6.0

4.0

2.0

0

0   0.2   0.4   0.6   0.8   1.0

Y'

(NONDIMENSIONAL SEMISPAN DISTANCE)
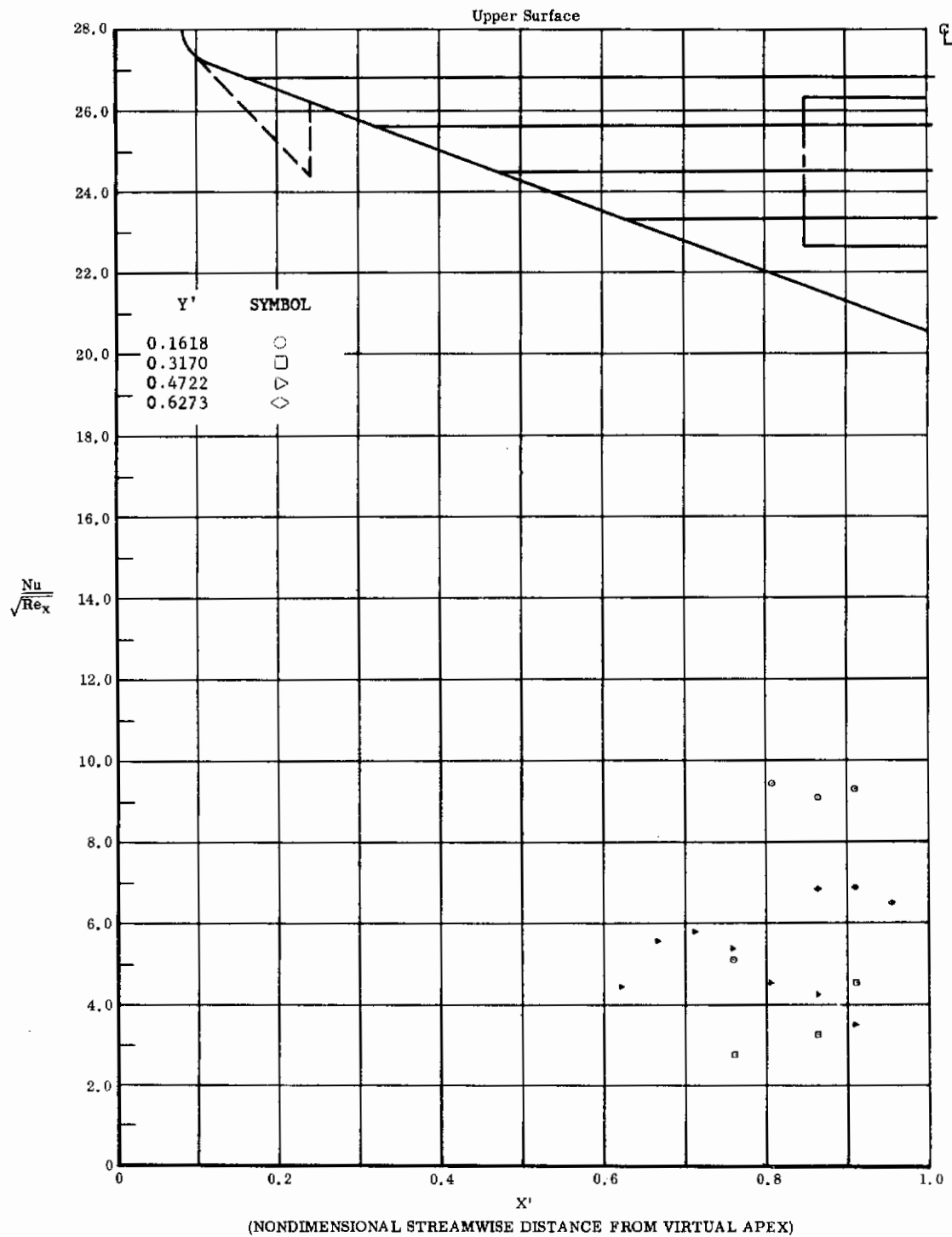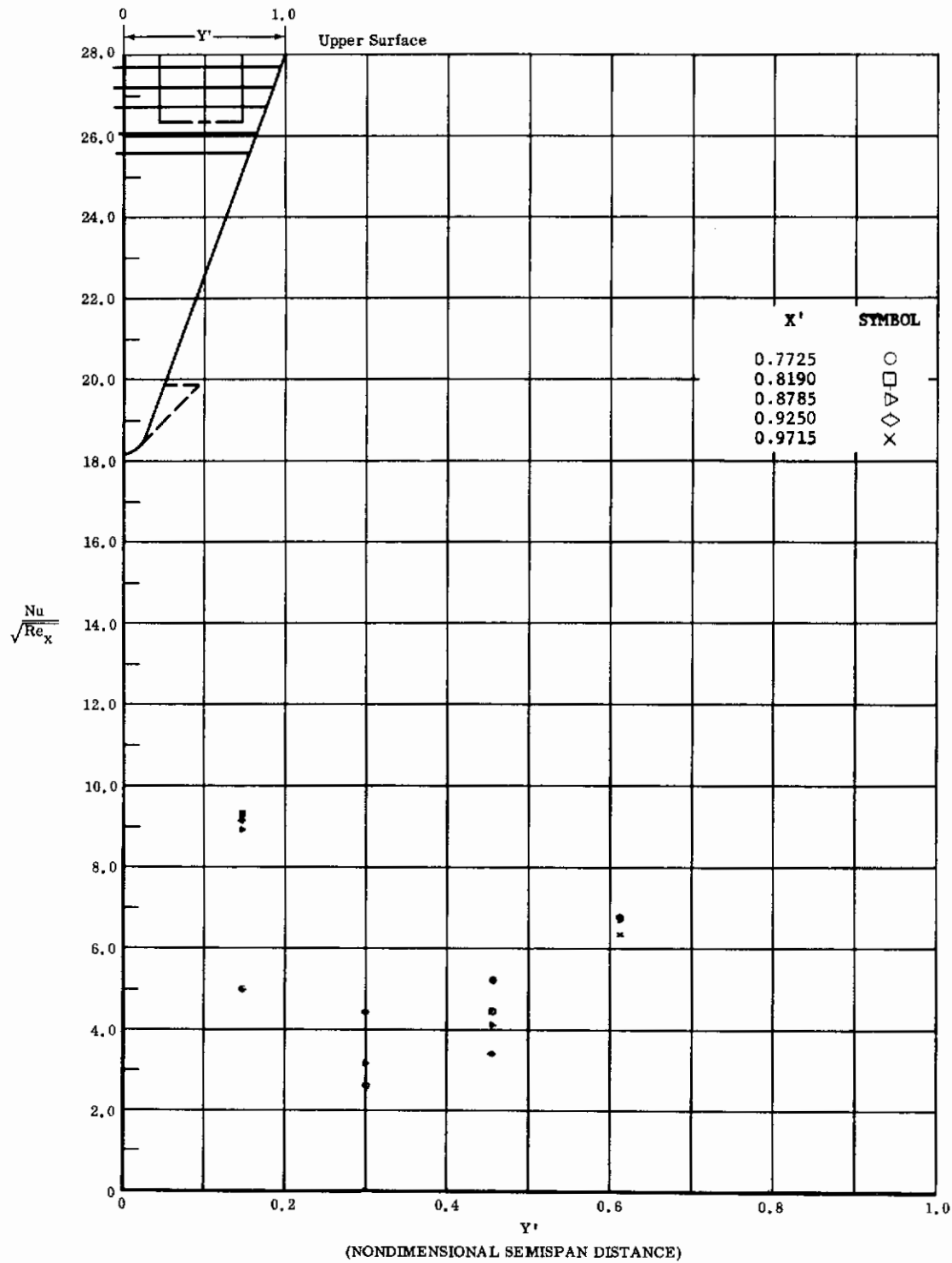
Fig. 12   Spanwise Distributions of Aerodynamic Heating Rates; Basic Configuration,
No Flap Deflections, $\alpha = -33°$, $\beta = 0°$, $Re_\infty/ft = 3,300,000$.

39
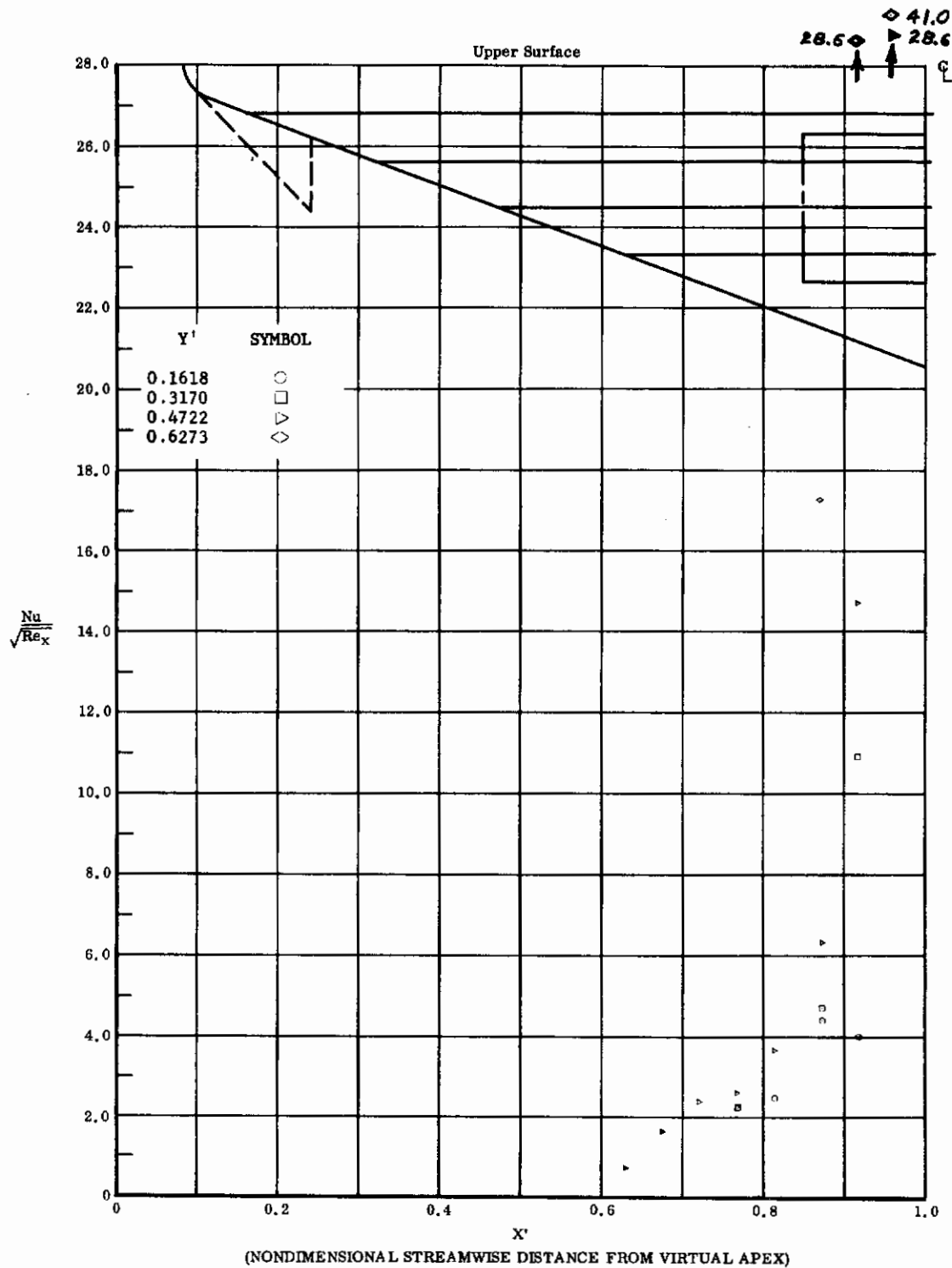
Fig. 13 Streamwise Distributions of Aerodynamic Heating Rates; Basic Configuration, Left and Right (Upper) Flaps Deflected -40°, $\alpha = 0°$, $\beta = 0°$, $Re_\infty/ft = 1,100,000$.

Fig. 13 Spanwise Distributions of Aerodynamic Heating Rates; Basic Configuration, Left and Right (Upper) Flaps Deflected -40°, $\alpha = 0°$, $\beta = 0°$, $Re_\infty/ft = 1,100,000.$

41

SEE FOLLOWING PAGES OF THIS FIGURE   FOR VALUES OF $\dfrac{Nu}{\sqrt{Re_x}} > 28$

$\dfrac{Nu}{\sqrt{Re_x}}$

X'

(NONDIMENSIONAL STREAMWISE DISTANCE FROM VIRTUAL APEX)

Y'	SYMBOL
0.1618	○
0.3170	□
0.4722	▷
0.6273	◇

Fig. 14   Streamwise Distributions of Aerodynamic Heating Rates; Basic Configuration,
Left and Right (Upper) Flaps Deflected -40°, α = 0°, β = 0°,
Re_∞/ft = 3,300,000.

42
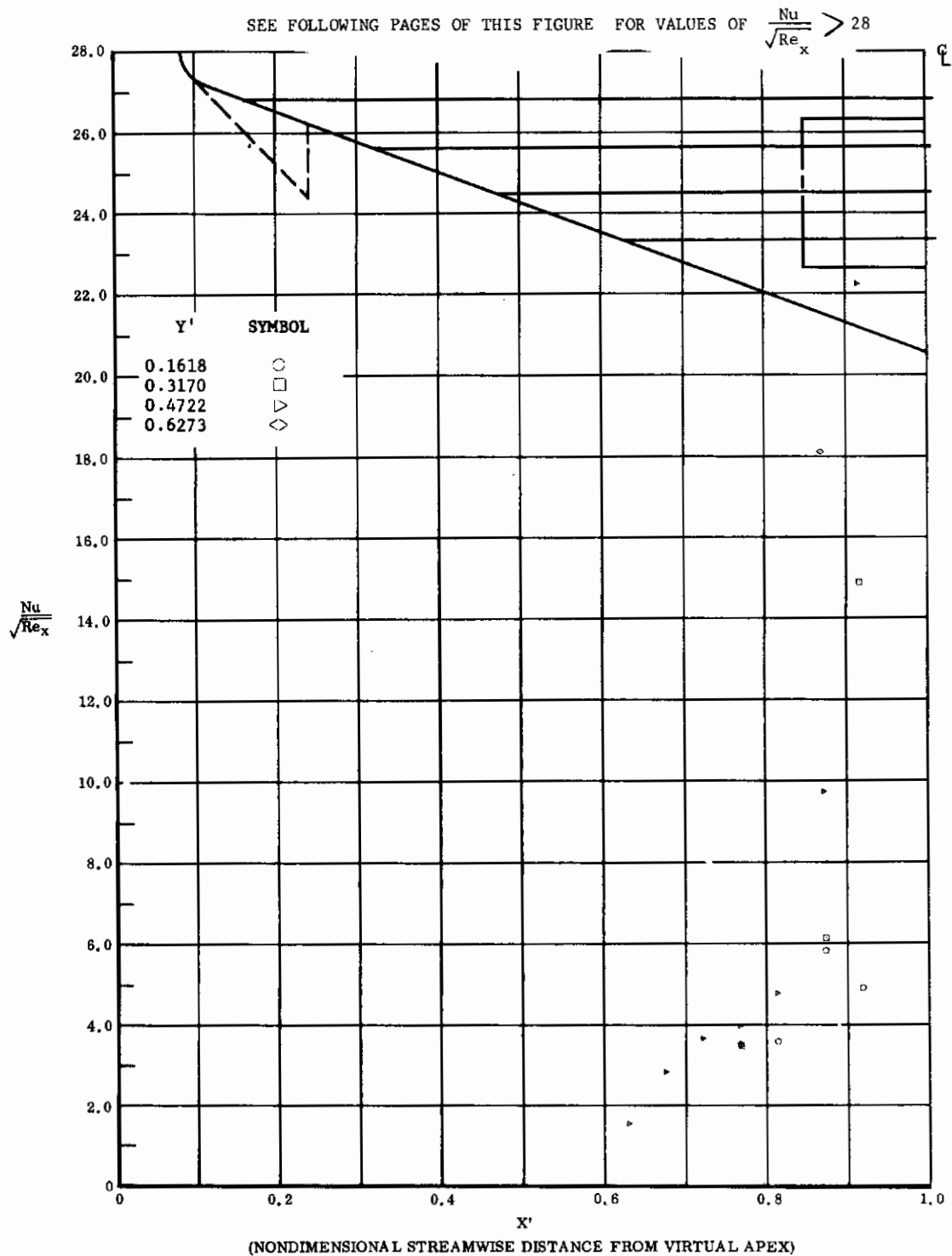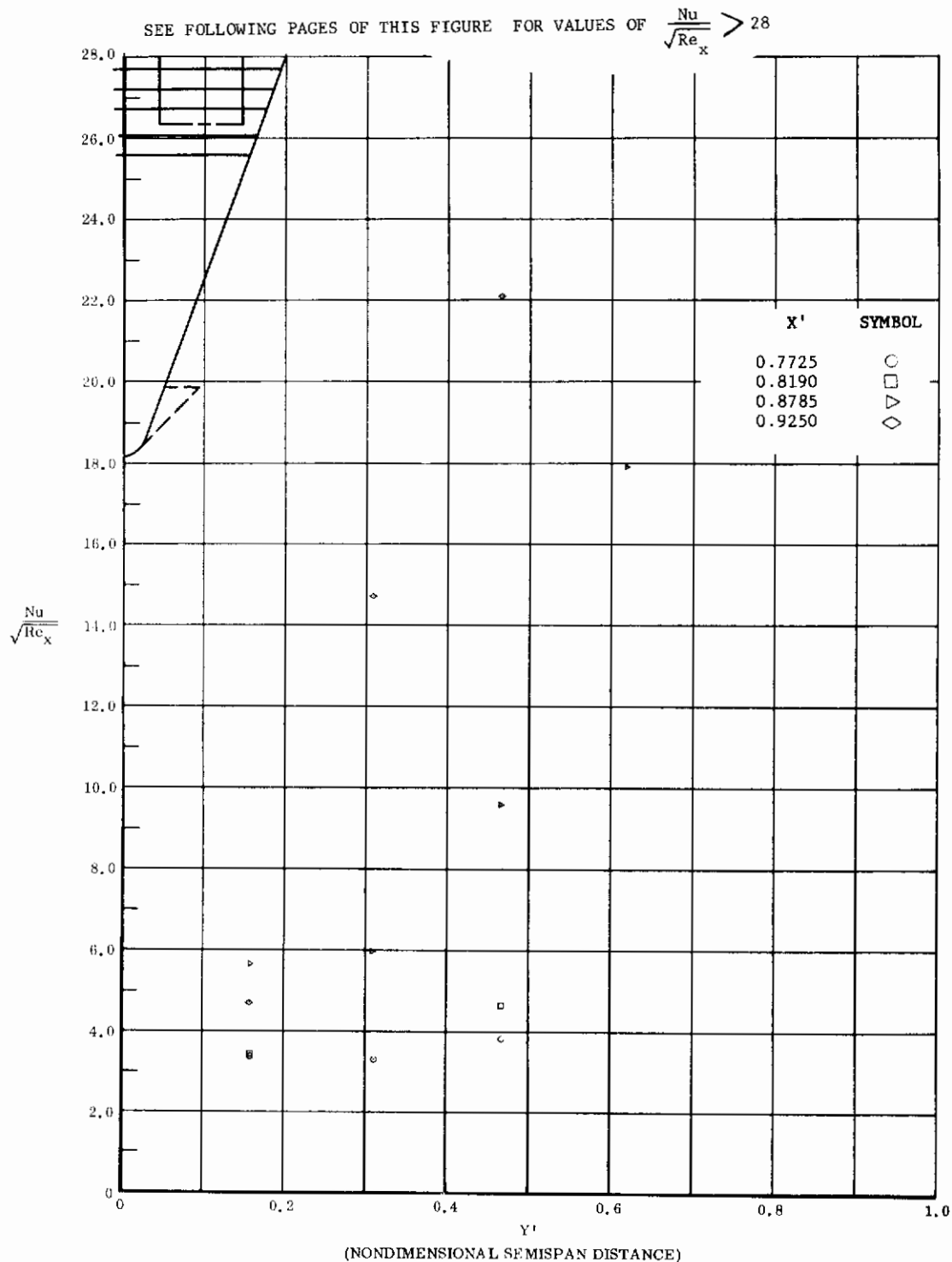
Fig. 14 Spanwise Distributions of Aerodynamic Heating Rates; Basic Configuration, Left and Right (Upper) Flaps Deflected -40°, $\alpha = 0°$, $\beta = 0°$, $Re_\infty/ft = 3,300,000$.

Fig. 14 Streamwise Distributions of Aerodynamic Heating Rates; Basic Configuration, Left and Right (Upper) Flaps Deflected -40°, $\alpha = 0°$, $\beta = 0°$, $Re_\infty/ft = 3,300,000$.

0   1.0

Y'

Upper Surface

80

70

60

50

$\dfrac{Nu}{\sqrt{Re_x}}$

40

30

20

0

X'	SYMBOL
0.8785	▷
0.9250	◇
0.9715	✕

SEE PRECEDING PAGES OF THIS FIGURE FOR VALUES OF $\dfrac{Nu}{\sqrt{Re_x}} < 20$

0   0.2   0.4   0.6   0.8   1.0

Y'

(NONDIMENSIONAL SEMISPAN DISTANCE)

Fig. 14   Spanwise Distributions of Aerodynamic Heating Rates; Basic Configuration,
Left and Right (Upper) Flaps Deflected -40°, $\alpha = 0°$, $\beta = 0°$,
$Re_\infty/ft = 3,300,000$.

45

Upper Surface

Y'	SYMBOL
0.1618	○
0.3170	□
0.4722	▷
0.6273	◇

$\dfrac{Nu}{\sqrt{Re_x}}$

X'

(NONDIMENSIONAL STREAMWISE DISTANCE FROM VIRTUAL APEX)
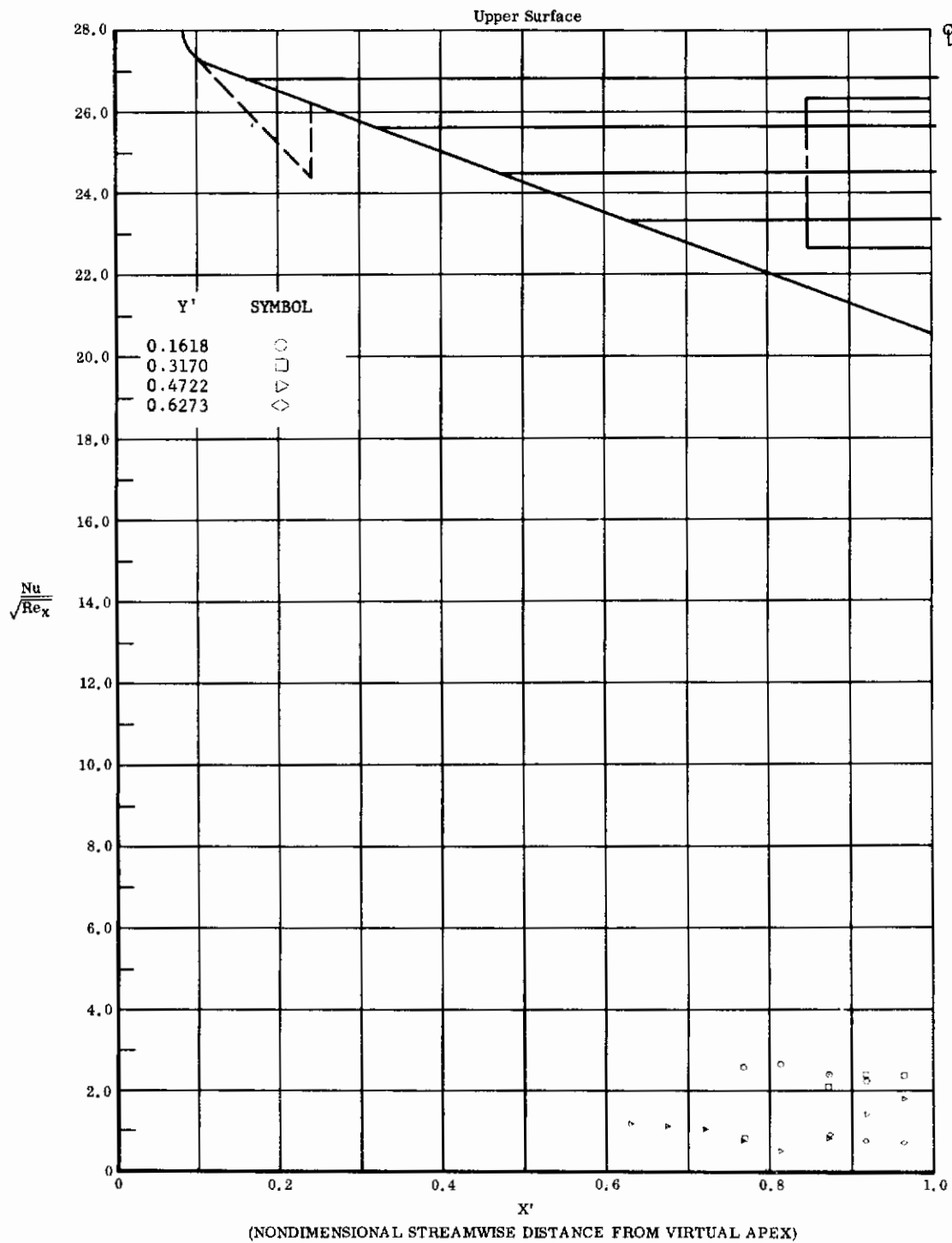
Fig. 15 Streamwise Distributions of Aerodynamic Heating Rates; Basic Configuration, Left (Upper) Flap Deflected -40°, $\alpha = 0°$, $\beta = 0°$, $Re_\infty/ft = 3,300,000$.

Fig. 15 Spanwise Distributions of Aerodynamic Heating Rates; Basic Configuration, Left (Upper) Flap Deflected -40°, $\alpha = 0°$, $\beta = 0°$, $Re_{\infty}/ft = 3,300,000$.

47

Fig. 16 Streamwise Distributions of Aerodynamic Heating Rates; Basic Configuration, Right (Upper) Flap Deflected -40°, α = 0°, β = 0°, Re_∞/ft = 3,300,000.

SEE FOLLOWING PAGES OF THIS FIGURE FOR VALUES OF $\frac{Nu}{\sqrt{Re_x}} > 28$

X'	SYMBOL
0.7725	○
0.8190	□
0.8785	▷
0.9250	◇

$\frac{Nu}{\sqrt{Re_x}}$

Y'

(NONDIMENSIONAL SEMISPAN DISTANCE)

Fig. 16 Spanwise Distributions of Aerodynamic Heating Rates; Basic Configuration, Right (Upper) Flap Deflected -40°, α = 0°, β = 0°, Re/ft = 3,300,000.
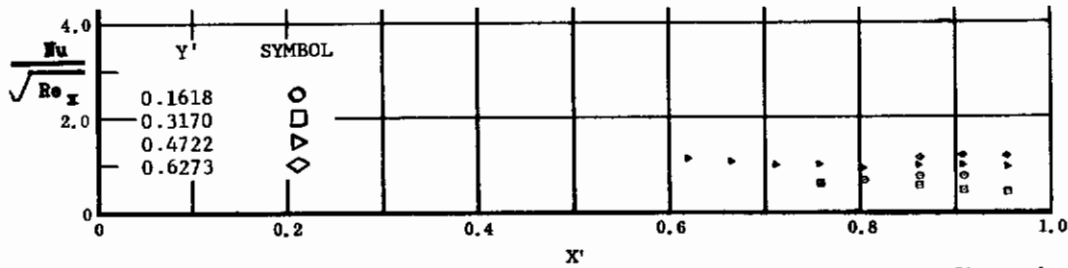
Fig. 15 Streamwise Distributions of Aerodynamic Heating Rates; Basic Configuration,
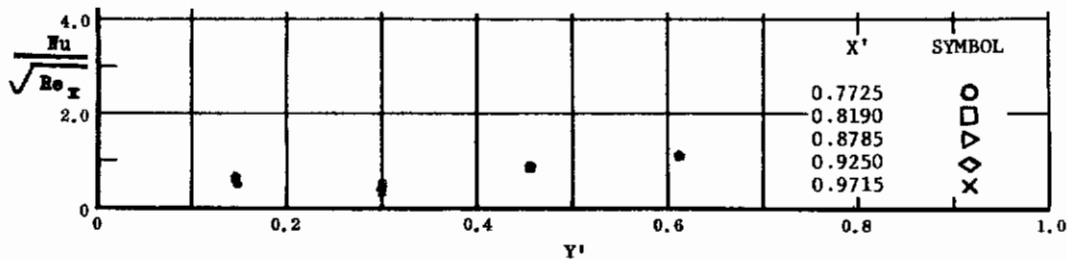Right (Upper) Flap Deflected -40°, $\alpha = 0°$, $\beta = 0°$, $Re_\infty/ft = 3,300,000$.

50

Fig. 16 Spanwise Distributions of Aerodynamic Heating Rates; Basic Configuration, Right (Upper) Flap Deflected -40°, $\alpha = 0°$, $\beta = 0°$, $Re_\infty/ft = 3,300,000$.

51
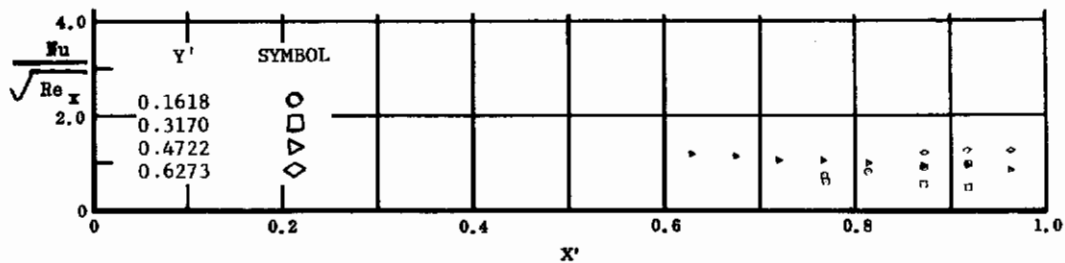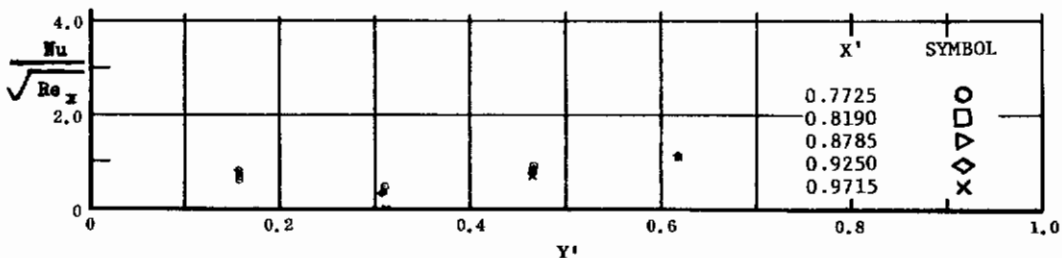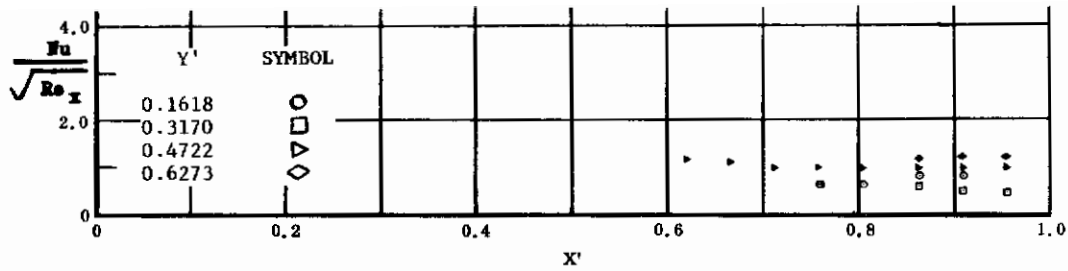
Fig. 17 Streamwise Distributions of Aerodynamic Heating Rates; Basic Configuration + Canards, Left and Right (Upper) Flaps Deflected - 40°, $\alpha = 0°$, $\beta = 0°$, $Re_\infty/ft = 3,300,000$.

52

SEE FOLLOWING PAGES OF THIS FIGURE FOR VALUES OF $\dfrac{Nu}{\sqrt{Re_x}} > 28$

X'	SYMBOL
0.7725	○
0.8190	⬚
0.8785	△
0.9250	◇

$\dfrac{Nu}{\sqrt{Re_x}}$

Y'

(NONDIMENSIONAL SEMISPAN DISTANCE)

Fig. 17 Spanwise Distributions of Aerodynamic Heating Rates; Basic Configuration
+ Canards, Left and Right (Upper) Flaps Deflected - 40°, $\alpha = 0°$, $\beta = 0°$,
$Re_\infty/ft = 3,300,000$.

53

Upper Surface

102.4 □
99.7 ◇
88.2 ▷ 89.3 □   ₵

80

70

60

50

$\dfrac{Nu}{\sqrt{Re_x}}$

Y'	SYMBOL
0.3170	□
0.4722	▷
0.6273	◇

40

30

20

SEE PRECEDING PAGES OF THIS FIGURE FOR VALUES OF $\dfrac{Nu}{\sqrt{Re_x}} < 20$

0

0   0.2   0.4   0.6   0.8   1.0

X'

(NONDIMENSIONAL STREAMWISE DISTANCE FROM VIRTUAL APEX)

Fig. 17 Streamwise Distributions of Aerodynamic Heating Rates; Basic Configuration + Canards, Left and Right (Upper) Flaps Deflected -40°, $\alpha = 0°$, $\beta = 0°$, $Re_\infty/ft = 3,300,000$.

54

Fig. 17 Spanwise Distributions of Aerodynamic Heating Rates; Basic Configuration
+ Canards, Left and Right (Upper) Flaps Deflected -40°, $\alpha = 0°$, $\beta = 0°$,
$Re_\infty/ft = 3,300,000$.

55

Fig. 18 Streamwise Distributions of Aerodynamic Heating Rates; Basic Configuration, Left and Right (Upper) Flaps Deflected -30°, $\alpha = 0°$, $\beta = 0°$, $Re_\infty/ft = 3,300,000$.

Fig. 18 Spanwise Distributions of Aerodynamic Heating Rates; Basic Configuration, Left and Right (upper) Flaps Deflected -30°, $\alpha = 0°$, $\beta = 0°$, $Re_\infty/ft = 3,300,000$.

57

Upper Surface
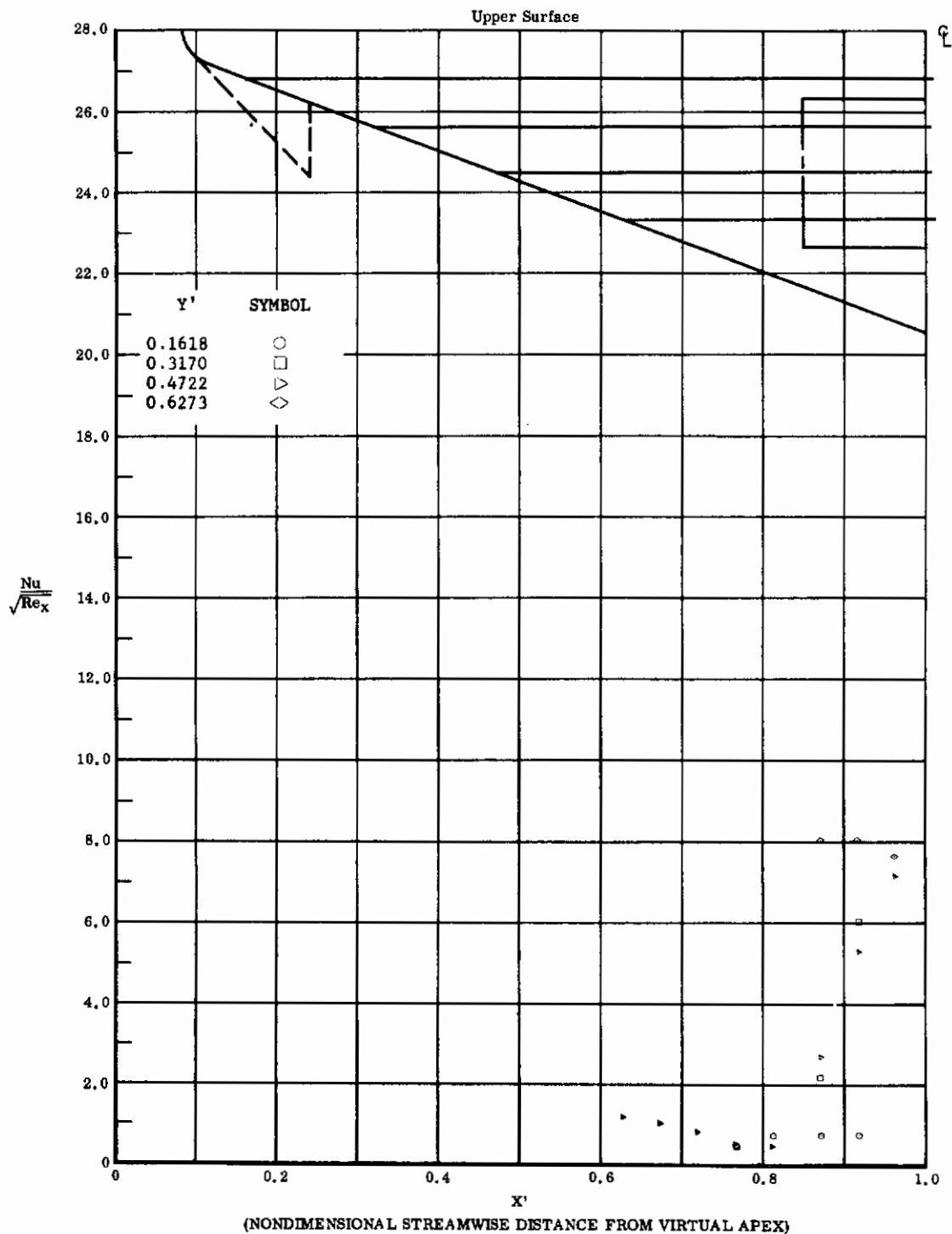
Fig. 19 Streamwise Distributions of Aerodynamic Heating Rates; Basic Configuration,
Left and Right (Upper) Flaps Deflected -20°, $\alpha = 0°$, $\beta = 0°$,
$Re_\infty/ft = 1,100,000$.

58
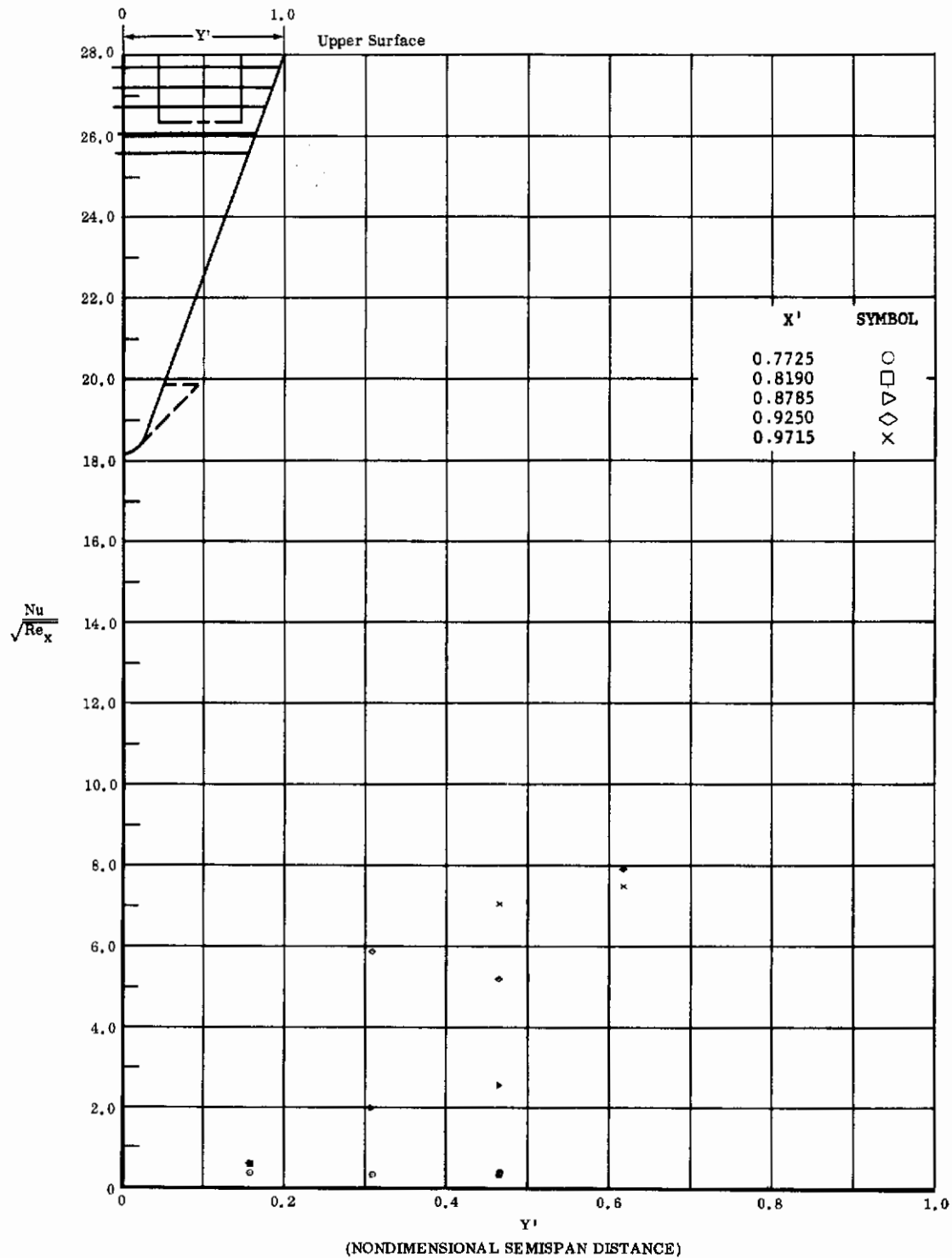
Fig. 19 Spanwise Distributions of Aerodynamic Heating Rates; Basic Configuration, Left and Right (Upper) Flaps Deflected -20°, $\alpha = 0°$, $\beta = 0°$, $Re_\infty/ft = 1,100,000.$

59
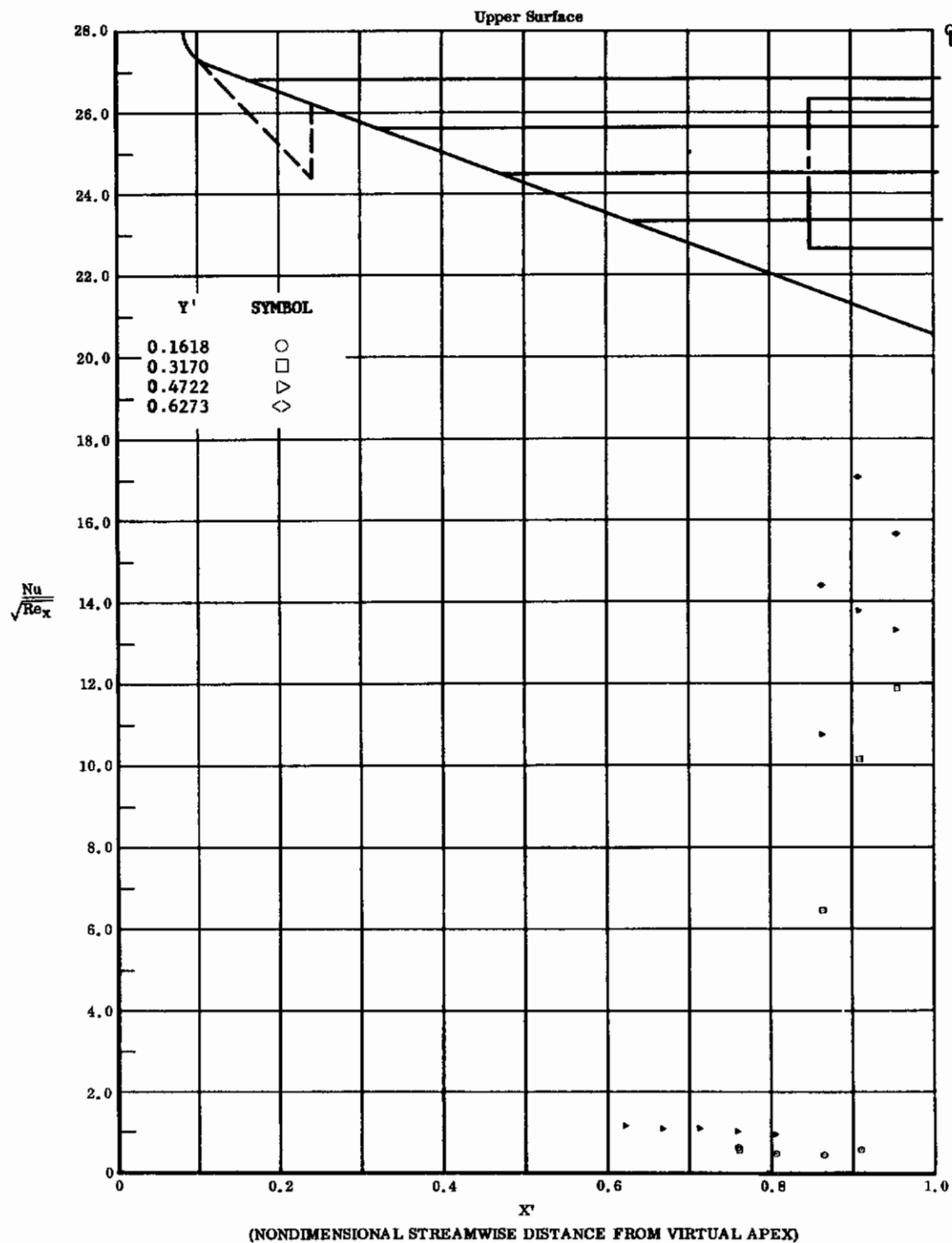
Fig. 20 Streamwise Distributions of Aerodynamic Heating Rates; Basic Configuration, Left and Right (Upper) Flaps Deflected -20°, $\alpha = 0°$, $\beta = 0°$, $Re_\infty/ft = 3,300,000$.

Fig. 20 Spanwise Distributions of Aerodynamic Heating Rates; Basic Configuration, Left and Right (Upper) Flaps Deflected -20°, $\alpha = 0°$, $\beta = 0°$, $Re_\infty/ft = 3,300,000.$

61

Upper Surface

Fig. 21 Streamwise Distributions of Aerodynamic Heating Rates; Basic Configuration, Left (Upper) Flap Deflected -20°, $\alpha = 0°$, $\beta = 0°$, $Re_\infty/ft = 3,300,000$.

62

Fig. 21   Spanwise Distributions of Aerodynamic Heating Rates; Basic Configuration, Left (Upper) Flap Deflected -20°, $\alpha = 0°$, $\beta = 0°$, $Re_\infty/ft = 3,300,000$.

The legend in the figure:

X'	SYMBOL
0.7725	◠
0.8190	□
0.8785	▷
0.9250	◇
0.9715	×

Axis labels: $\frac{Nu}{\sqrt{Re_x}}$ (vertical), Y' (NONDIMENSIONAL SEMISPAN DISTANCE) (horizontal), Upper Surface.

Fig. 22 Streamwise Distributions of Aerodynamic Heating Rates; Basic Configuration, Right (Upper) Flap Deflected -20°, $\alpha = 0°$, $\beta = 0°$, Re_∞/ft = 3,300,000.

64

Fig. 22   Spanwise Distributions of Aerodynamic Heating Rates; Basic Configuration, Right (Upper) Flap Deflected -20°, α = 0°, β = 0°, Re∞/ft = 3,300,000.

65

Upper Surface

Fig. 23 Streamwise Distributions of Aerodynamic Heating Rates; Basic Configuration
+ Canards, Left and Right (Upper) Flaps Deflected -20°, α = 0°, β = 0°,
Re∞/ft = 3,300,000.

66

Fig. 23 Spanwise Distributions of Aerodynamic Heating Rates; Basic Configuration
+ Canards, Left and Right (Upper) Flaps Deflected -20°, $\alpha = 0°$, $\beta = 0°$,
$Re_\infty/ft = 3,300,000$.

67

Fig. 24 Streamwise Distributions of Aerodynamic Heating Rates; Basic Configuration,
Left and Right (Upper) Flaps Deflected -10°, $\alpha = 0°$, $\beta = 0°$,
$Re_\infty/ft = 3,300,000$.
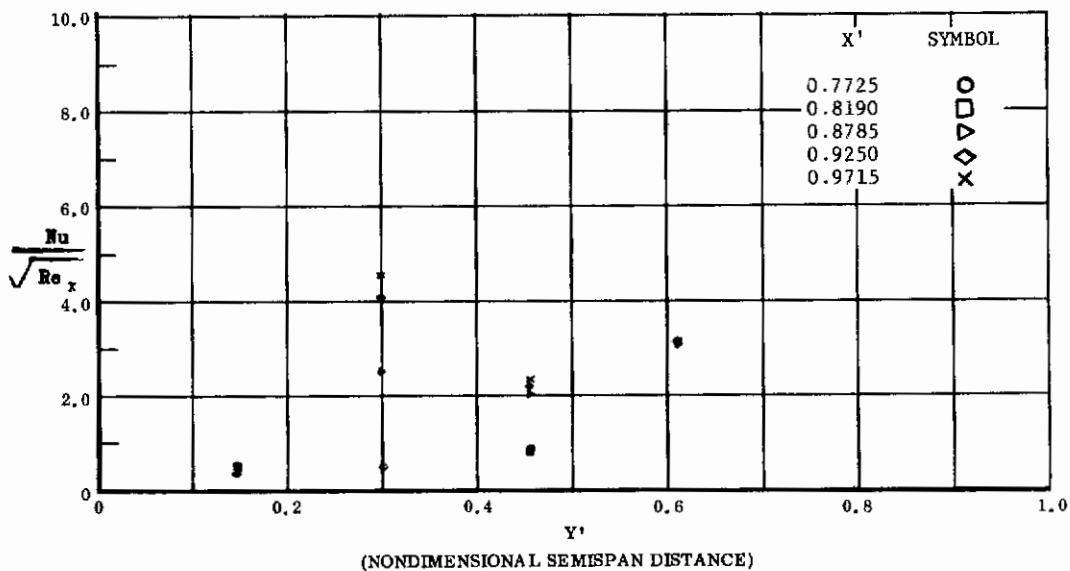
Fig. 24 Spanwise Distributions of Aerodynamic Heating Rates; Basic Configuration,
Left and Right (Upper) Flaps Deflected -10°, $\alpha = 0°$, $\beta = 0°$,
$Re_\infty/ft = 3,300,000$.

68
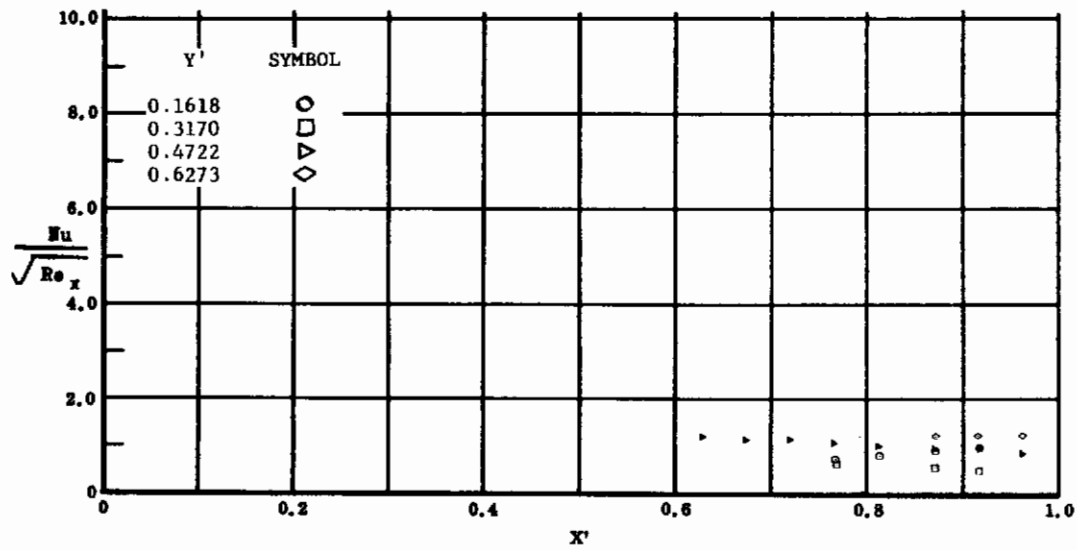
Fig. 25 Streamwise Distributions of Aerodynamic Heating Rates; Basic Configuration, No Flap Deflections, $\alpha = 0°$, $\beta = 0°$, $Re_\infty/ft = 1,100,000$.
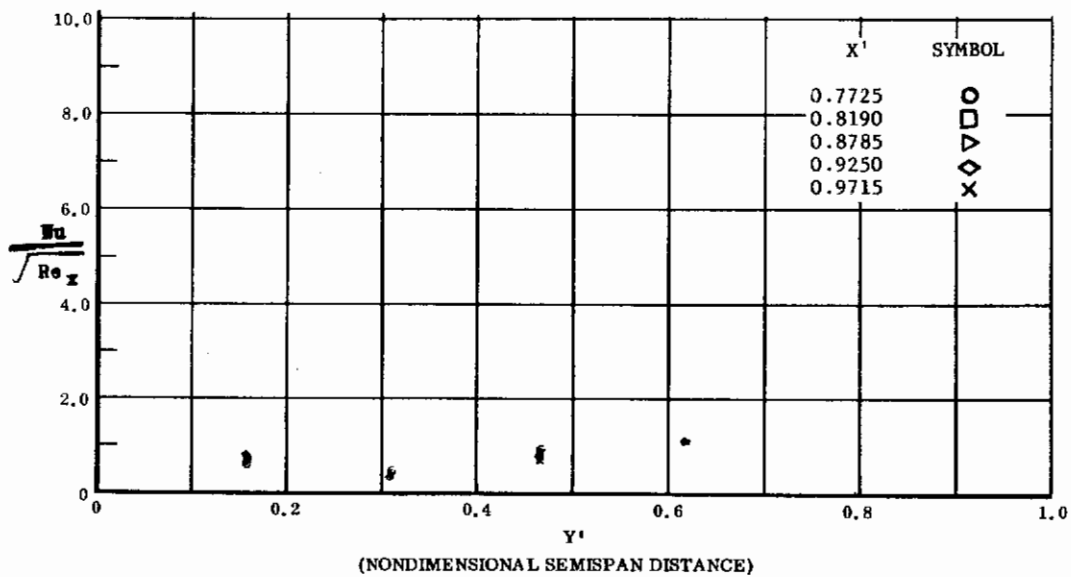
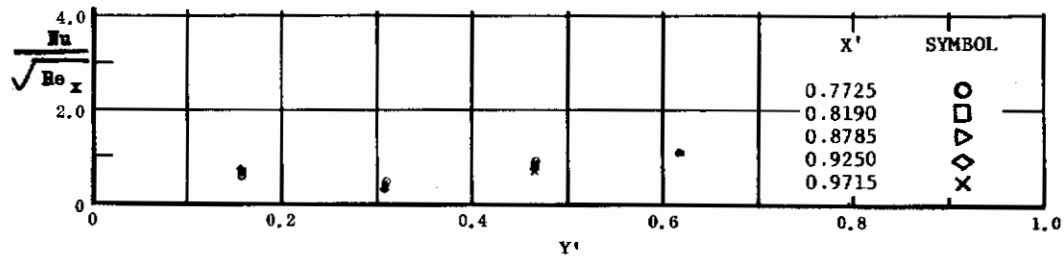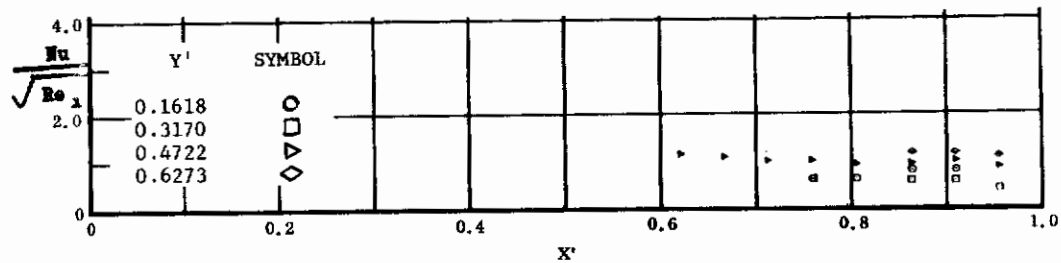Fig. 25 Spanwise Distributions of Aerodynamic Heating Rates; Basic Configuration, No Flap Deflections, $\alpha = 0°$, $\beta = 0°$, $Re_\infty/ft = 1,100,000$.

69
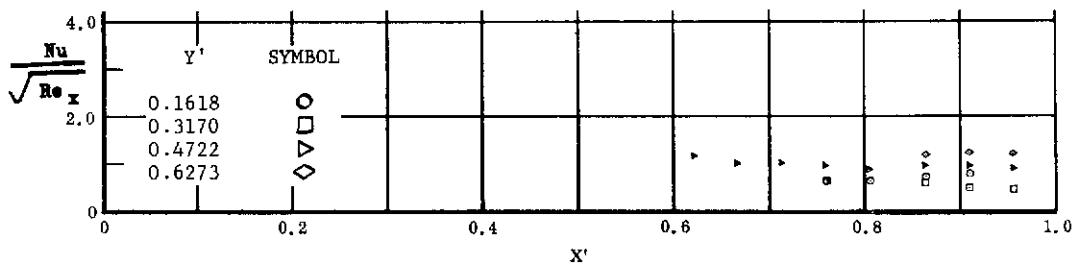
Fig. 26   Streamwise Distributions of Aerodynamic Heating Rates; Basic Configuration, No Flap Deflections, $\alpha = 0°$, $\beta = 0°$, $Re_\infty/ft = 3,300,000$.
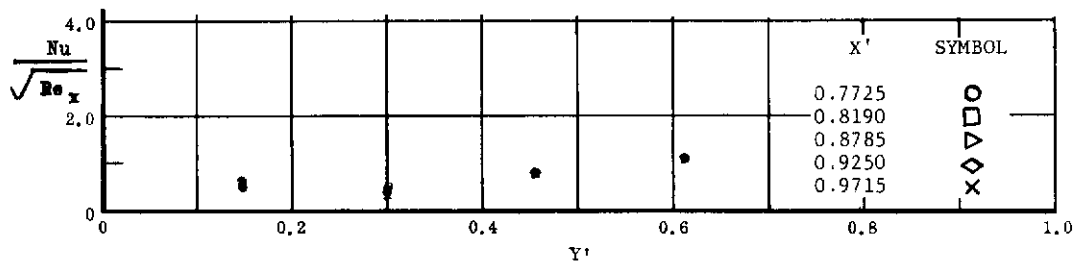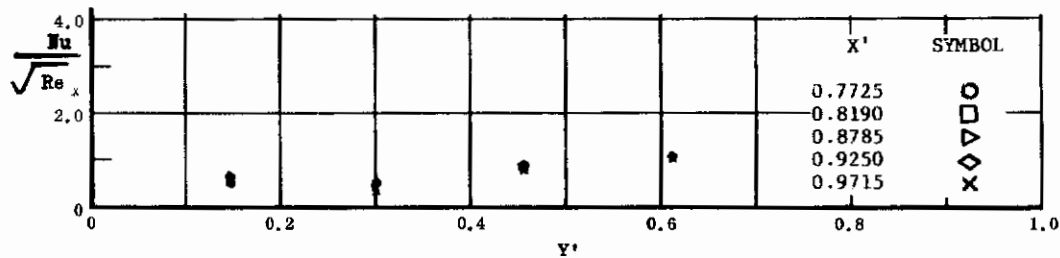

Fig. 26   Spanwise Distributions of Aerodynamic Heating Rates; Basic Configuration, No Flap Deflections, $\alpha = 0°$, $\beta = 0°$, $Re_\infty/ft = 3,300,000$.
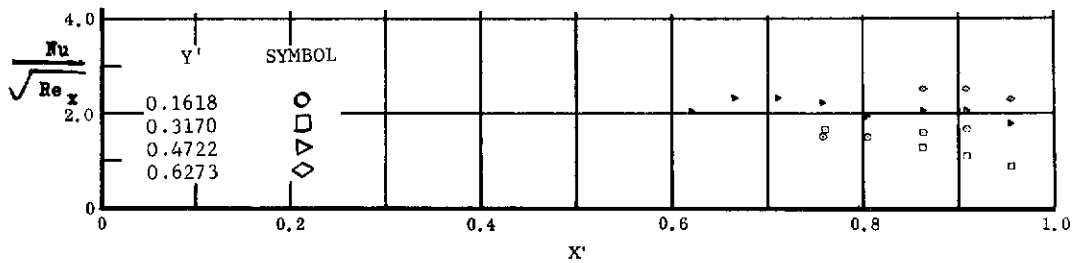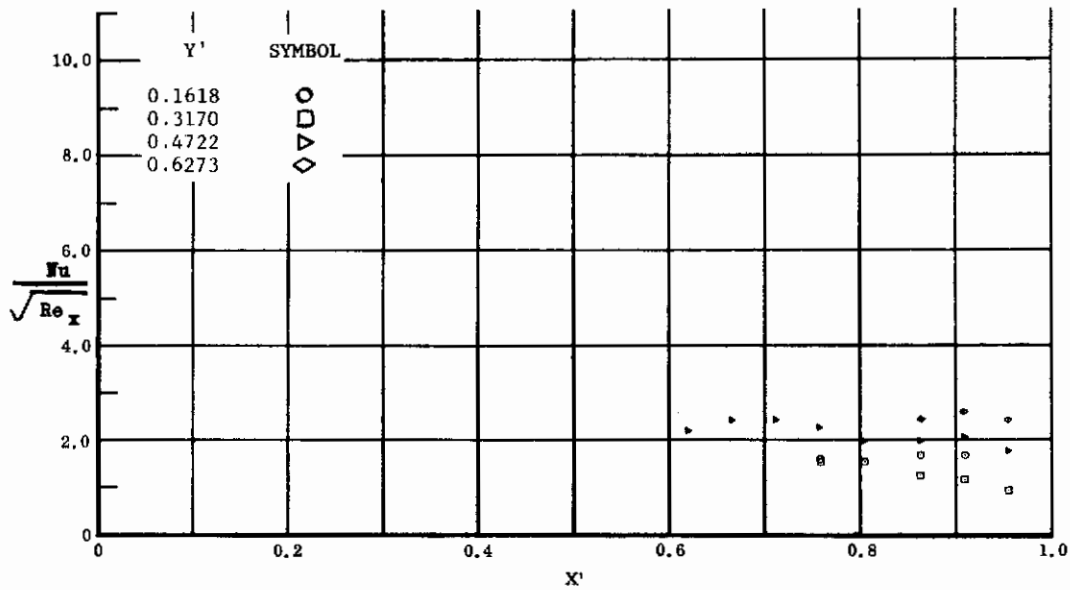

Fig. 27   Streamwise Distributions of Aerodynamic Heating Rates; Basic Configuration + Canards, No Flap Deflections, $\alpha = 0°$, $\beta = 0°$, $Re_\infty/ft = 3,300,000$.
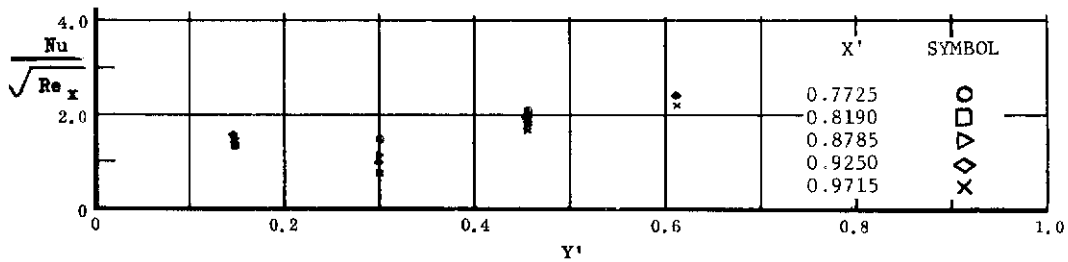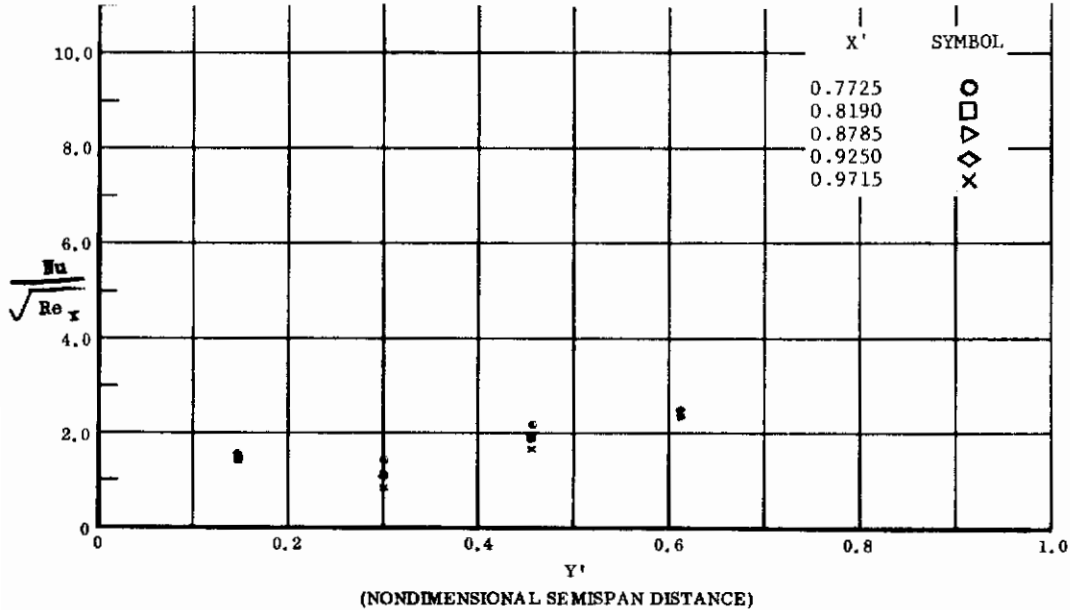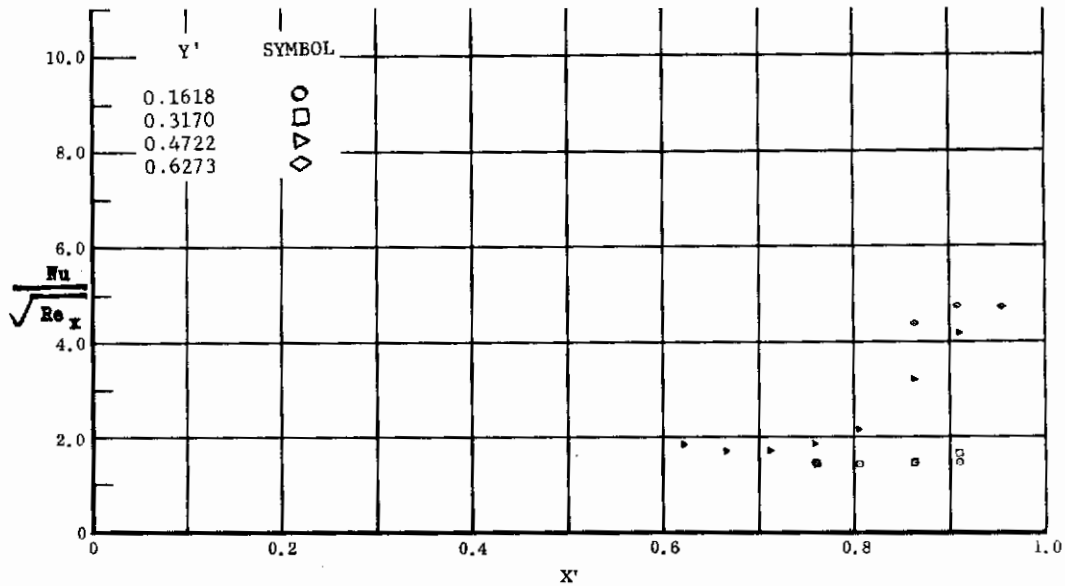

Fig. 27   Spanwise Distributions of Aerodynamic Heating Rates; Basic Configuration + Canards, No Flap Deflections, $\alpha = 0°$, $\beta = 0°$, $Re_\infty/ft = 3,300,000$.

70
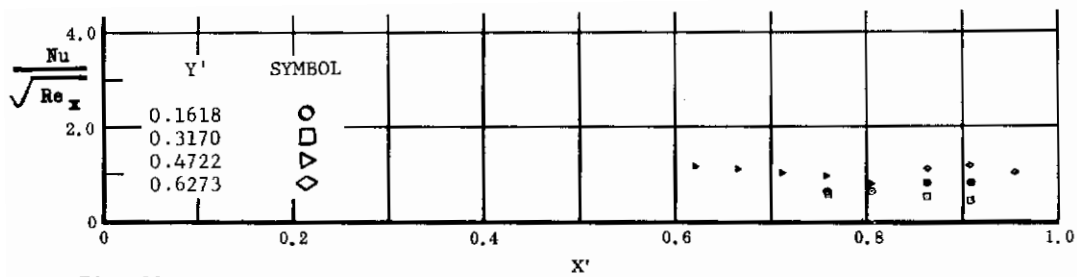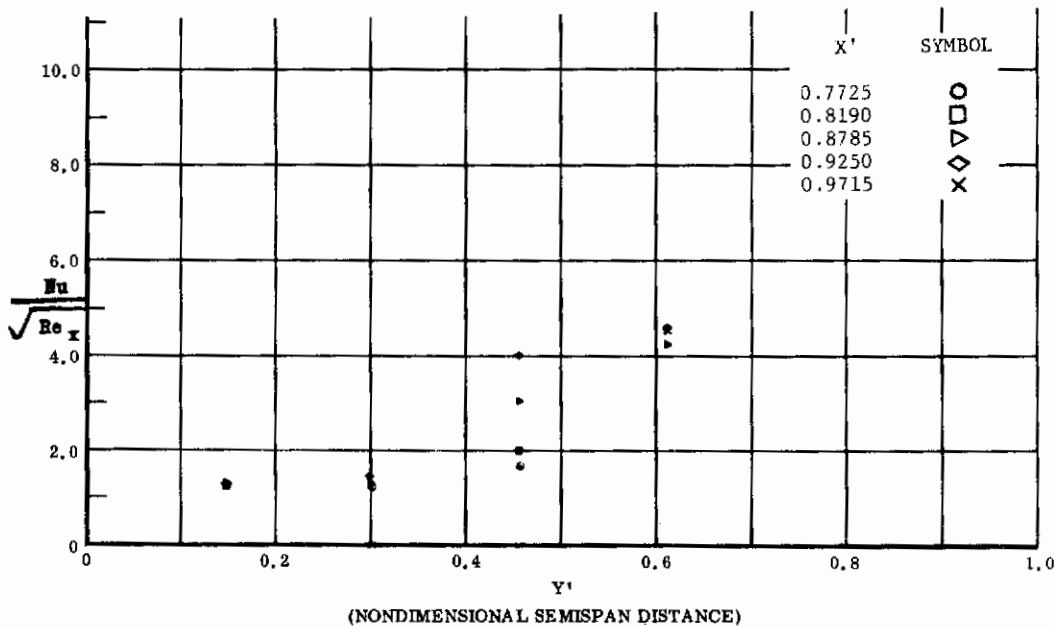
Fig. 28 Streamwise Distributions of Aerodynamic Heating Rates; Basic Configuration + Fin ($\delta = 0$), No Flap Deflections, $\alpha = 0°$, $\beta = 0°$, $Re_\infty/ft = 3,300,000$.
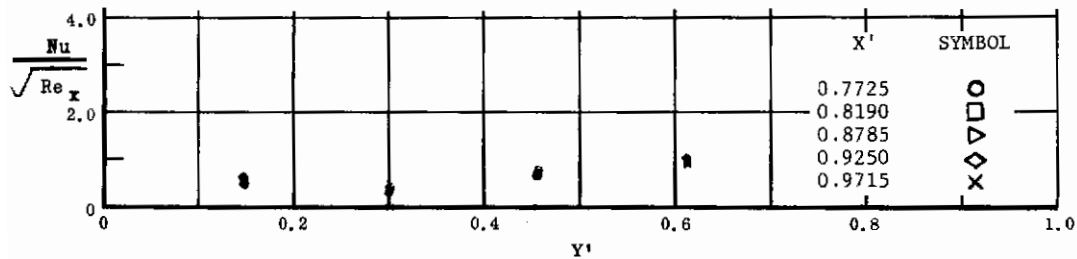
Fig. 28 Spanwise Distributions of Aerodynamic Heating Rates; Basic Configuration + Fin ($\delta = 0$), No Flap Deflections, $\alpha = 0°$, $\beta = 0°$, $Re_\infty/ft = 3,300,000$.
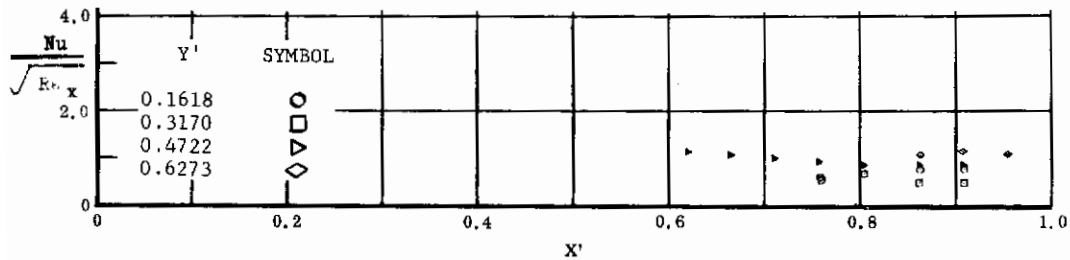
Fig. 29 Streamwise Distributions of Aerodynamic Heating Rates; Basic Configuration + Fin ($\delta = 15°$), No Flap Deflections, $\alpha = 0°$, $\beta = 0°$, $Re_\infty/ft = 3,300,000$.
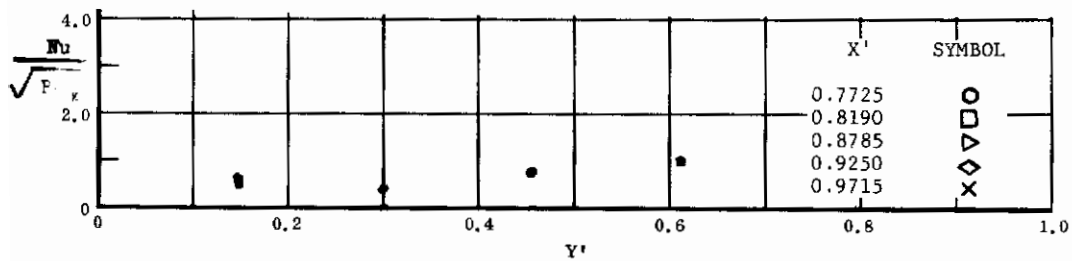
Fig. 29 Spanwise Distributions of Aerodynamic Heating Rates; Basic Configuration + Fin ($\delta = 15°$), No Flap Deflections, $\alpha = 0°$, $\beta = 0°$, $Re_\infty/ft = 3,300,000$.
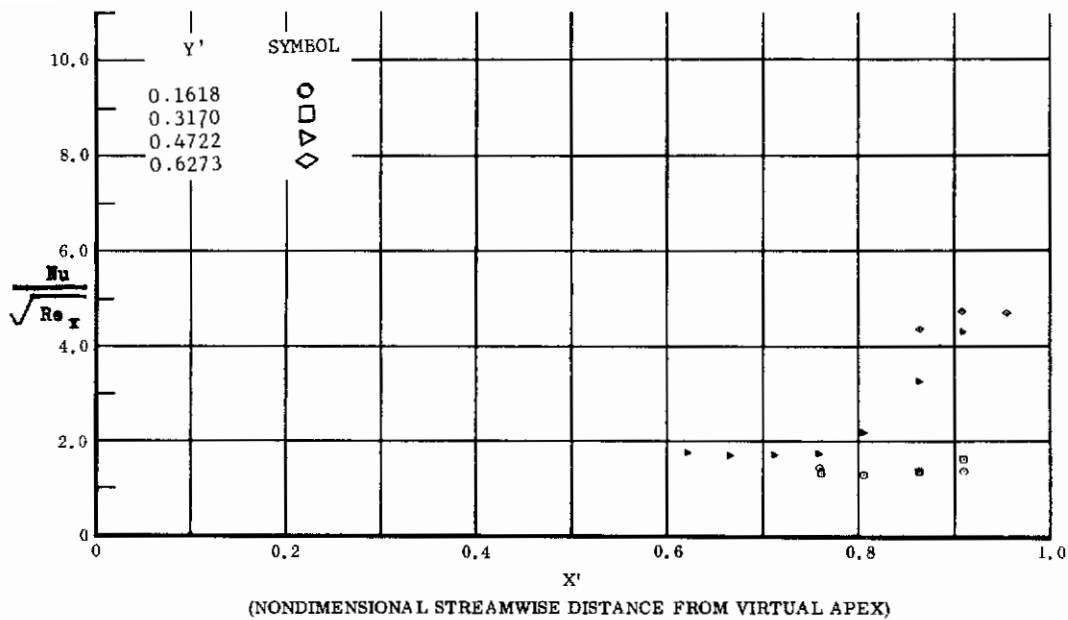
Fig. 30 Streamwise Distributions of Aerodynamic Heating Rates; Basic Configuration, Bottom Flaps Deflected +10°, $\alpha = 0°$, $\beta = 0°$, Re_∞/ft = 3,300,000.
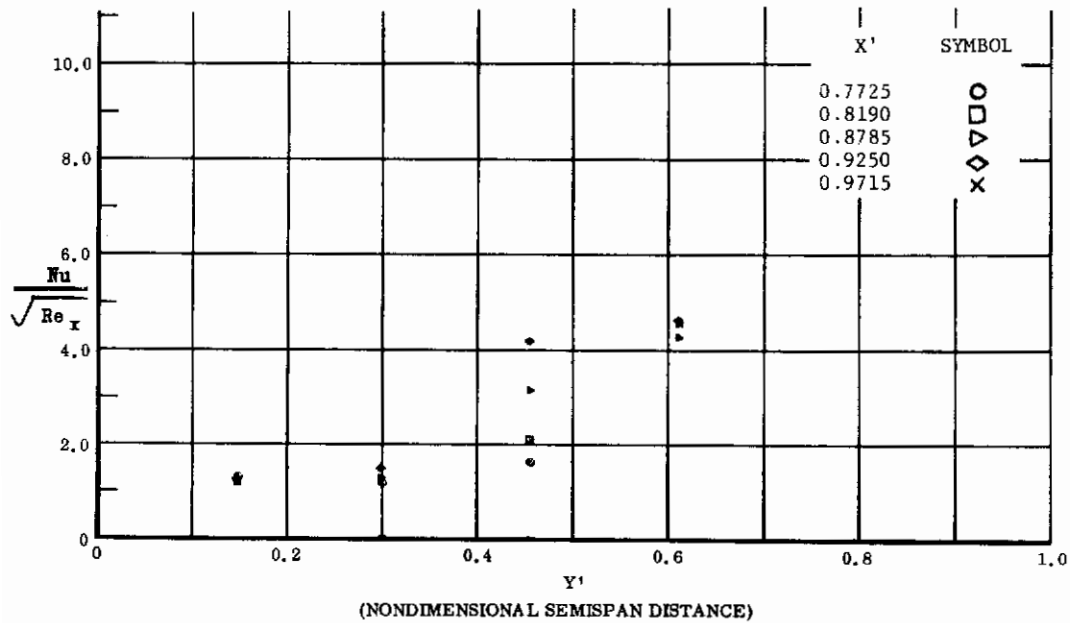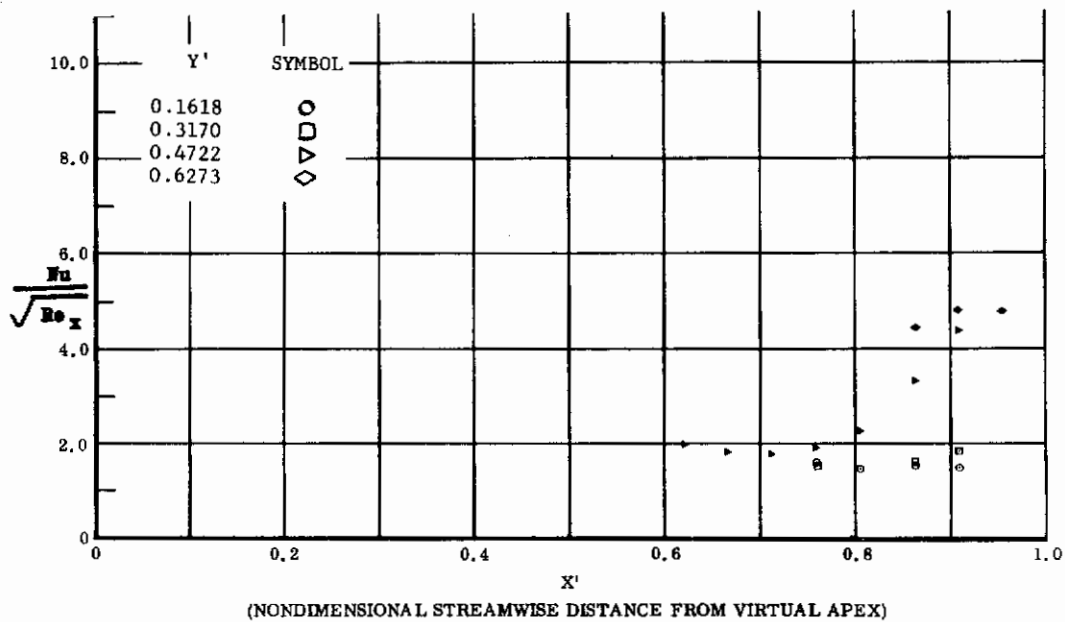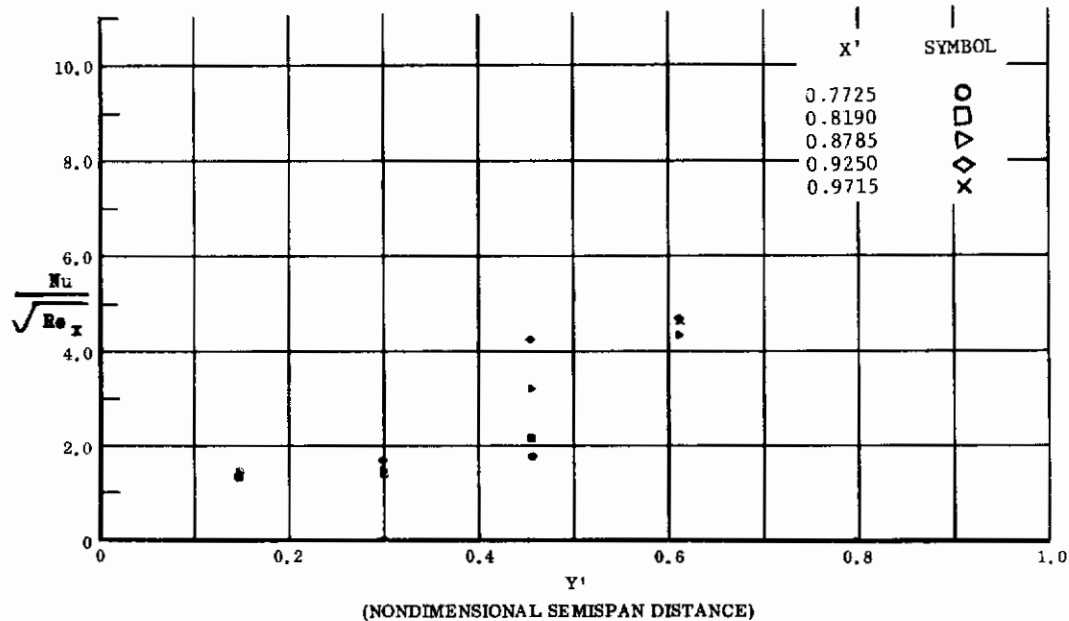
Fig. 30 Spanwise Distributions of Aerodynamic Heating Rates; Basic Configuration, Bottom Flaps Deflected +10°, $\alpha = 0°$, $\beta = 0°$, Re_∞/ft = 3,300,000.

Fig. 31 Streamwise Distributions of Aerodynamic Heating Rates; Basic Configuration, Bottom Flaps Deflected +20°, $\alpha = 0°$, $\beta = 0°$, Re_∞/ft = 1,100,000.

Fig. 31 Spanwise Distributions of Aerodynamic Heating Rates; Basic Configuration, Bottom Flaps Deflected +20°, $\alpha = 0°$, $\beta = 0°$, Re_∞/ft = 1,100,000.

72

Fig. 32 Streamwise Distributions of Aerodynamic Heating Rates; Basic Configuration, Bottom Flaps Deflected +20°, $\alpha = 0°$, $\beta = 0°$, $Re_\infty/ft = 3,300,000$.
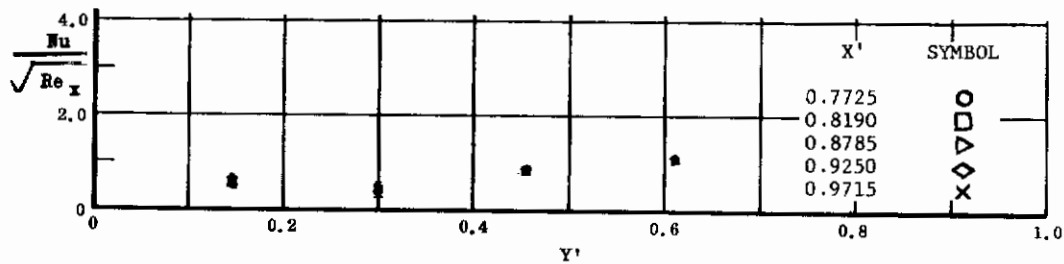
Fig. 32 Spanwise Distributions of Aerodynamic Heating Rates; Basic Configuration, Bottom Flaps Deflected +20°, $\alpha = 0°$, $\beta = 0°$, $Re_\infty/ft = 3,300,000$.
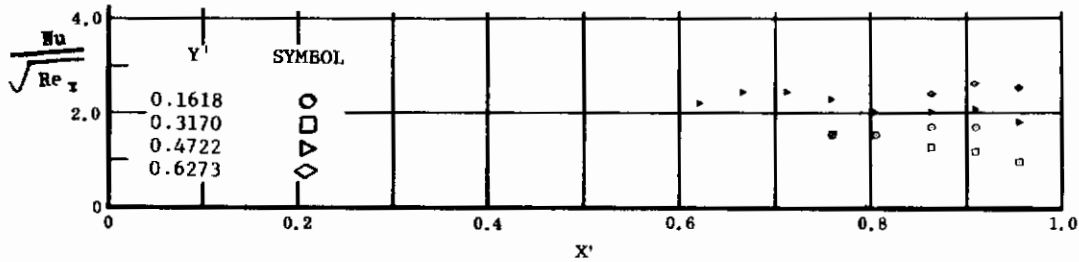
Fig. 33 Streamwise Distributions of Aerodynamic Heating Rates; Basic Configuration + Canards, Bottom Flaps Deflected +20°, $\alpha = 0°$, $\beta = 0°$, $Re_\infty/ft = 3,300,000$.
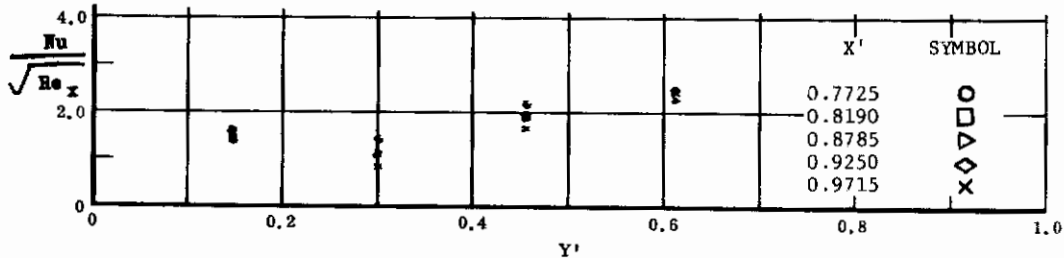
Fig. 33 Spanwise Distributions of Aerodynamic Heating Rates; Basic Configuration + Canards, Bottom Flaps Deflected +20°, $\alpha = 0°$, $\beta = 0°$, $Re_\infty/ft = 3,300,000$.

73
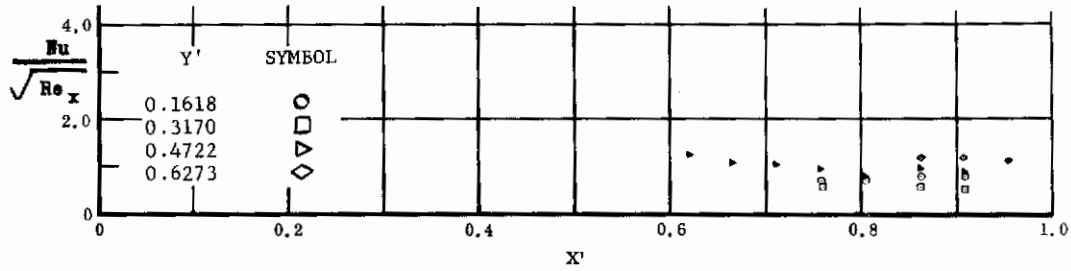
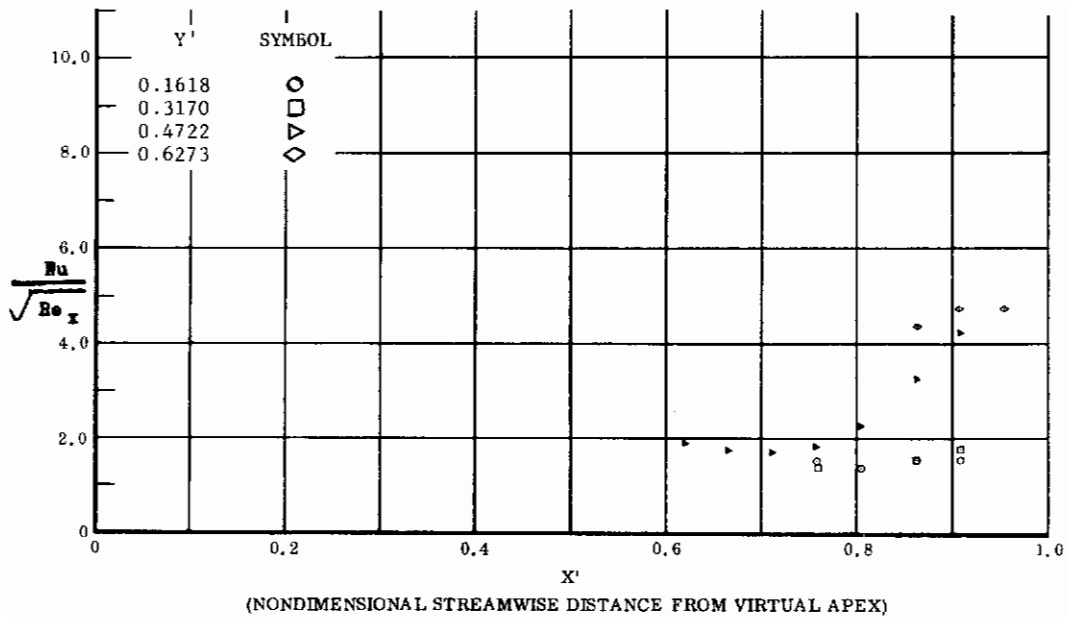Fig. 34 Streamwise Distributions of Aerodynamic Heating Rates; Basic Configuration + Fin ($\delta = 0$), Bottom Flaps Deflected +20°, $\alpha = 0°$, $\beta = 0°$, $Re_\infty/ft = 3,300,000$.
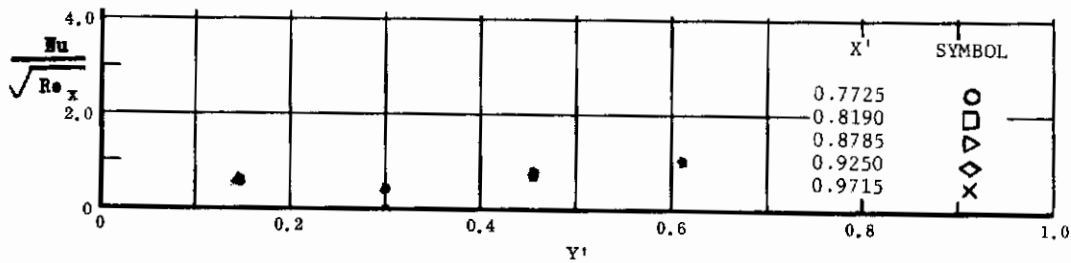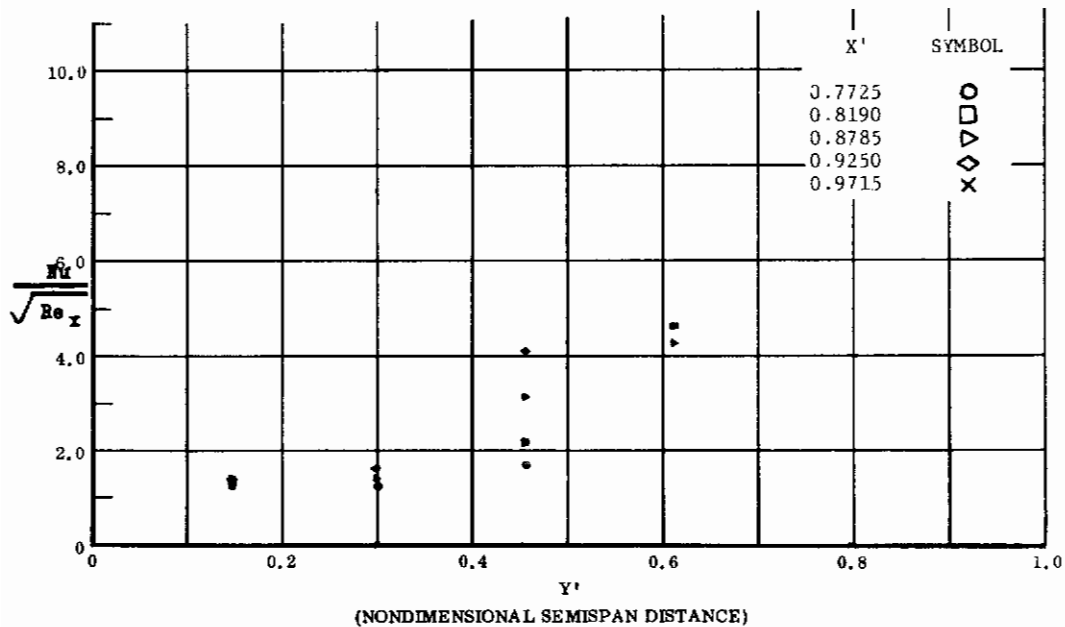

Fig. 34 Spanwise Distributions of Aerodynamic Heating Rates; Basic Configuration + Fin ($\delta = 0$), Bottom Flaps Deflected +20°, $\alpha = 0°$, $\beta = 0°$, $Re_\infty/ft = 3,300,000$.
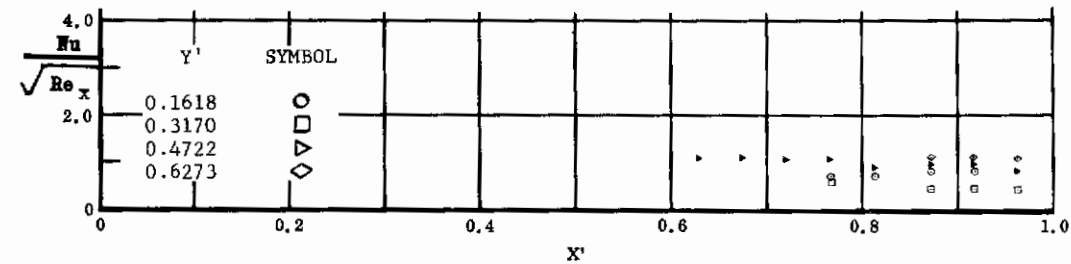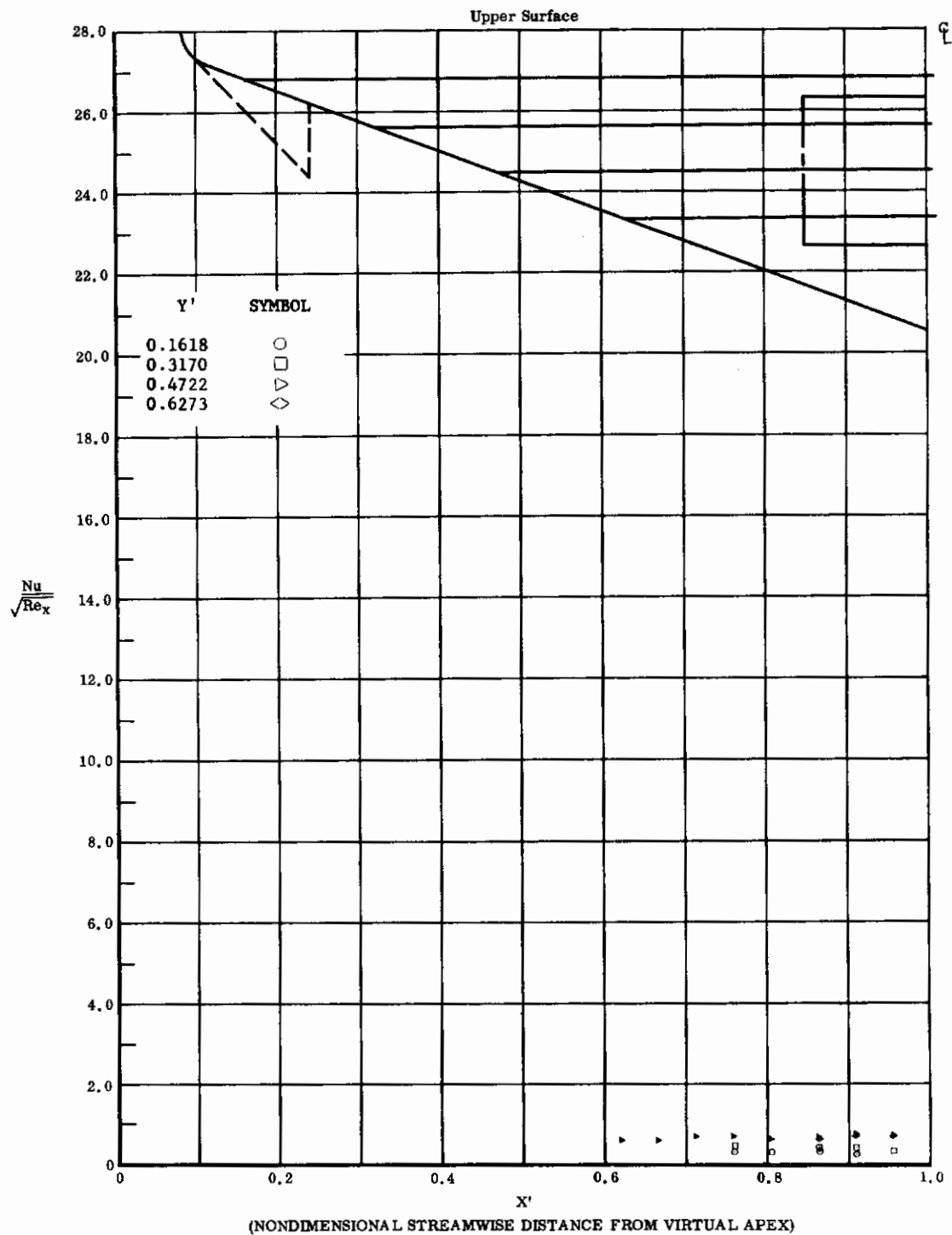

Fig. 35 Streamwise Distributions of Aerodynamic Heating Rates; Basic Configuration + Longer Chord Flaps, Bottom Flaps Deflected +20°, $\alpha = 0°$, $\beta = 0°$, $Re_\infty/ft = 1,100,000$.
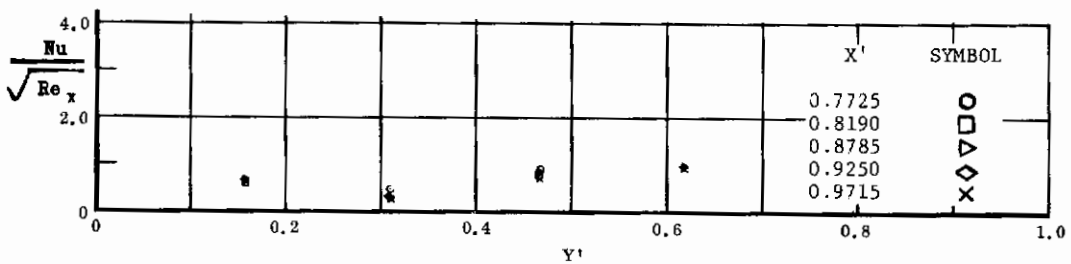
Fig. 35 Spanwise Distributions of Aerodynamic Heating Rates; Basic Configuration + Longer Chord Flaps, Bottom Flaps Deflected +20°, $\alpha = 0°$, $\beta = 0°$, $Re_\infty/ft = 1,100,000$.
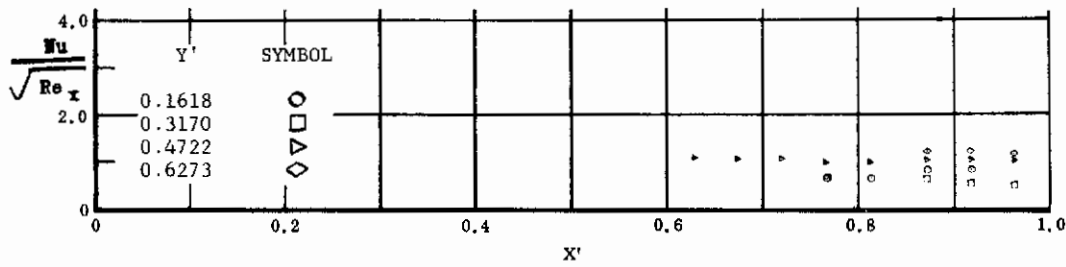
Fig. 36 Streamwise Distributions of Aerodynamic Heating Rates; Basic Configuration + Longer Chord Flaps, Bottom Flaps Deflected +20°, $\alpha = 0°$, $\beta = 0°$, $Re_\infty/ft = 3,300,000$.
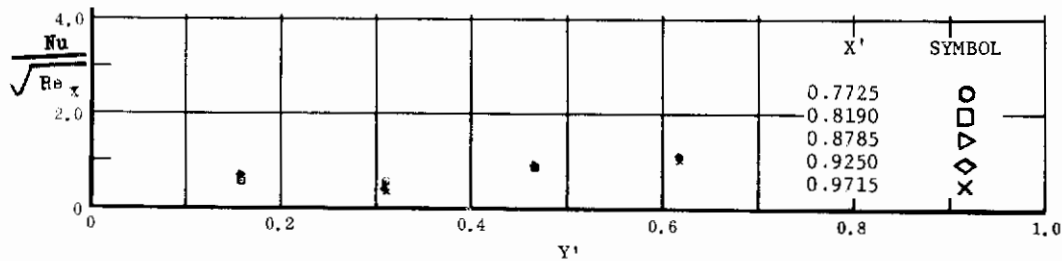
Fig. 36 Spanwise Distributions of Aerodynamic Heating Rates; Basic Configuration + Longer Chord Flaps, Bottom Flaps Deflected +20°, $\alpha = 0°$, $\beta = 0°$, $Re_\infty/ft = 3,300,000$.
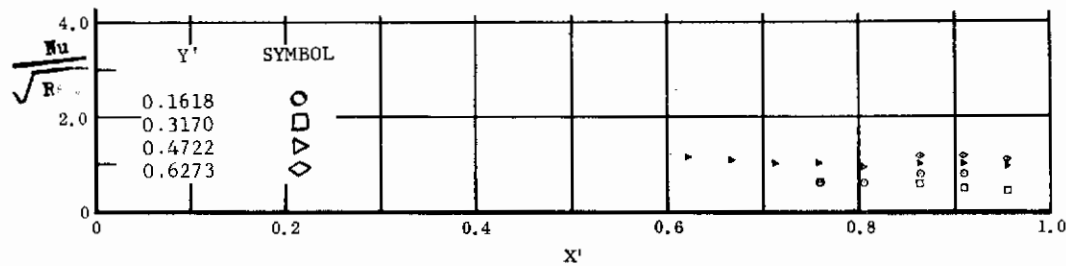
Fig. 37 Streamwise Distributions of Aerodynamic Heating Rates; Basic Configuration, Bottom Flaps Deflected +30°, $\alpha = 0°$, $\beta = 0°$, $Re_\infty/ft = 3,300,000$.
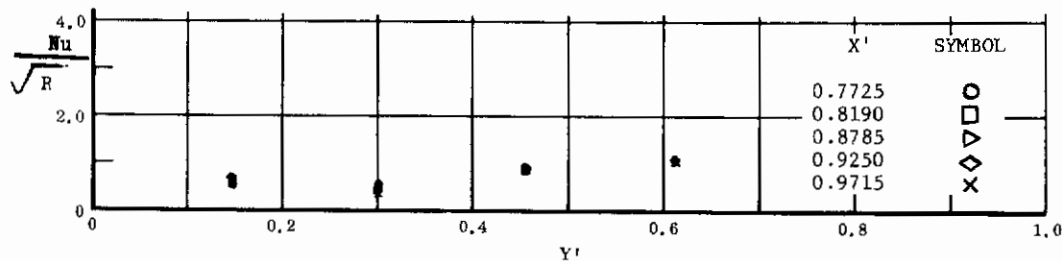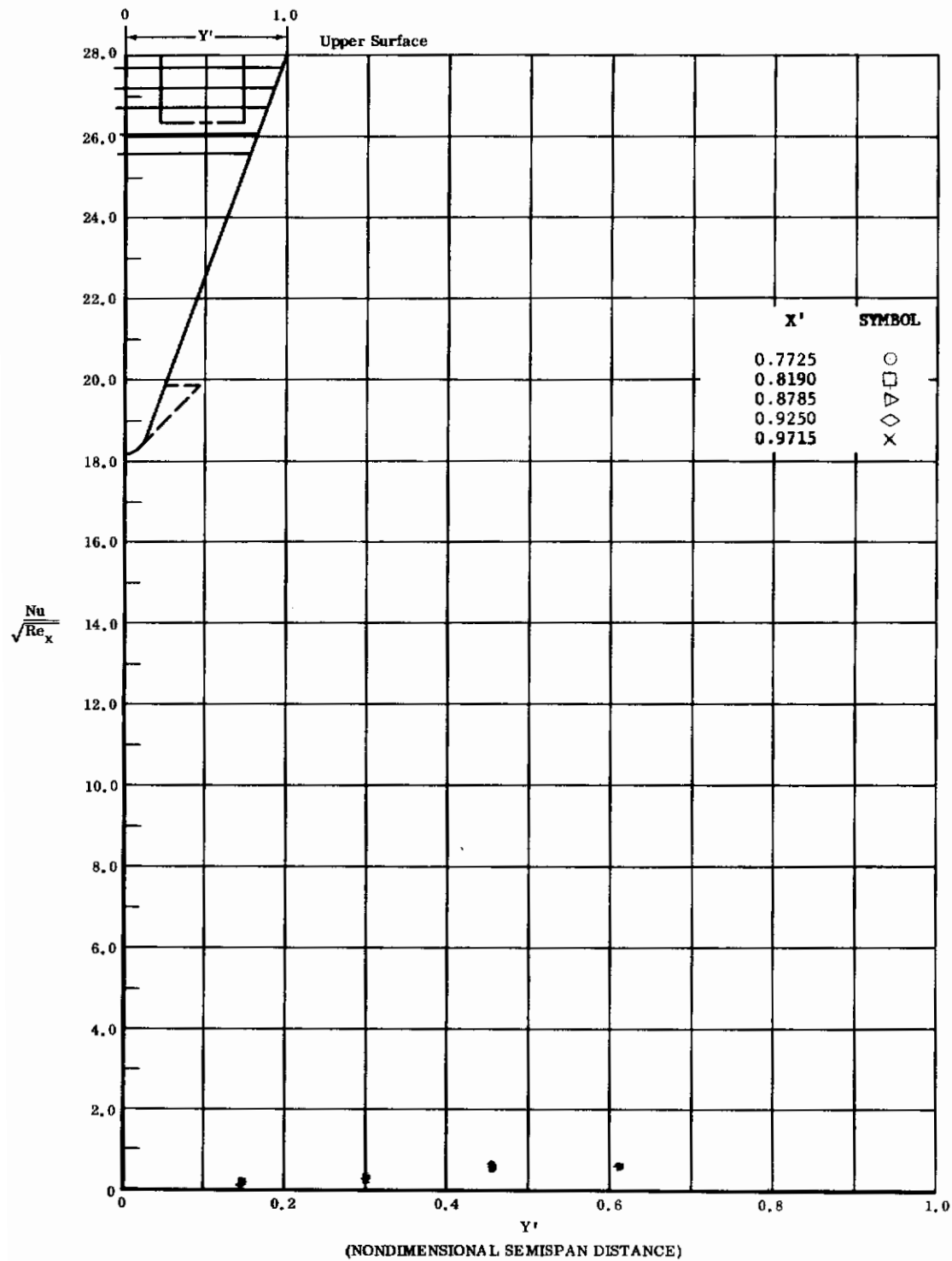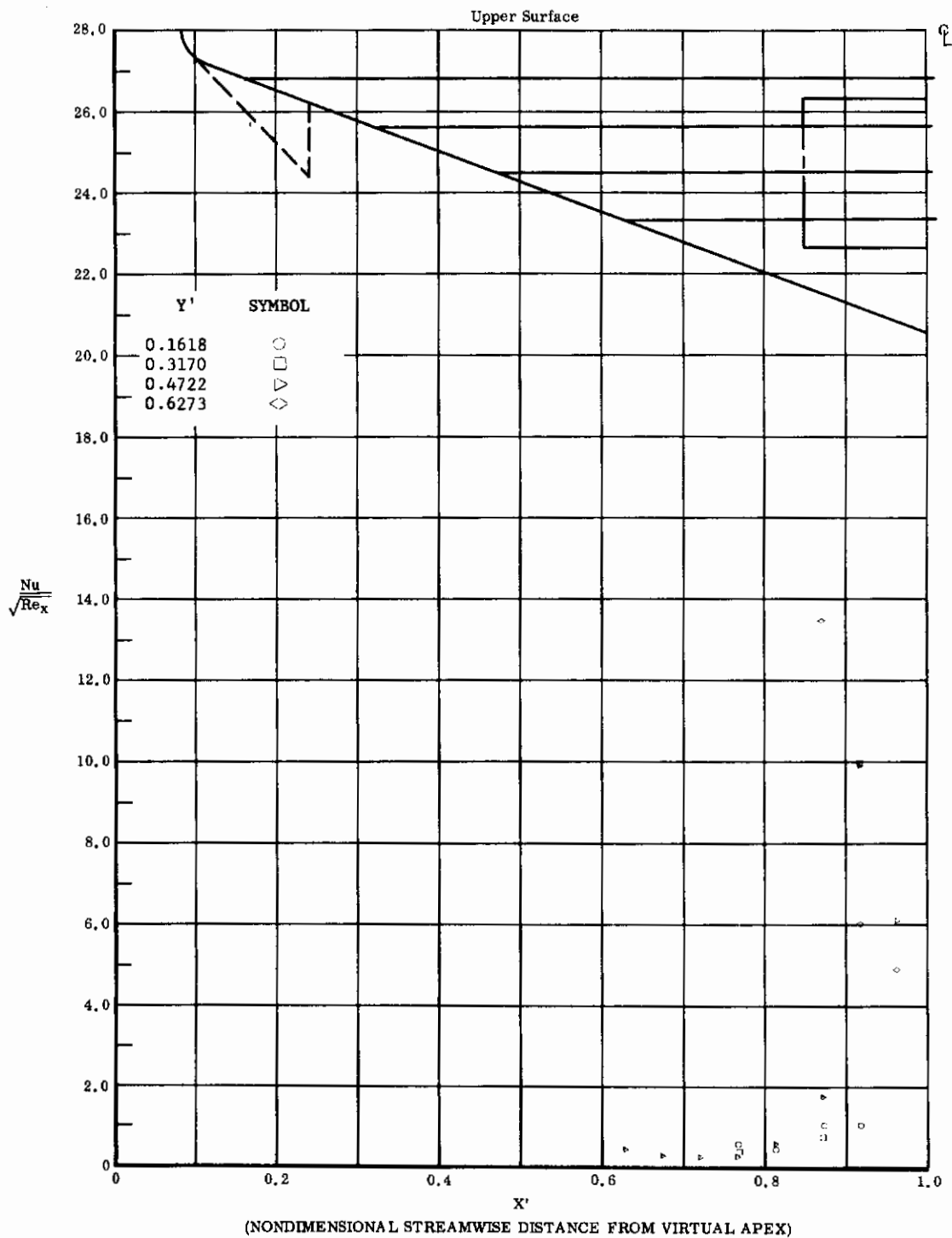

Fig. 37 Spanwise Distributions of Aerodynamic Heating Rates; Basic Configuration, Bottom Flaps Deflected +30°, $\alpha = 0°$, $\beta = 0°$, $Re_\infty/ft = 3,300,000$.

75
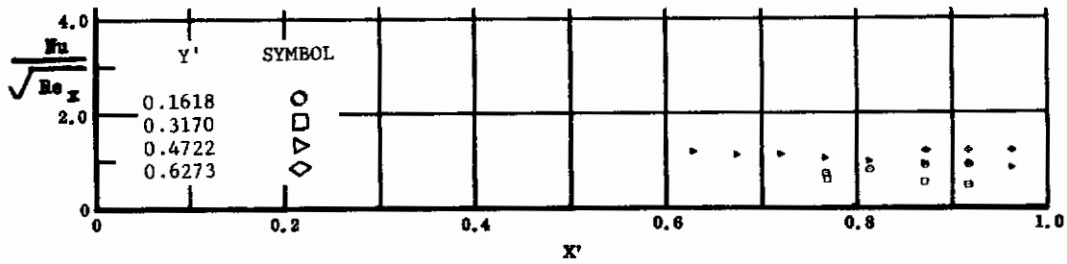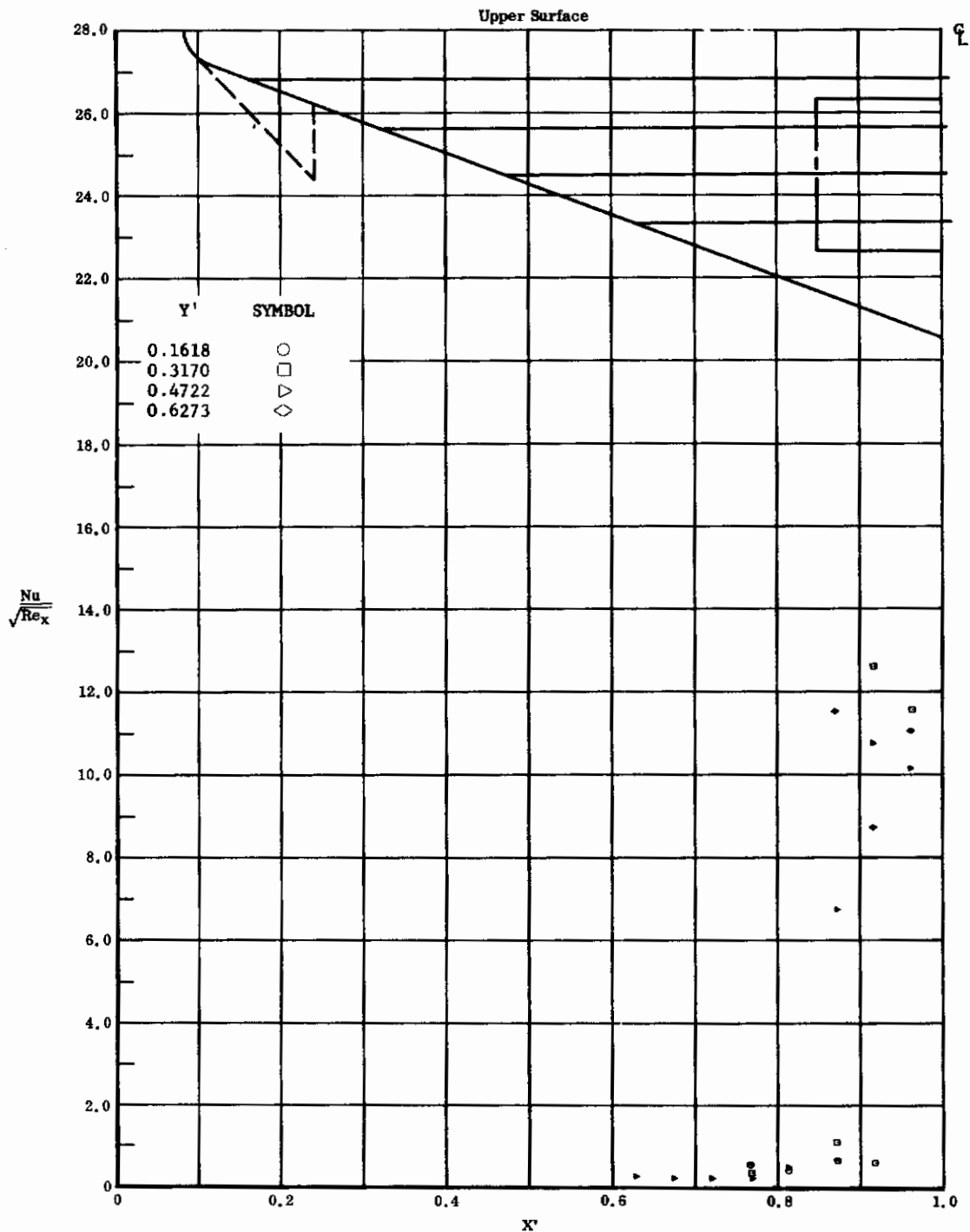
Fig. 38   Streamwise Distributions of Aerodynamic Heating Rates; Basic Configuration, Bottom Flaps Deflected +40°, $\alpha = 0°$, $\beta = 0°$, $Re_\infty/ft = 1,100,000$.

Fig. 38   Spanwise Distributions of Aerodynamic Heating Rates; Basic Configuration, Bottom Flaps Deflected +40°, $\alpha = 0°$, $\beta = 0°$, $Re_\infty/ft = 1,100,000$.

Fig. 39   Streamwise Distributions of Aerodynamic Heating Rates; Basic Configuration, Bottom Flaps Deflected +40°, $\alpha = 0°$, $\beta = 0°$, $Re_\infty/ft = 3,300,000$.

Fig. 39   Spanwise Distributions of Aerodynamic Heating Rates; Basic Configuration, Bottom Flaps Deflected +40°, $\alpha = 0$, $\beta = 0°$, $Re_\infty/ft = 3,300,000$.

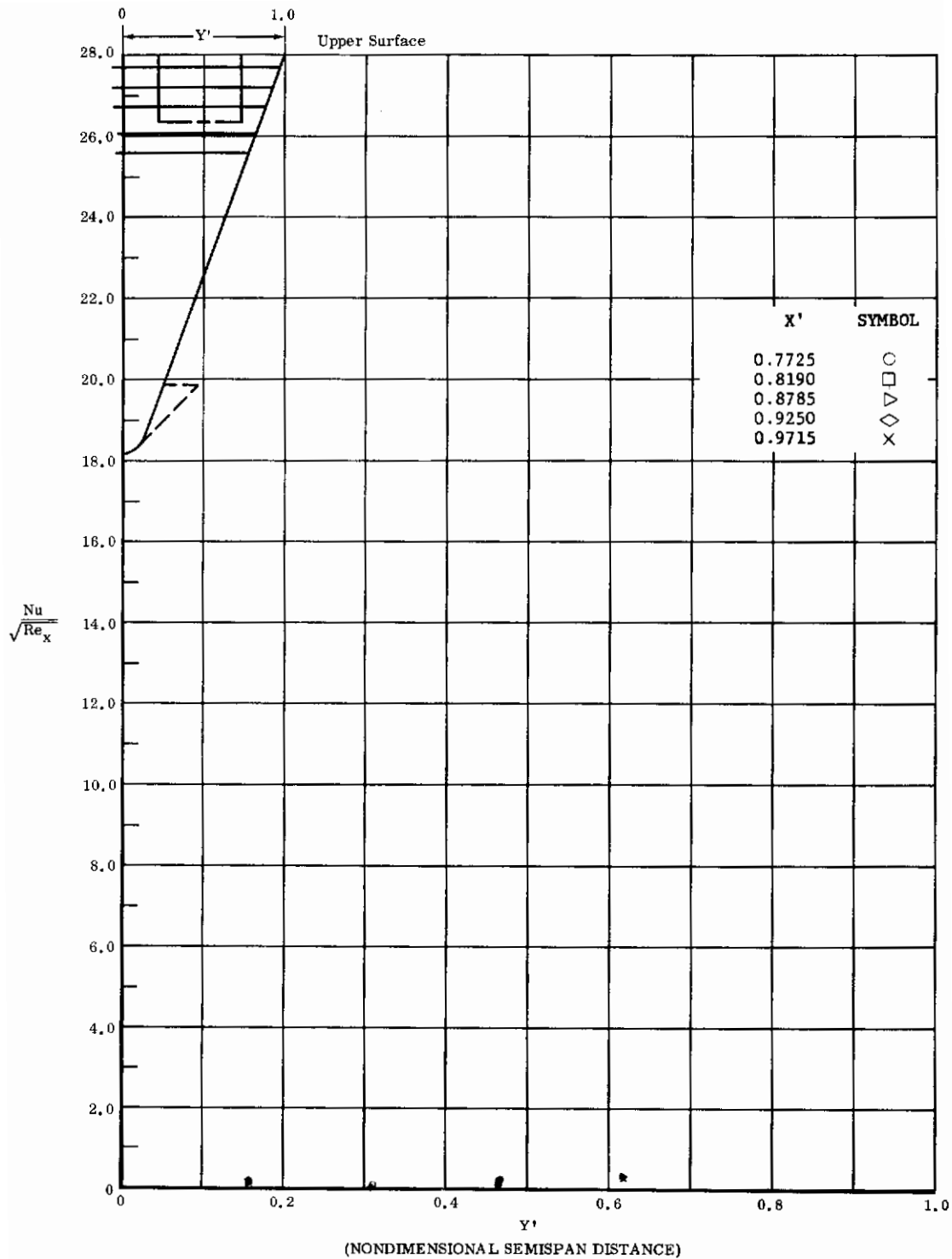Fig. 40 Streamwise Distributions of Aerodynamic Heating Rates; Basic Configuration + Canards, Bottom Flaps Deflected +40°, $\alpha = 0°$, $\beta = 0°$, $Re_\infty/ft = 3,300,000$.

Fig. 40 Spanwise Distributions of Aerodynamic Heating Rates; Basic Configuration + Canards, Bottom Flaps Deflected +40°, $\alpha = 0°$, $\beta = 0°$, $Re_\infty/ft = 3,300,000$.

77

Fig. 41 Streamwise Distributions of Aerodynamic Heating Rates; Basic Configuration, No Flap Deflections, $\alpha = 0°$, $\beta = +12°$, $Re_{\infty}/ft = 3,300,000$.

Fig. 41 Spanwise Distributions of Aerodynamic Heating Rates; Basic Configuration, No Flap Deflections, $\alpha = 0°$, $\beta = +12°$, $Re_{\infty}/ft = 3,300,000$.

78

$$\frac{Nu}{\sqrt{Re_x}}$$

Y'   SYMBOL

0.1618   ○
0.3170   □
0.4722   ▷
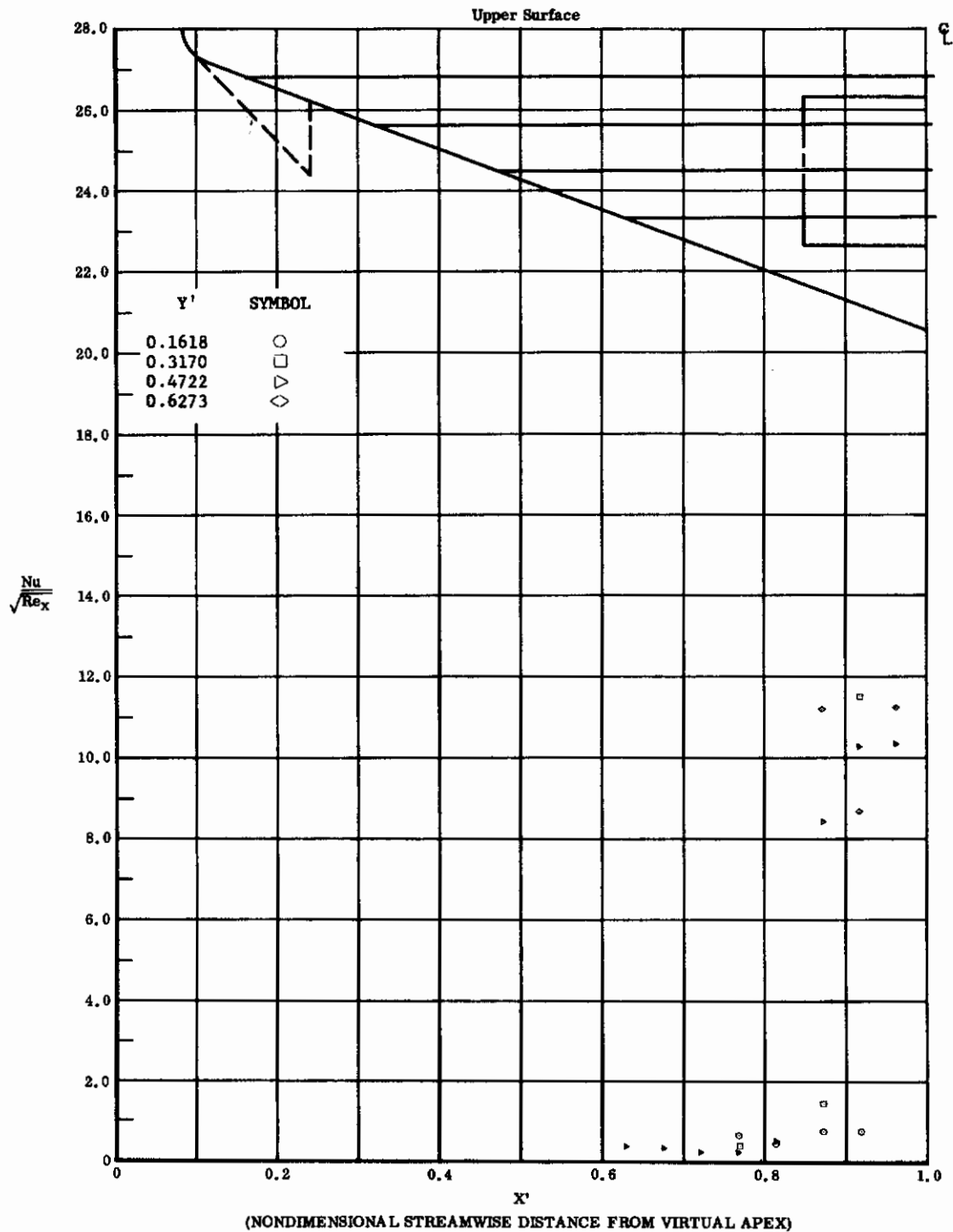0.6273   ◇

X'
(NONDIMENSIONAL STREAMWISE DISTANCE FROM VIRTUAL APEX)

Fig. 42   Streamwise Distributions of Aerodynamic Heating Rates; Basic Configuration, Bottom Flaps Deflected +20°, $\alpha = 0°$, $\beta = +12°$, $Re_\infty/ft = 3,300,000$.

$$\frac{Nu}{\sqrt{Re_x}}$$

X'   SYMBOL

0.7725   ○
0.8190   □
0.8785   ▷
0.9250   ◇
0.9715   ×

Y'
(NONDIMENSIONAL SEMISPAN DISTANCE)

Fig. 42   Spanwise Distributions of Aerodynamic Heating Rates; Basic Configuration, Bottom Flaps Deflected +20°, $\alpha = 0°$, $\beta = +12°$, $Re_\infty/ft = 3,300,000$.

79

Fig. 43   Streamwise Distributions of Aerodynamic Heating Rates; Basic Configuration + Fin (δ = 0), No Flap Deflections, α = 0°, β = +12°, Re_∞/ft = 3,300,000.

Fig. 43   Spanwise Distributions of Aerodynamic Heating Rates; Basic Configuration + Fin (δ = 0), No Flap Deflections, α = 0°, β = +12°, Re_∞/ft = 3,300,000.

80

Fig. 44 Streamwise Distributions of Aerodynamic Heating Rates; Basic Configuration
+ Fin (δ = 15°), No Flap Deflections, α = 0°, β = +12°, Re/ft = 3,300,000.

Fig. 44 Spanwise Distributions of Aerodynamic Heating Rates; Basic Configuration
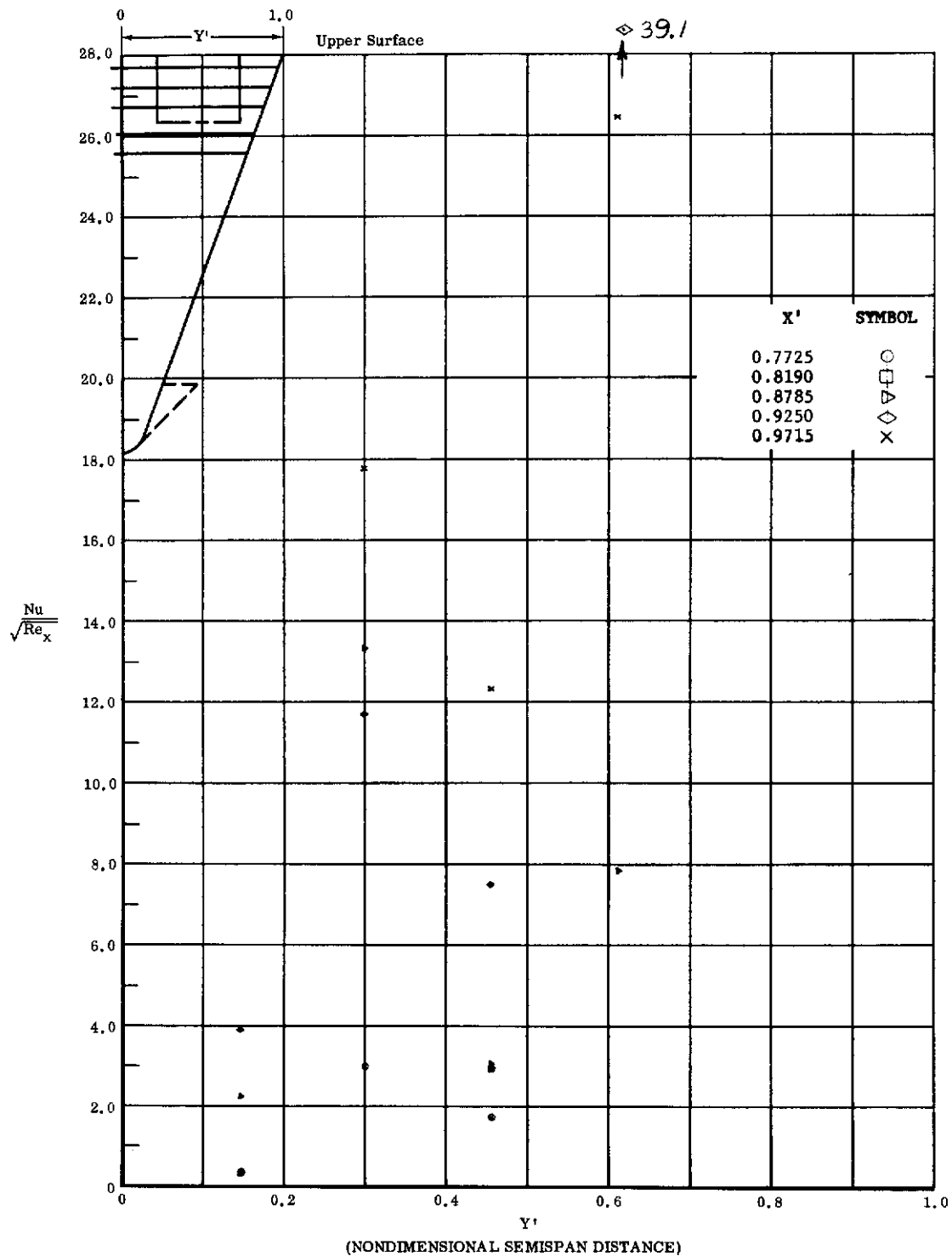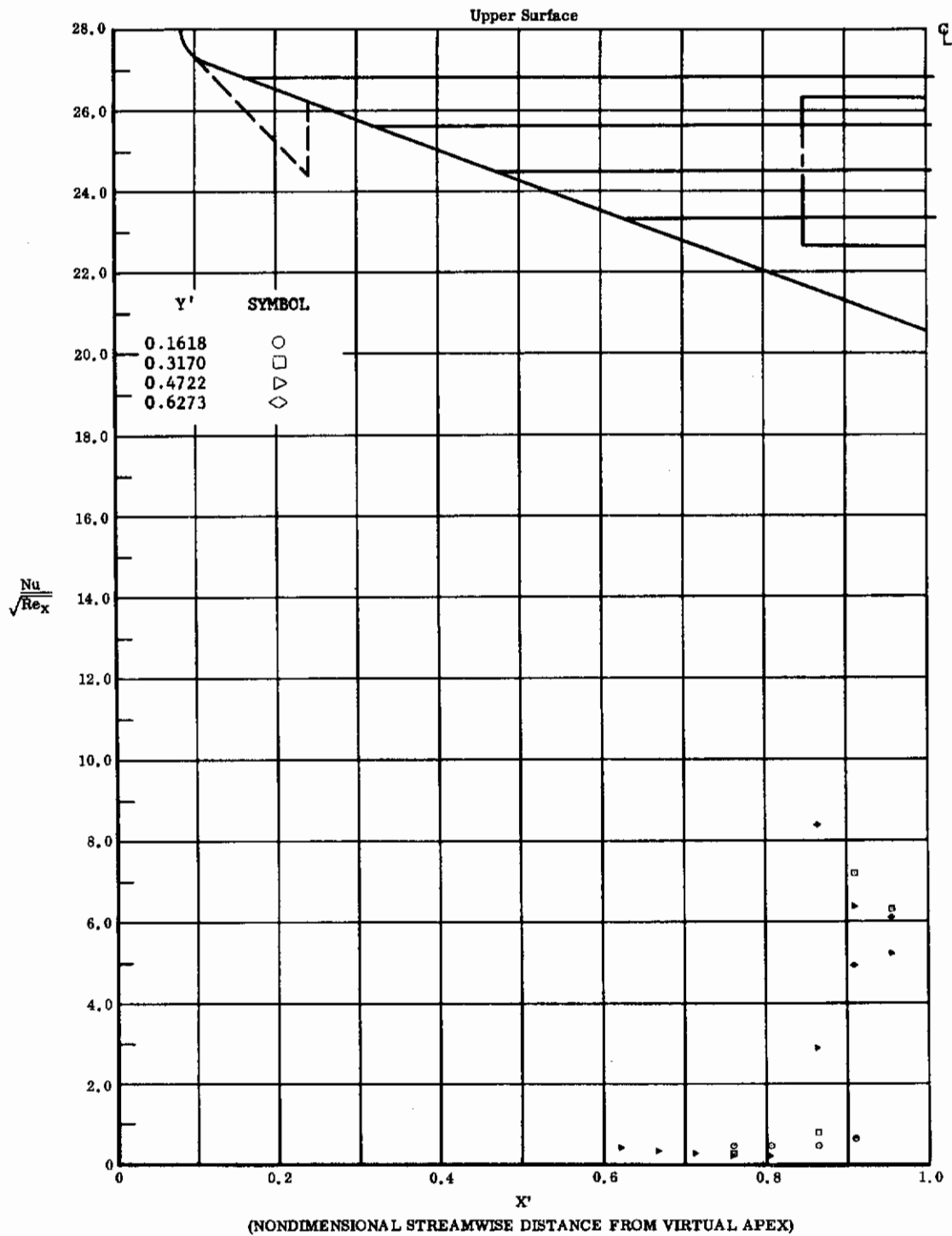+ Fin (δ = 15°), No Flap Deflections, α = 0°, β = +12°, Re/ft = 3,300,000.

81
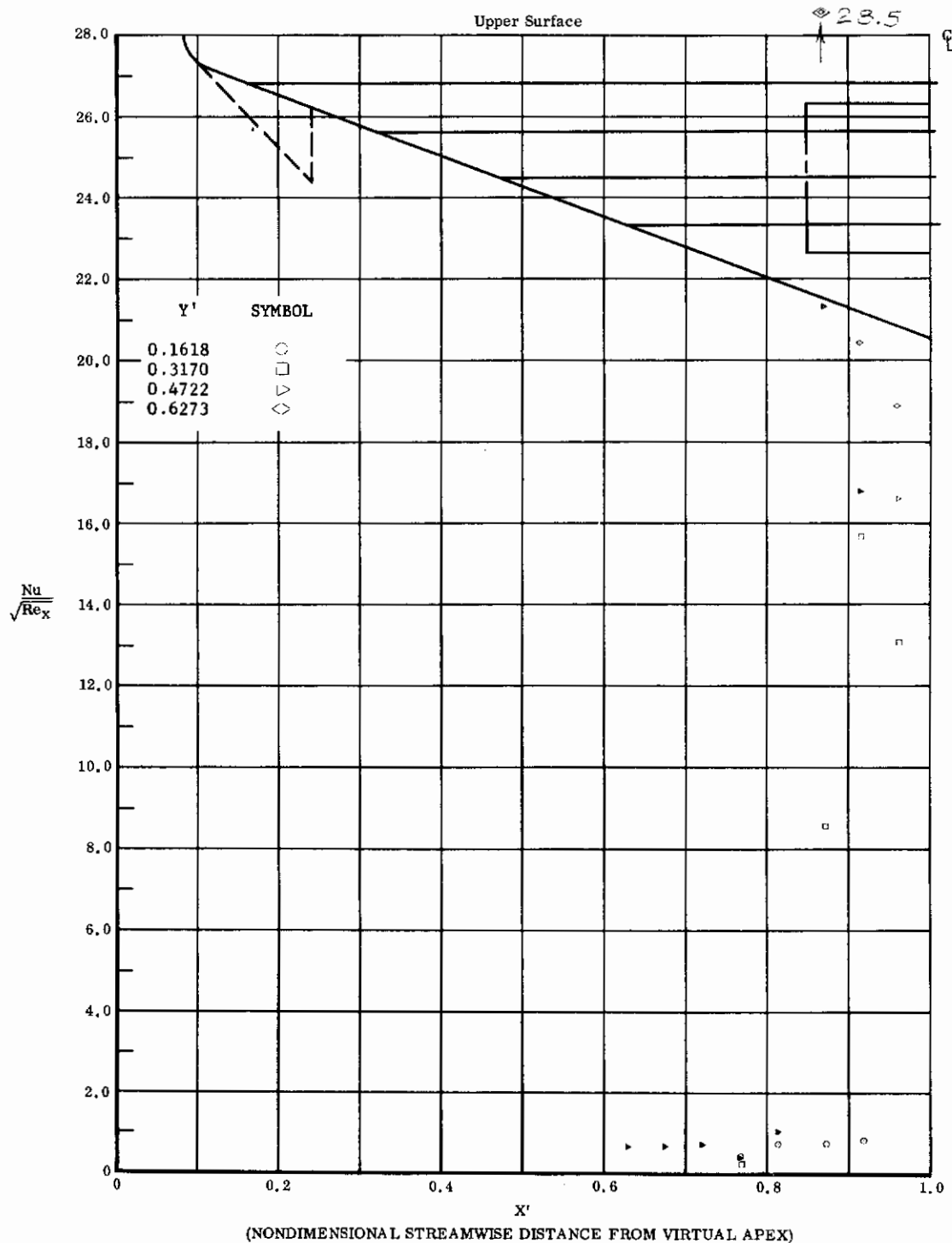
Fig. 45 Streamwise Distributions of Aerodynamic Heating Rates; Basic Configuration, Left and Right (Upper) Flaps Deflected -40°, $\alpha = +7°$, $\beta = 0°$, $Re_\infty/ft = 3,300,000$.
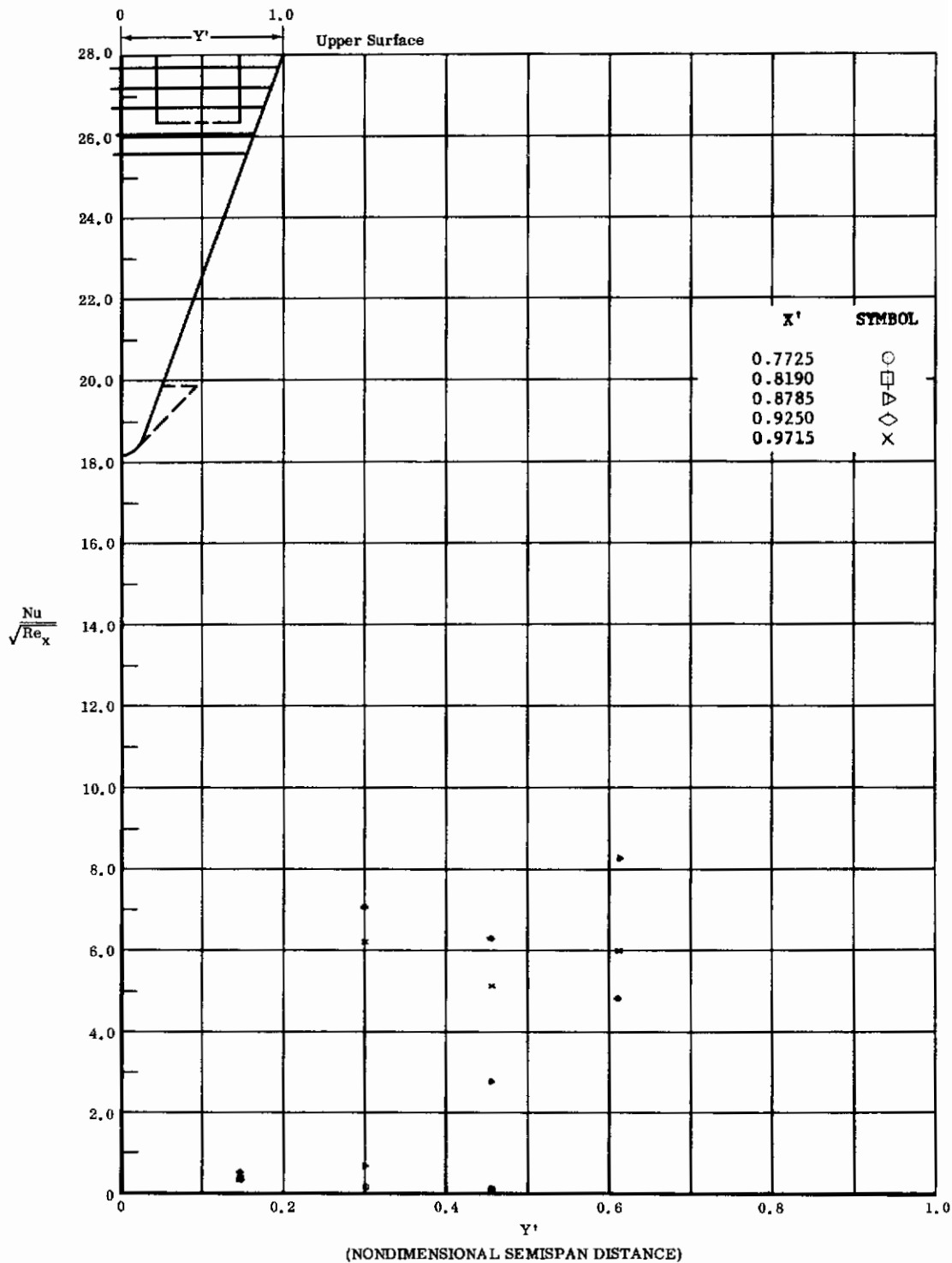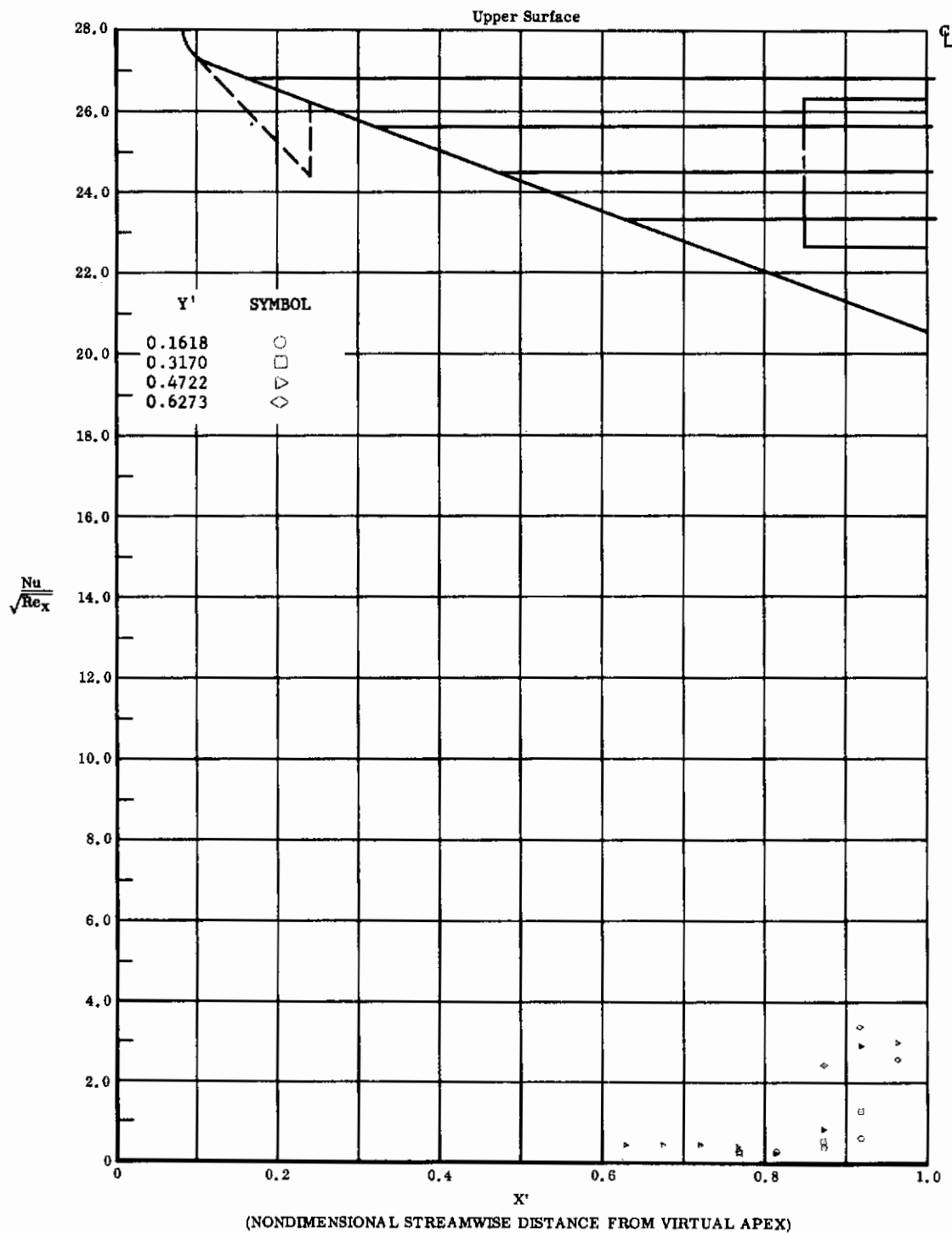
82
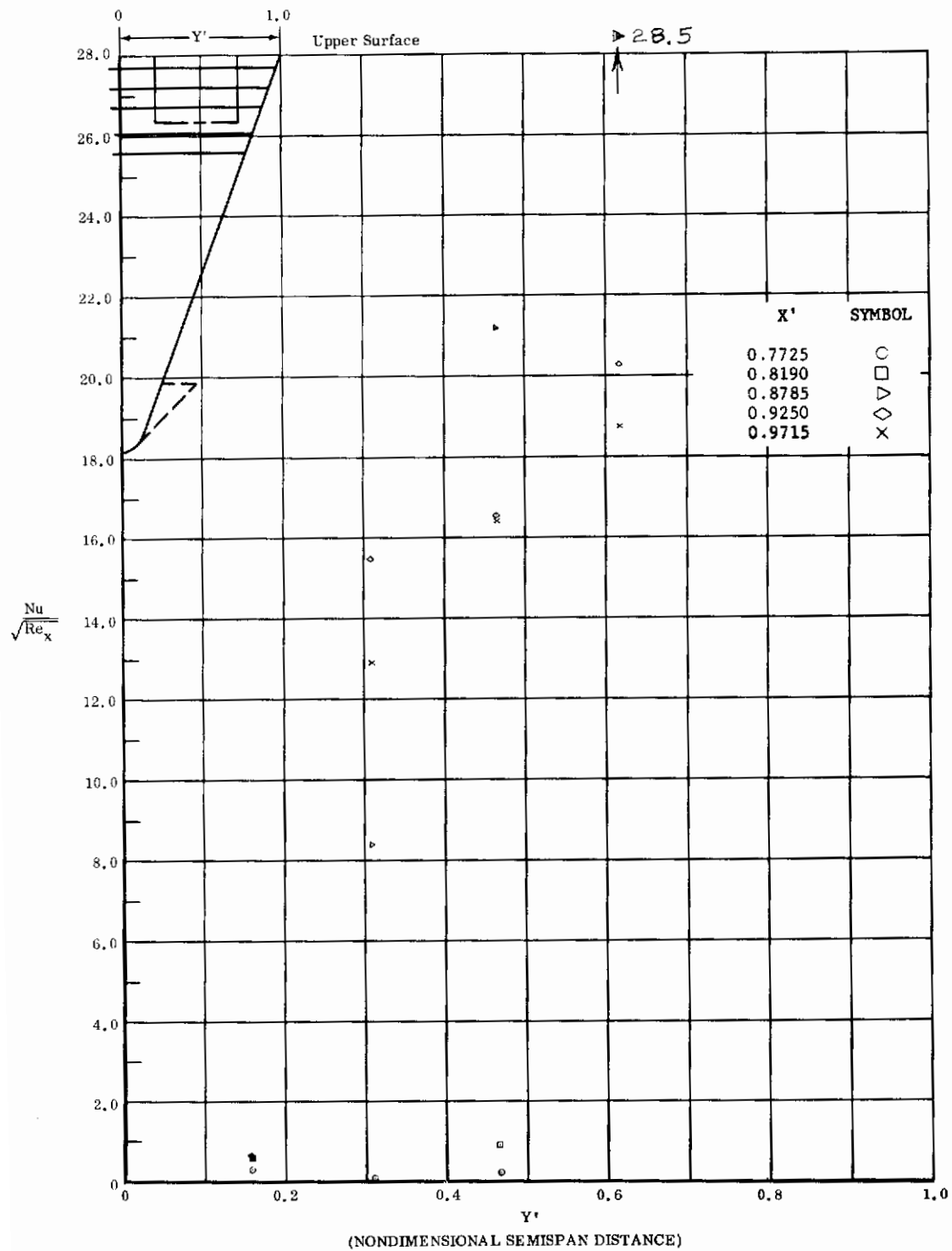
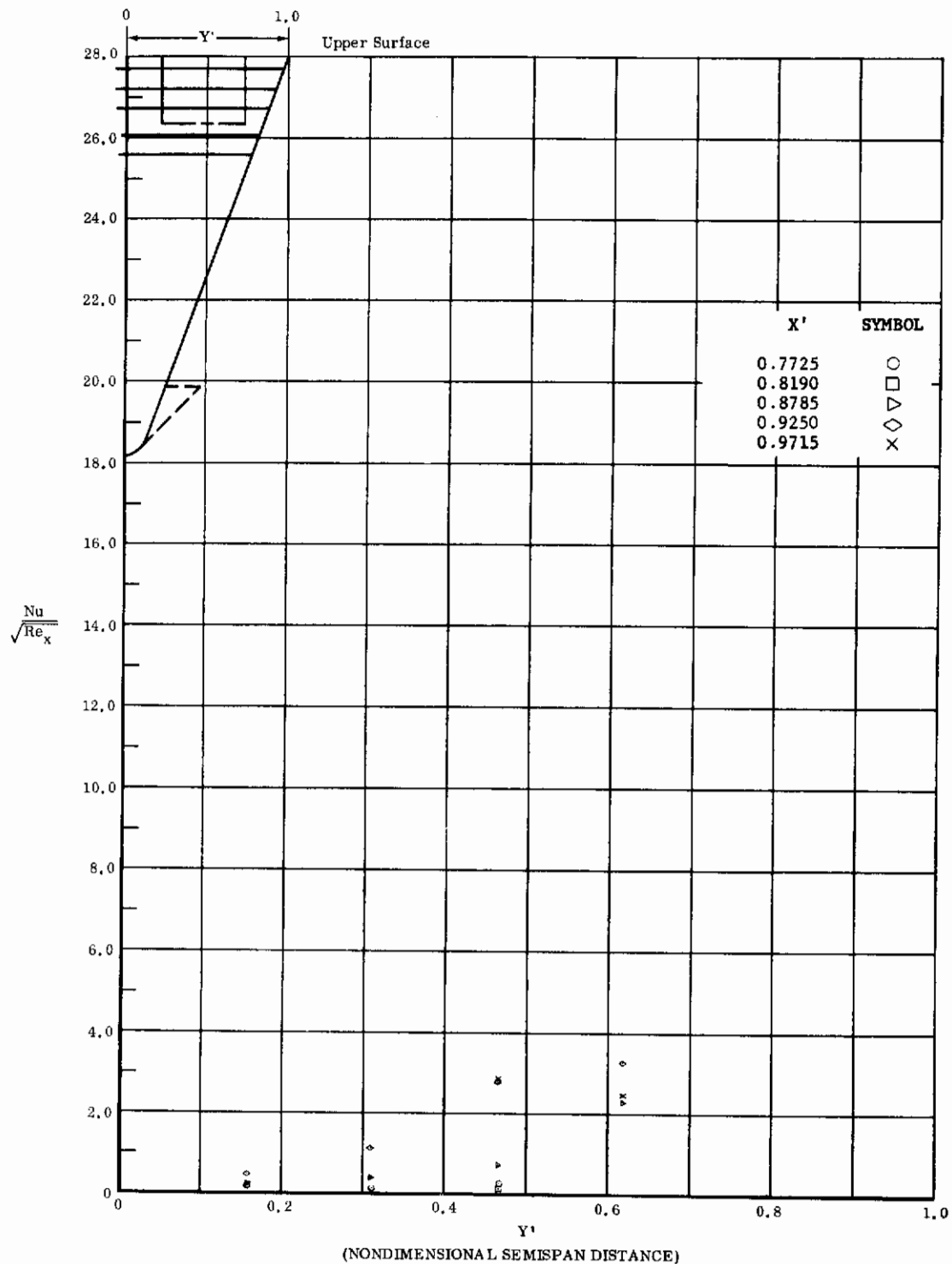Fig. 45 Spanwise Distributions of Aerodynamic Heating Rates; Basic Configuration, Left and Right (upper) Flaps Deflected -40°, $\alpha = +7°$, $\beta = 0°$, $Re_\infty/ft = 3,300,000.$

83

Upper Surface

Fig. 46   Streamwise Distributions of Aerodynamic Heating Rates; Basic Configuration, Bottom Flaps Deflected +40°, α = +7°, β = 0°, Re_∞/ft = 3,300,000.

Y'	SYMBOL
0.1618	◯
0.3170	□
0.4722	▷
0.6273	◇

$\dfrac{Nu}{\sqrt{Re_x}}$

X'
(NONDIMENSIONAL STREAMWISE DISTANCE FROM VIRTUAL APEX)

84

Fig. 46 Spanwise Distributions of Aerodynamic Heating Rates; Basic Configuration, Bottom Flaps Deflected +40°, $\alpha = +7°$, $\beta = 0°$, $Re_\infty/ft = 3,300,000$.
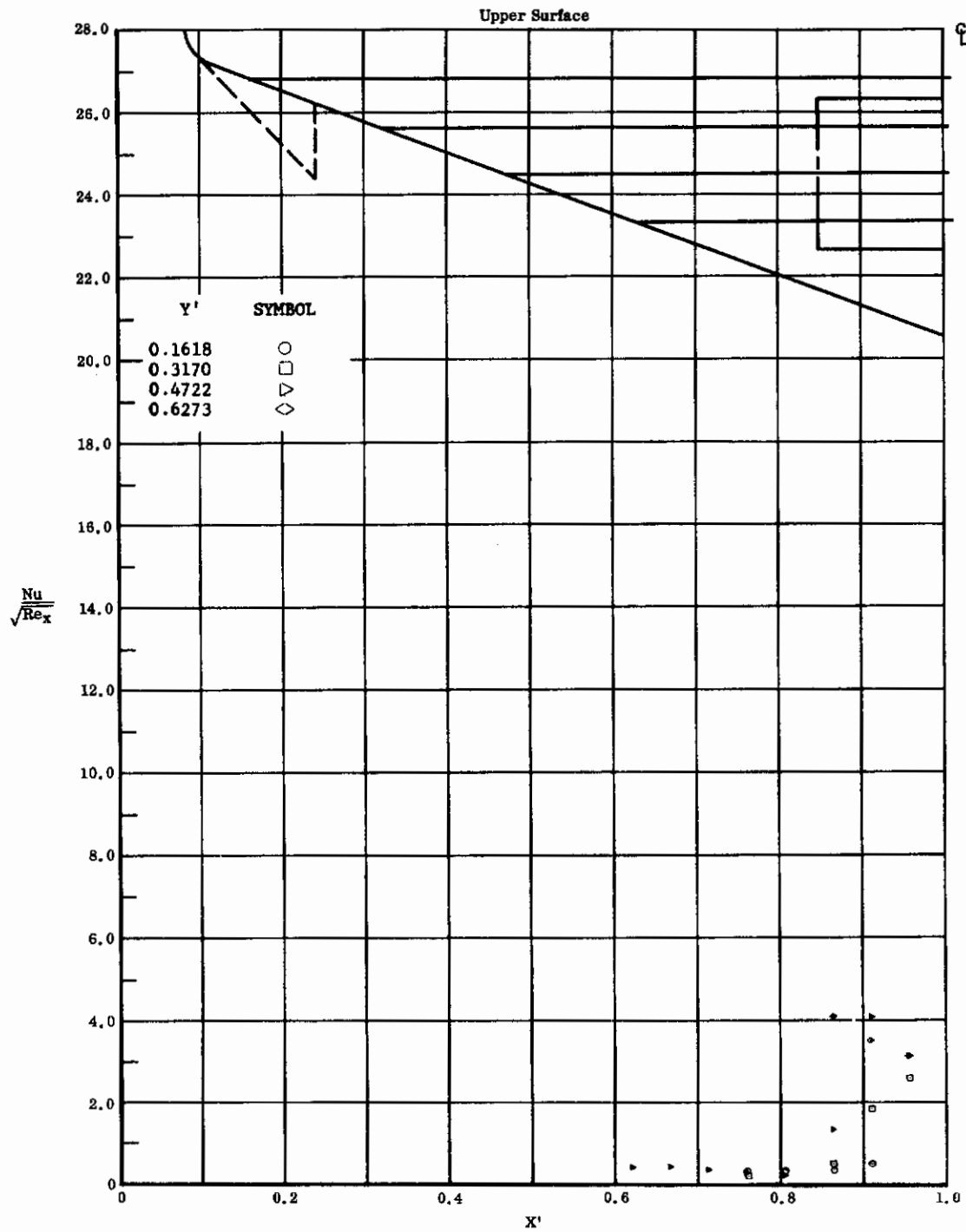
Upper Surface

Fig. 47 Streamwise Distributions of Aerodynamic Heating Rates; Basic Configuration,
Left and Right (Upper) Flaps Deflected -40°, α = +14.3°, β = 0°,
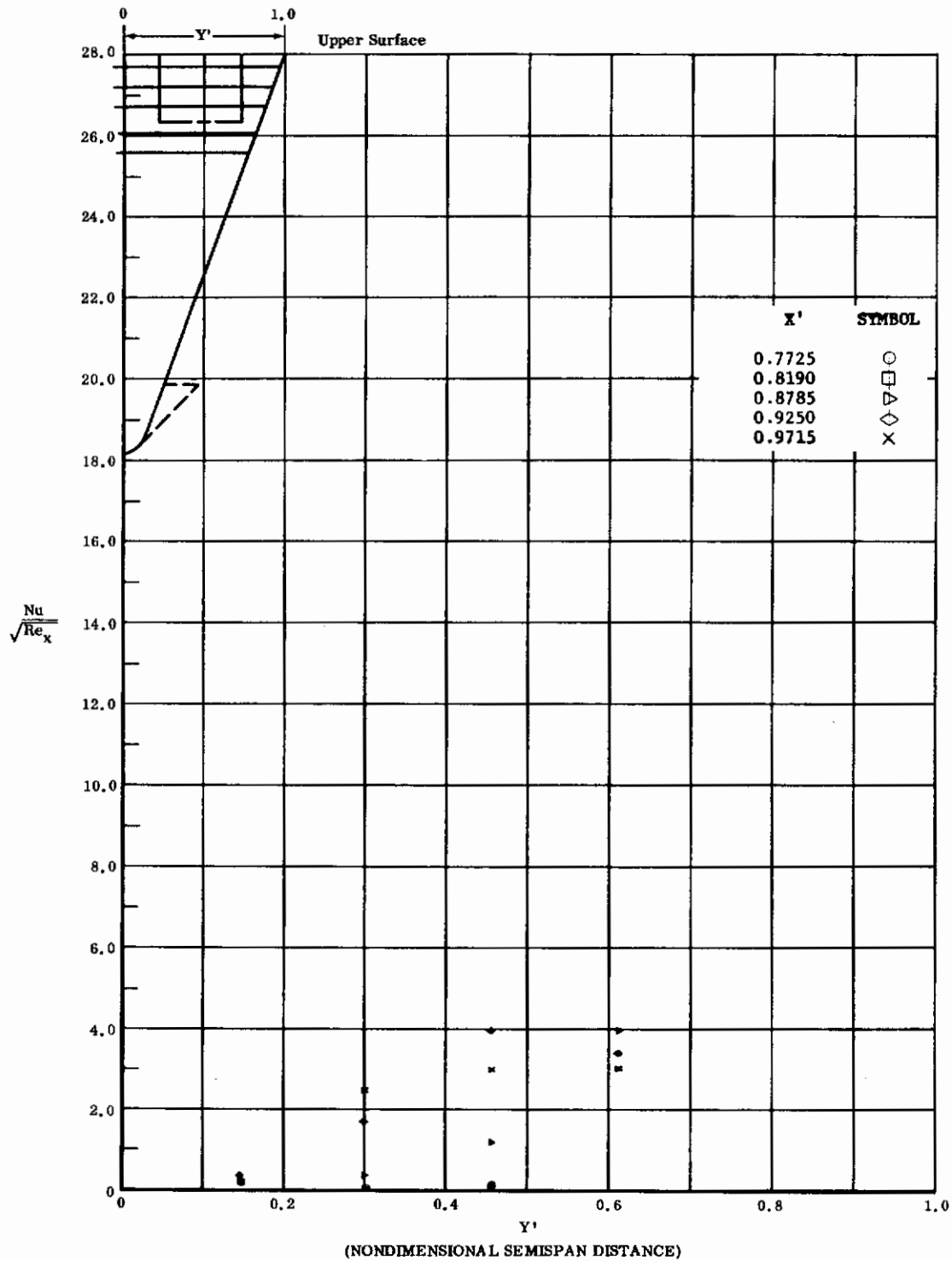Re_∞/ft = 1,100,000.

86
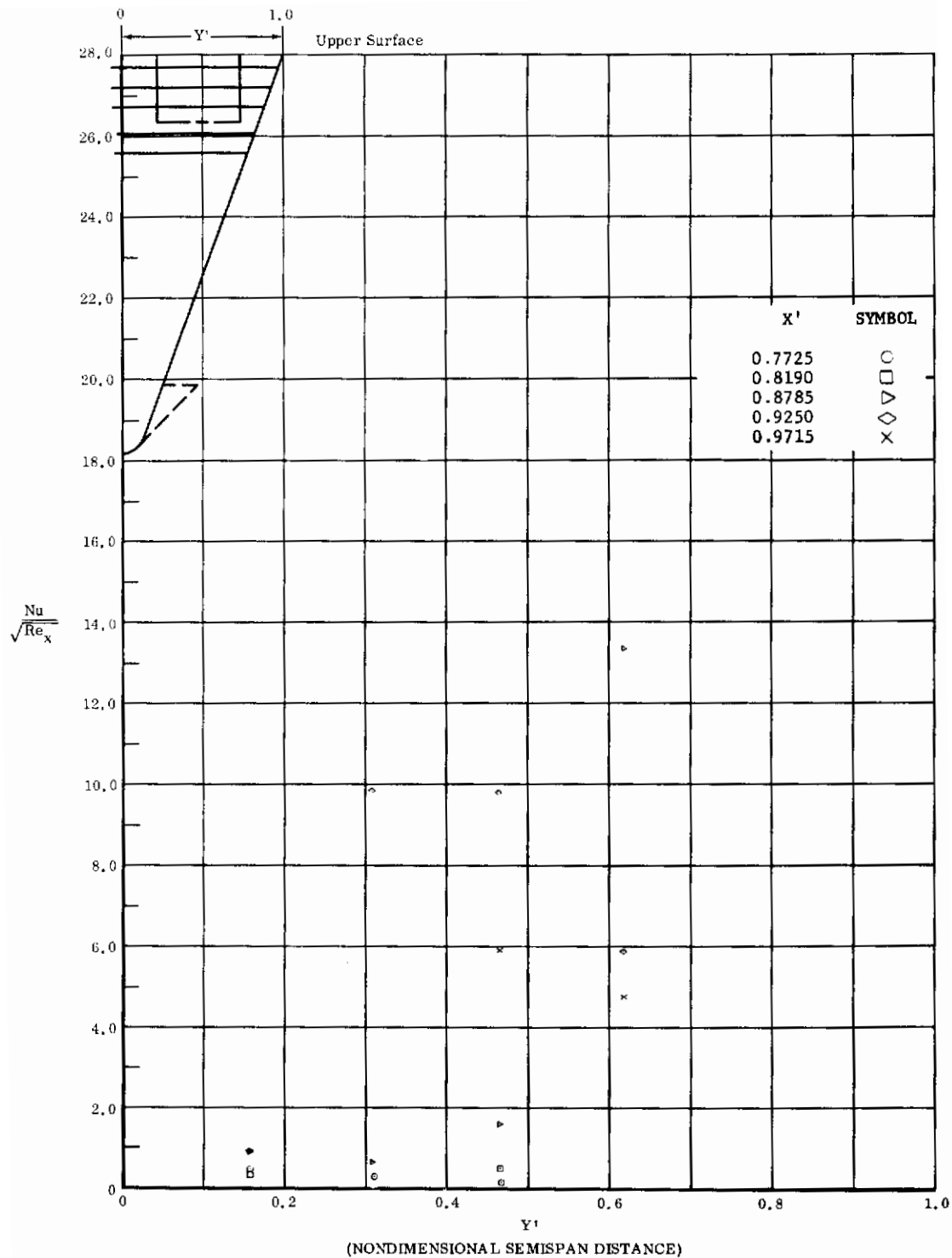
Fig. 47 Spanwise Distributions of Aerodynamic Heating Rates; Basic Configuration,
Left and Right (Upper) Flaps Deflected -40°, α = +14.3°, β = 0°,
Re$_\infty$/ft = 1,100,000.

87

Upper Surface

Fig. 48 Streamwise Distributions of Aerodynamic Heating Rates; Basic Configuration, Left and Right (Upper) Flaps Deflected -40°, $\alpha = +14.3°$, $\beta = 0°$, $Re_\infty/ft = 3,300,000$.

88

0   1.0

Y'   Upper Surface

$\frac{Nu}{\sqrt{Re_x}}$

X'	SYMBOL
0.7725	○
0.8190	⊡
0.8785	▷
0.9250	◇
0.9715	×

Y'

(NONDIMENSIONAL SEMISPAN DISTANCE)
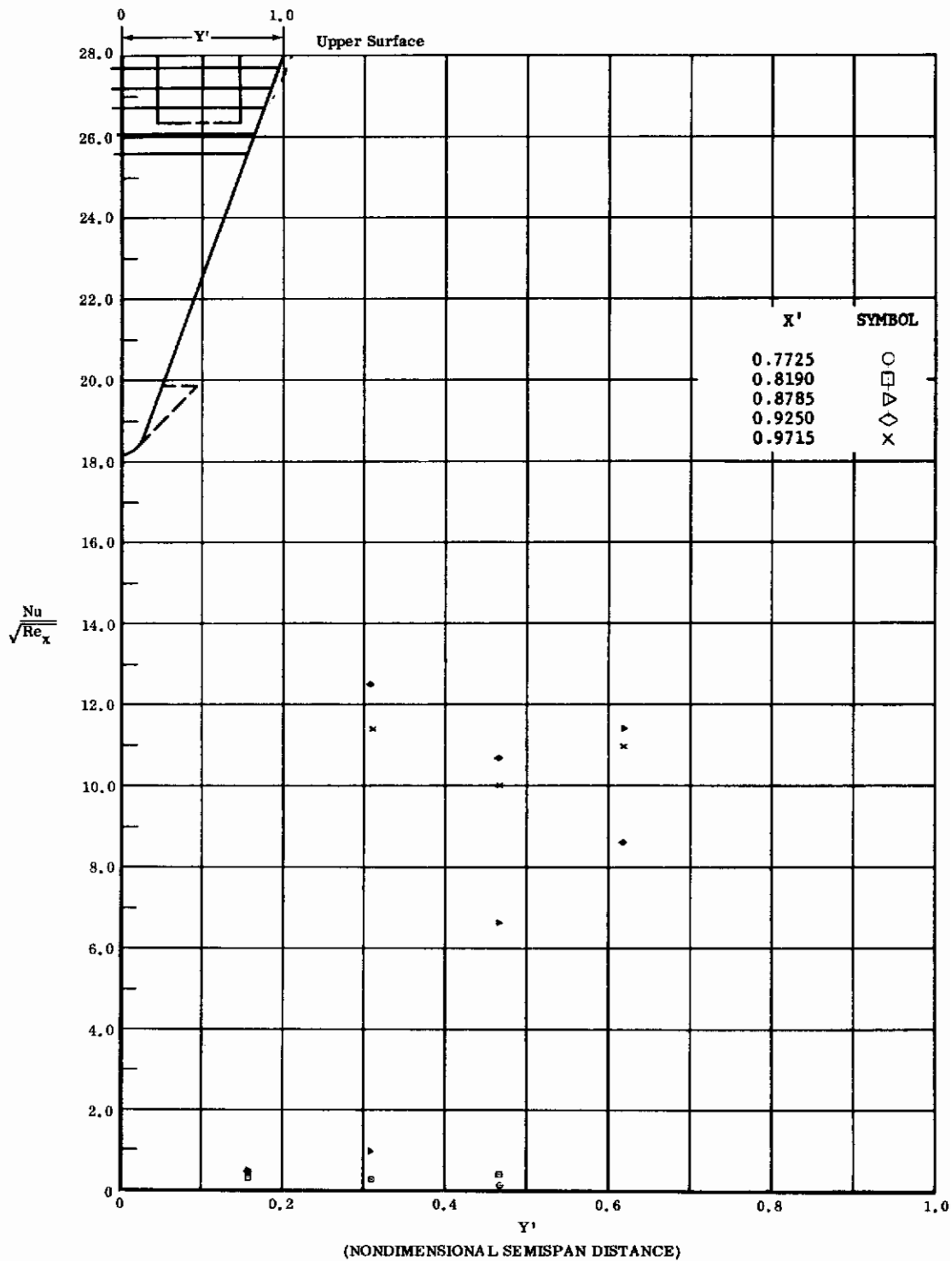
Fig. 48 Spanwise Distributions of Aerodynamic Heating Rates; Basic Configuration,
Left and Right (Upper) Flaps Deflected -40°, α = +14.3°, β = 0°,
Re_∞/ft = 3,300,000.

Upper Surface
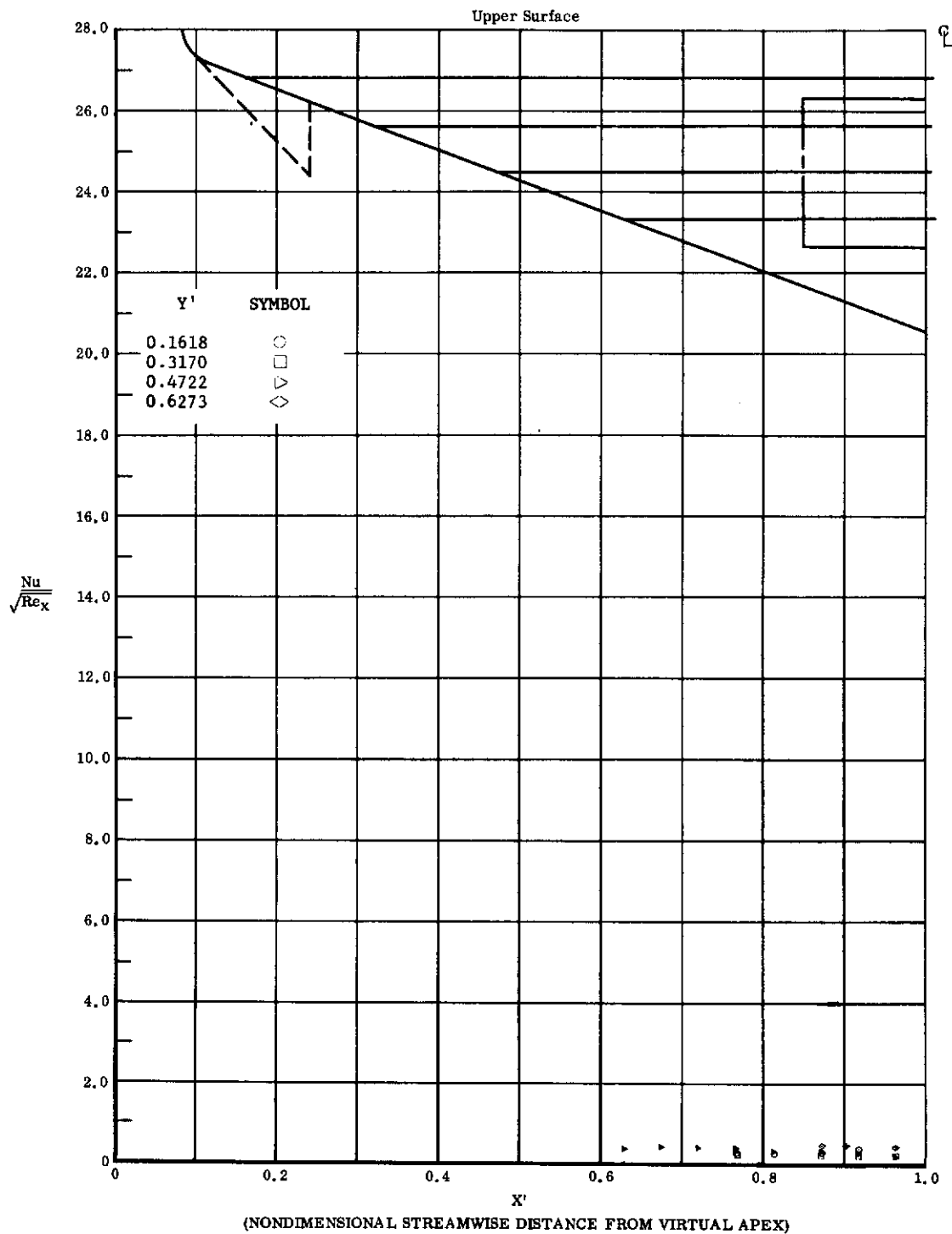
Fig. 49 Streamwise Distributions of Aerodynamic Heating Rates; Basic Configuration, Left (Upper) Flap Deflected -40°, α = +14.3°, β = 0°, Re_{∞}/ft = 3,300,000.
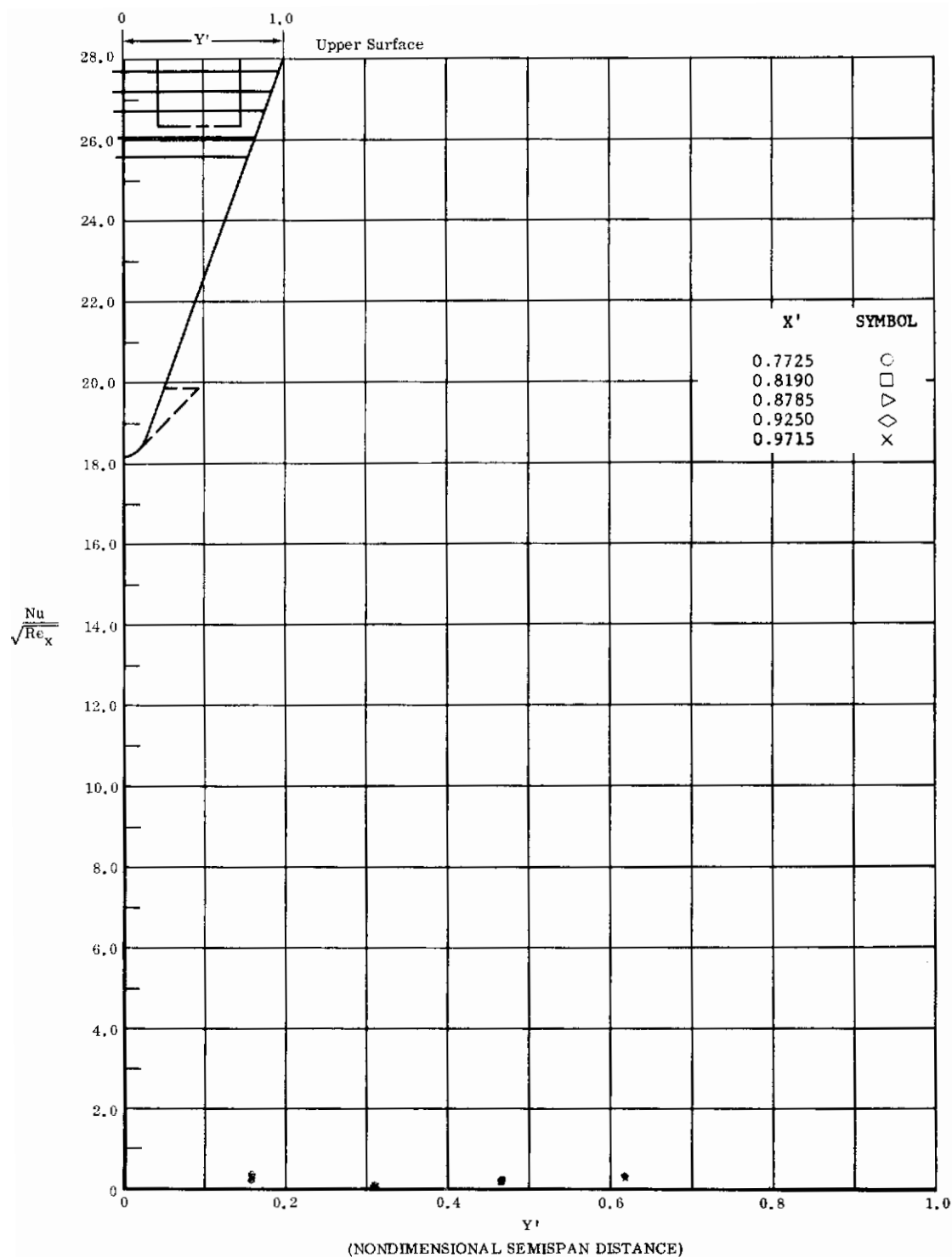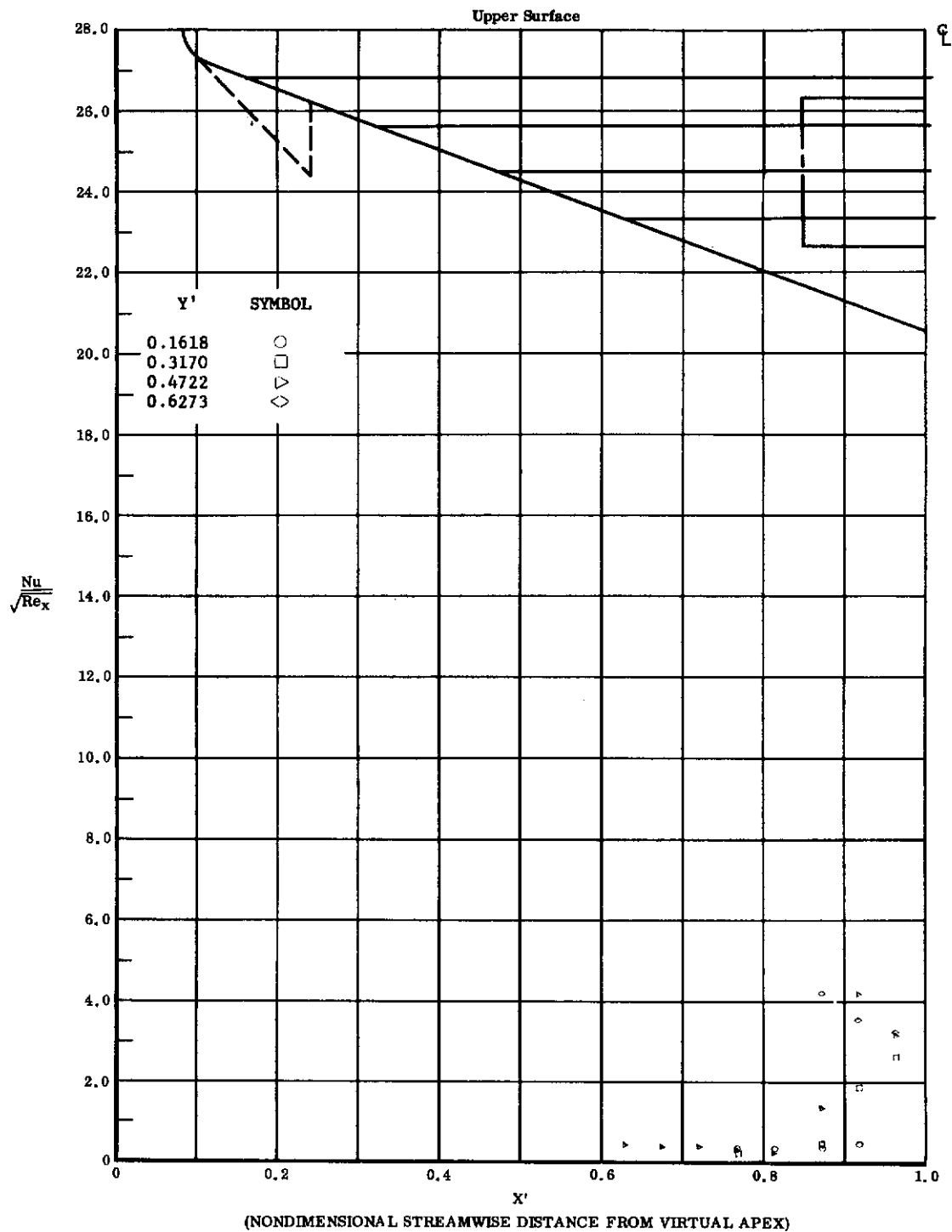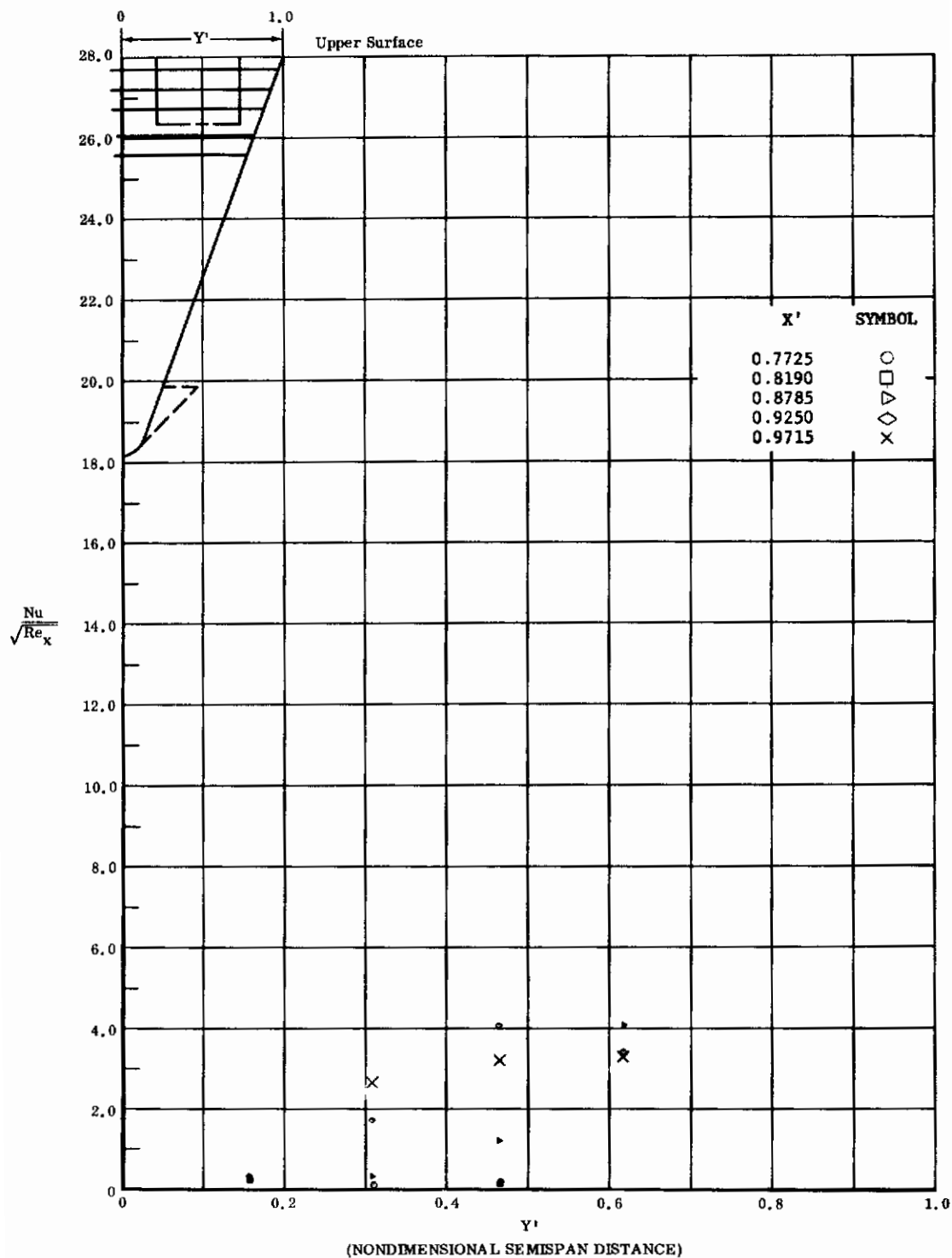
Fig. 49 Spanwise Distributions of Aerodynamic Heating Rates; Basic Configuration, Left (Upper) Flap Deflected -40°, α = +14.3°, β = 0°, Re_∞/ft = 3,300,000.

91

Fig. 50 Streamwise Distributions of Aerodynamic Heating Rates; Basic Configuration, Right (Upper) Flap Deflected -40°, α = +14.3°, β = 0°, Re_∞/ft = 3,300,000.

92

Fig. 50   Spanwise Distributions of Aerodynamic Heating Rates; Basic Configuration,
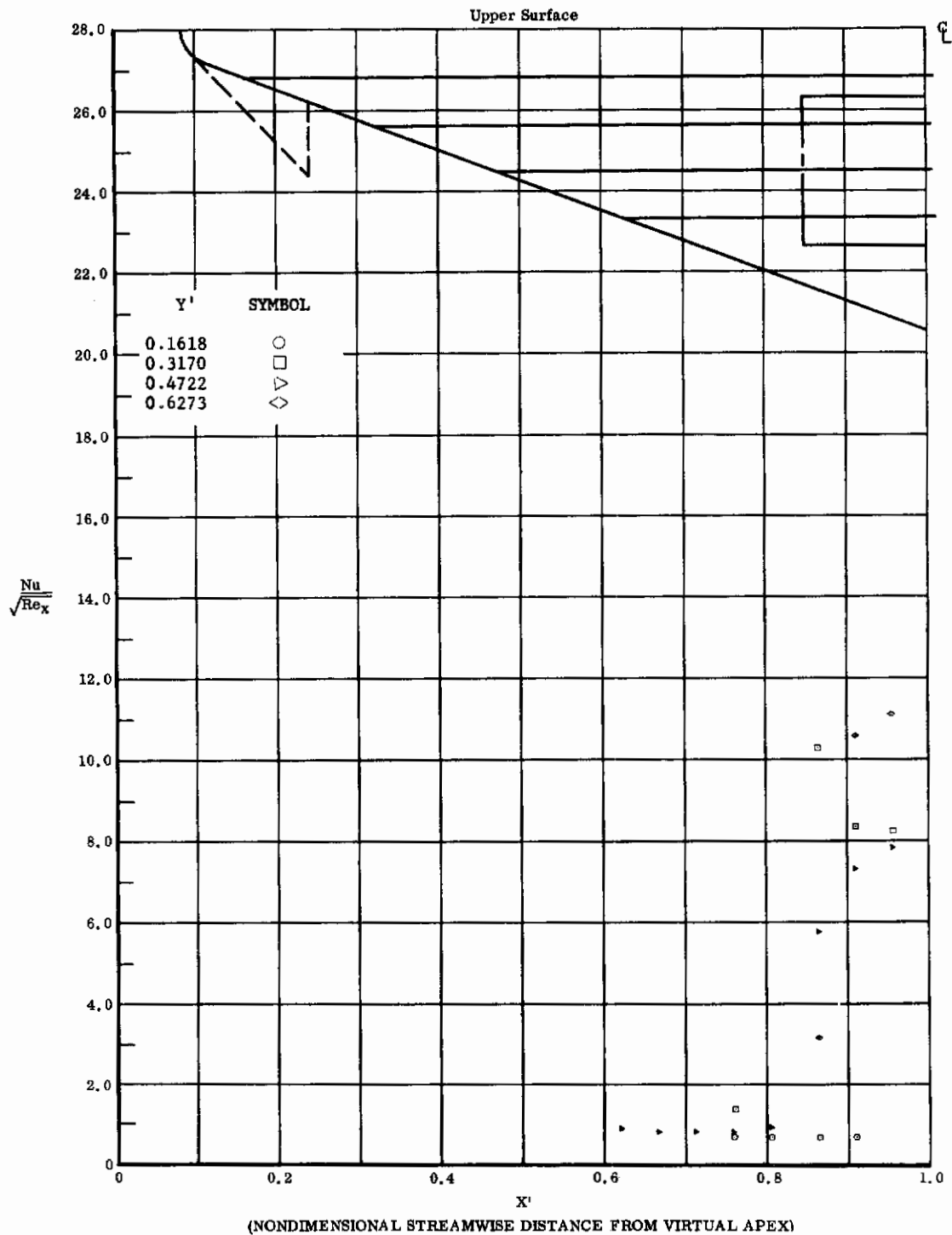Right (Upper) Flap Deflected -40°, $\alpha \approx +14.3°$, $\beta = 0°$, $Re_\infty/ft = 3,300,000$.
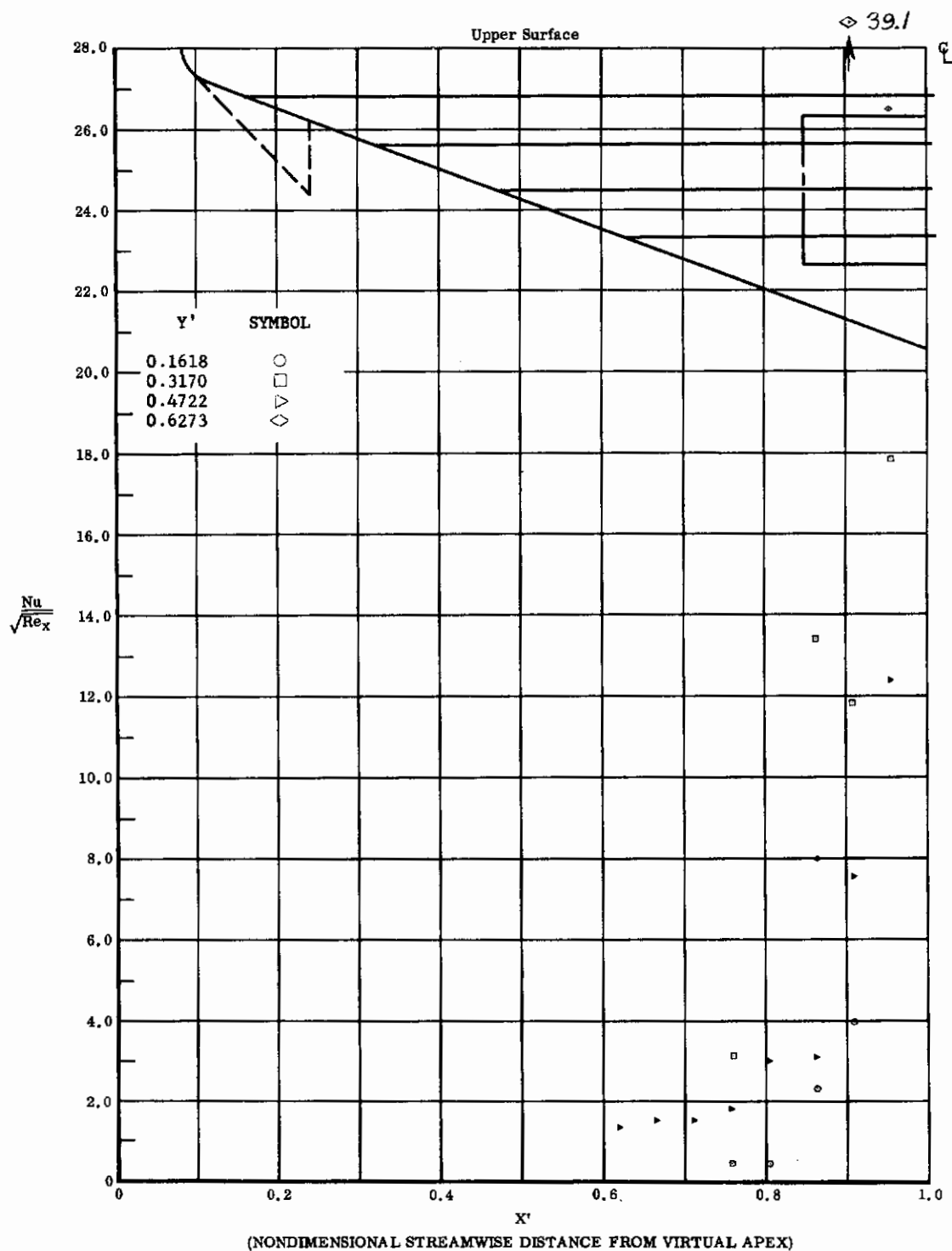
Fig. 51 Streamwise Distributions of Aerodynamic Heating Rates; Basic Configuration
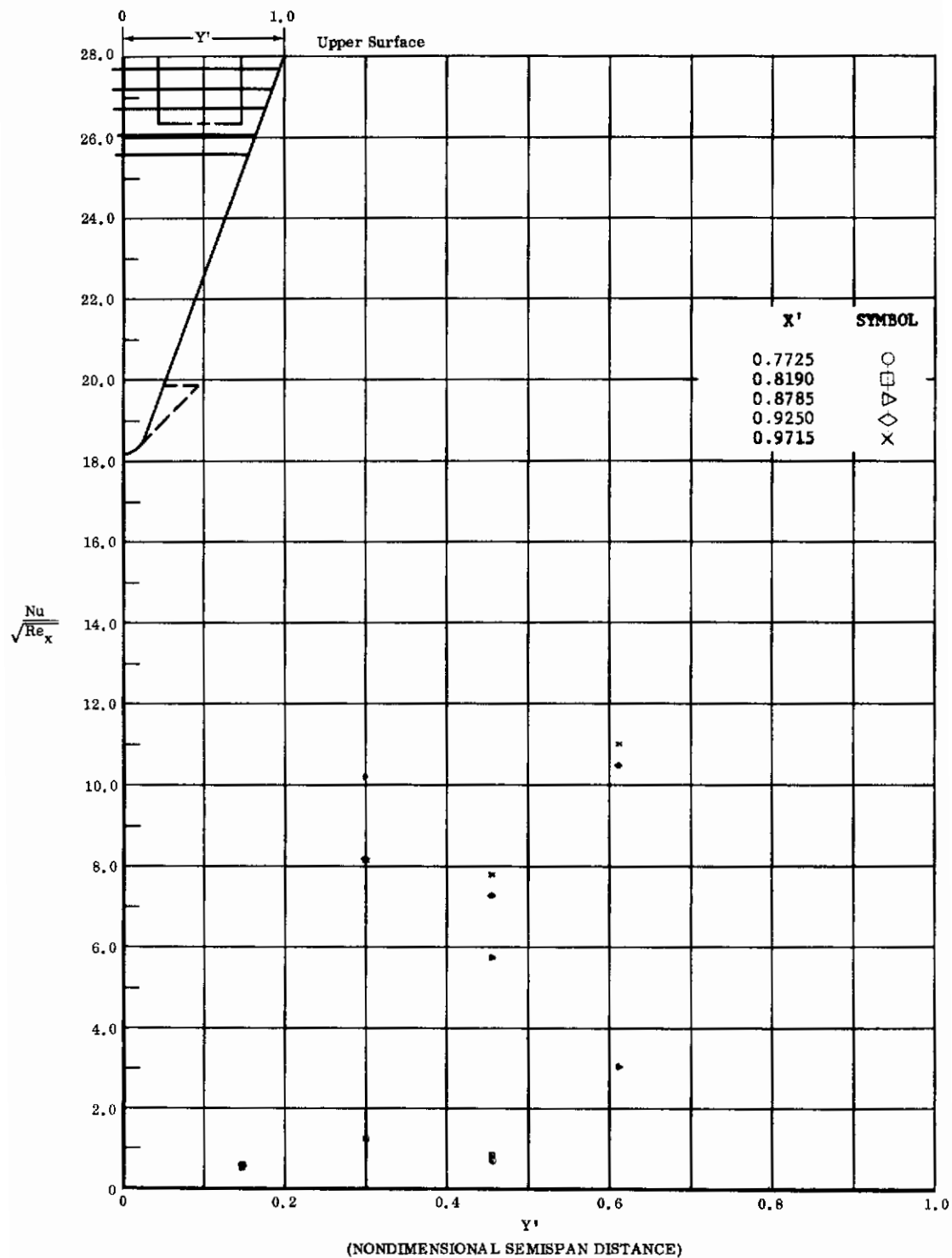+ Canards, Left and Right (Upper) Flaps Deflected -40°, α = +14.3°,
β = 0°, Re∞/ft = 3,300,000.

Fig. 51 Spanwise Distributions of Aerodynamic Heating Rates; Basic Configuration + Canards, Left and Right (Upper) Flaps Deflected -40°, α = +14.3°, β = 0°, Re_∞/ft = 3,300,000.
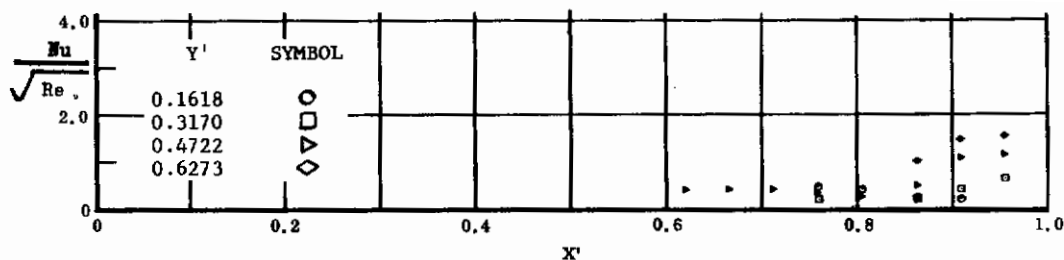
95

Fig. 52 Streamwise Distributions of Aerodynamic Heating Rates; Basic Configuration, Left and Right (Upper) Flaps Deflected -30°, α = +14.3°, β = 0°, $Re_\infty/ft = 3,300,000$.
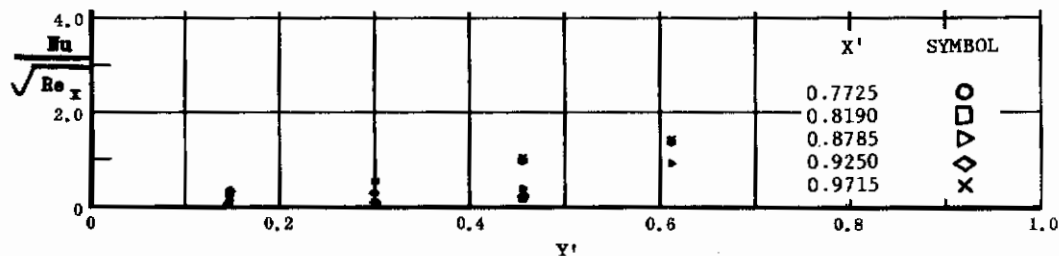
96

Fig. 52 Spanwise Distributions of Aerodynamic Heating Rates; Basic Configuration, Left and Right (Upper) Flaps Deflected -30°, α = +14.3°, β = 0°, Re$_\infty$/ft = 3,300,000.

97

Fig. 53 Streamwise Distributions of Aerodynamic Heating Rates; Basic Configuration, Left and Right (Upper) Flaps Deflected -20°, α = +14.3°, β = 0°, Re_∞/ft = 1,100,000.

98

Fig. 53 Spanwise Distributions of Aerodynamic Heating Rates; Basic Configuration, Left and Right (Upper) Flaps Deflected -20°, α = +14.3°, β = 0°, Re_∞/ft = 1,100,000.

99

Fig. 54 Streamwise Distributions of Aerodynamic Heating Rates; Basic Configuration, Left and Right (Upper) Flaps Deflected -20°, $\alpha = +14.3°$, $\beta = 0°$, $Re_{\infty}/ft = 3,300,000$.

100

Fig. 54 Spanwise Distributions of Aerodynamic Heating Rates; Basic Configuration,
Left and Right (Upper) Flaps Deflected -20°, α = +14.3°, β = 0°,
Re∞/ft = 3,300,000.

101
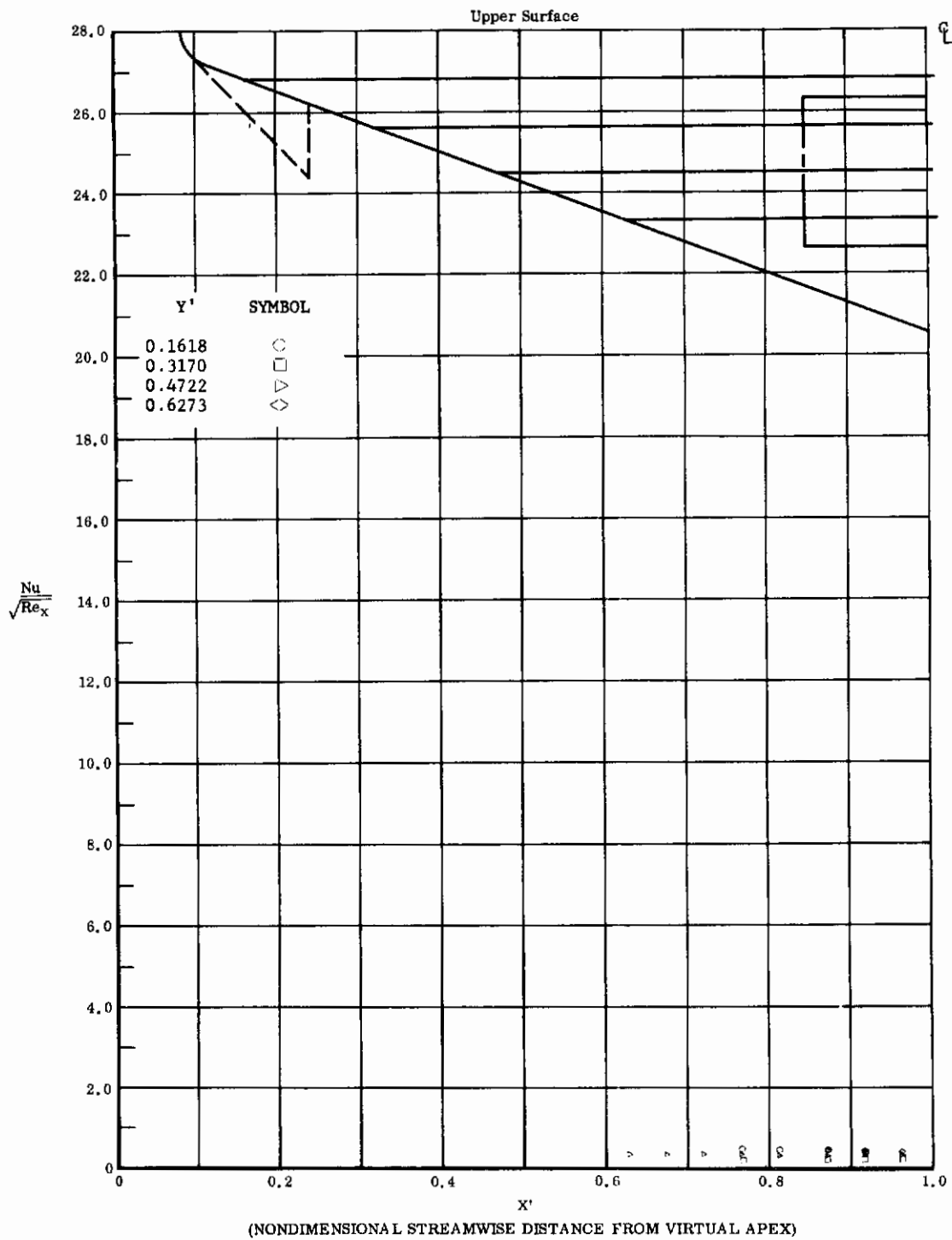
Fig. 55 Streamwise Distributions of Aerodynamic Heating Rates; Basic Configuration, Left (Upper) Flap Deflected -20°, $\alpha = +14.3°$, $\beta = 0°$, $Re_\infty/ft = 3,300,000$.

Fig. 55 Spanwise Distributions of Aerodynamic Heating Rates; Basic Configuration, Left (Upper) Flap Deflected -20°, α = +14.3°, β = 0°, Re_∞/ft = 3,300,000.

103

Fig. 56 Streamwise Distributions of Aerodynamic Heating Rates; Basic Configuration,
Right (Upper) Flap Deflected -20°, α = +14.3°, β = 0°, Re_∞/ft = 3,300,000.

104

Fig. 56 Spanwise Distributions of Aerodynamic Heating Rates; Basic Configuration,
Right (Upper) Flap Deflected -20°, α = +14.3°, β = 0°, Re_∞/ft = 3,300,000.

105

Upper Surface

Fig. 57   Streamwise Distributions of Aerodynamic Heating Rates; Basic Configuration
+ Canards, Left and Right (Upper) Flaps Deflected -20°, α = +14.3°,
β = 0°, Re_∞/ft = 3,300,000.

106

Fig. 57 Spanwise Distributions of Aerodynamic Heating Rates; Basic Configuration + Canards, Left and Right (Upper) Flaps Deflected -20°, α = +14.3°, β = 0°, Re∞/ft = 3,300,000.
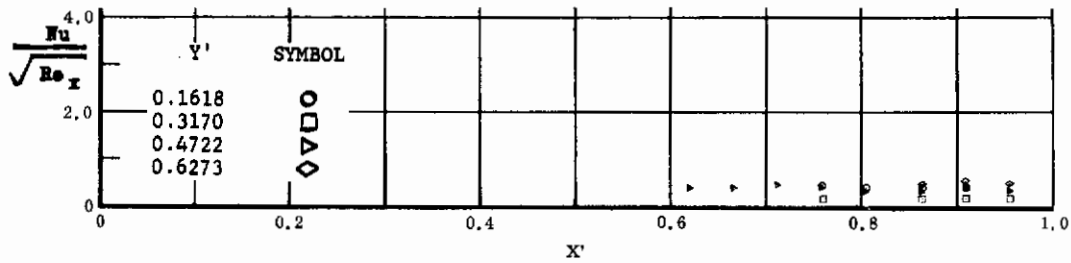
107

Fig. 58 Streamwise Distributions of Aerodynamic Heating Rates; Basic Configuration, Left and Right (Upper) Flaps Deflected -10°, $\alpha = +14.3°$, $\beta = 0°$, $Re_\infty/ft = 3,300,000$.

Fig. 58 Spanwise Distributions of Aerodynamic Heating Rates; Basic Configuration, Left and Right (Upper) Flaps Deflected -10°, $\alpha = +14.3°$, $\beta = 0°$, $Re_\infty/ft = 3,300,000$.
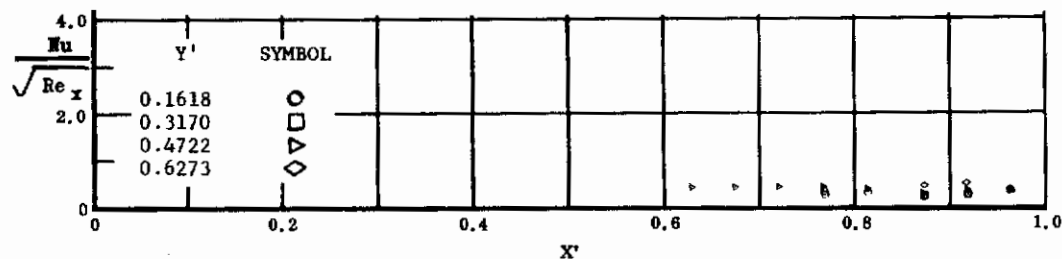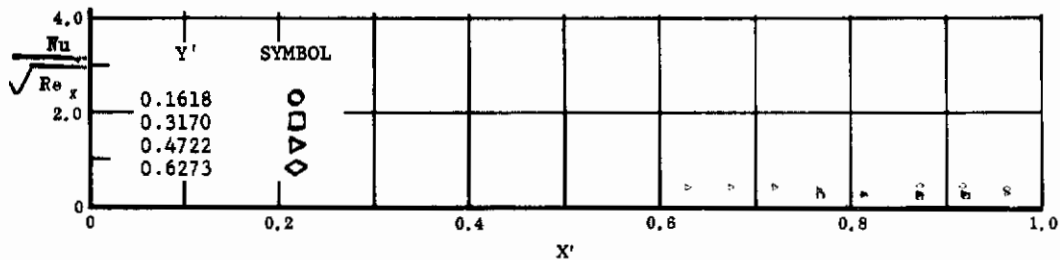
Fig. 59 Streamwise Distributions of Aerodynamic Heating Rates; Basic Configuration, No Flap Deflections, $\alpha = +14.3°$, $\beta = 0°$, $Re_\infty/ft = 1,100,000$.
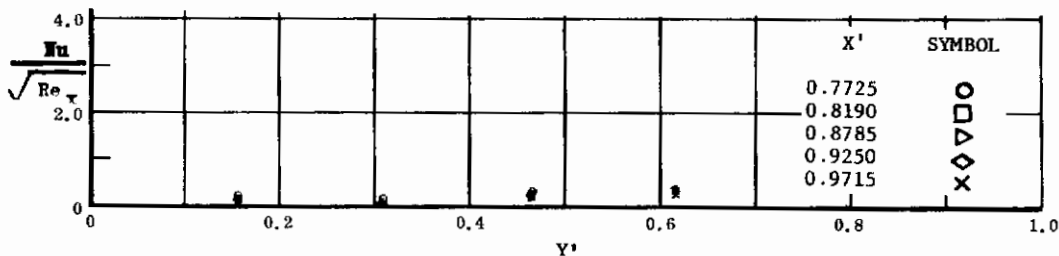
Fig. 59 Spanwise Distributions of Aerodynamic Heating Rates; Basic Configuration, No Flap Deflections, $\alpha = +14.3°$, $\beta = 0°$, $Re_\infty/ft = 1,100,000$.
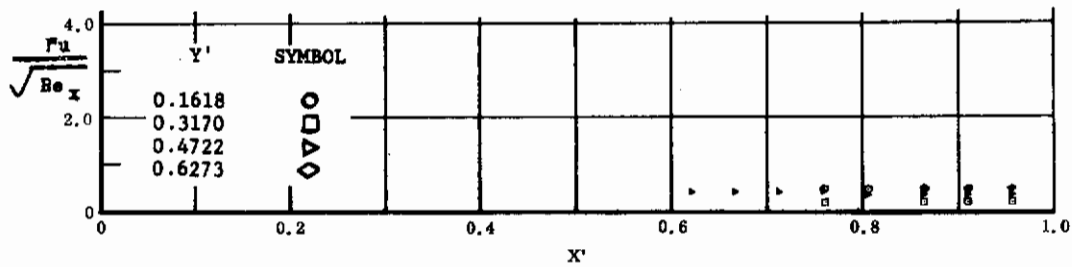
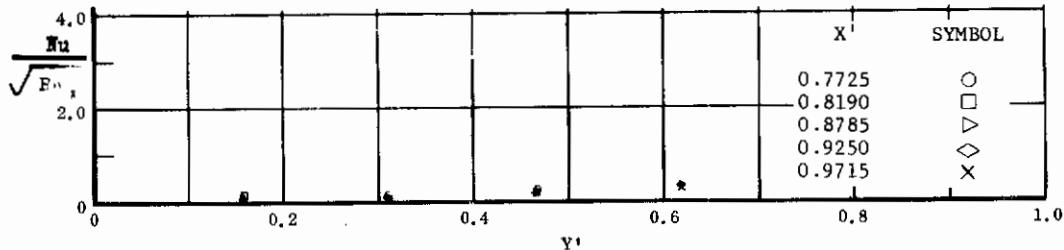Fig. 60 Streamwise Distributions of Aerodynamic Heating Rates; Basic Configuration, No Flap Deflections, $\alpha = +14.3°$, $\beta = 0°$, $Re_\infty/ft = 3,300,000$.
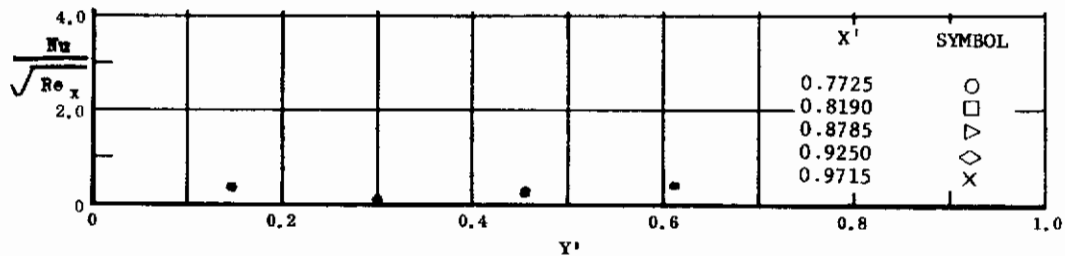
Fig. 60 Spanwise Distributions of Aerodynamic Heating Rates; Basic Configuration, No Flap Deflections, $\alpha = +14.3°$, $\beta = 0°$, $Re_\infty/ft = 3,300,000$.
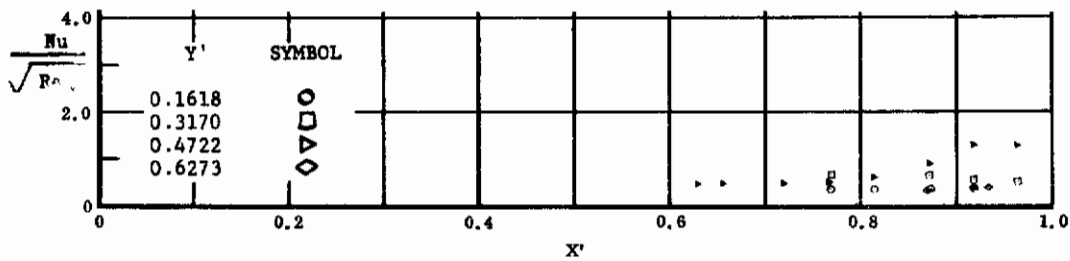
Fig. 61 Streamwise Distributions of Aerodynamic Heating Rates; Basic Configuration + Canards, No Flap Deflections, $\alpha = +14.3°$, $\beta = 0°$, $Re_\infty/ft = 3,300,000$.
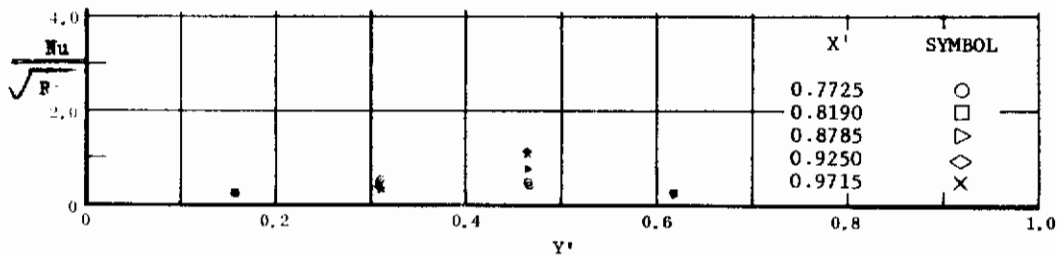
Fig. 61 Spanwise Distributions of Aerodynamic Heating Rates; Basic Configuration + Canards, No Flap Deflections, $\alpha = +14.3°$, $\beta = 0°$, $Re_\infty/ft = 3,300,000$.
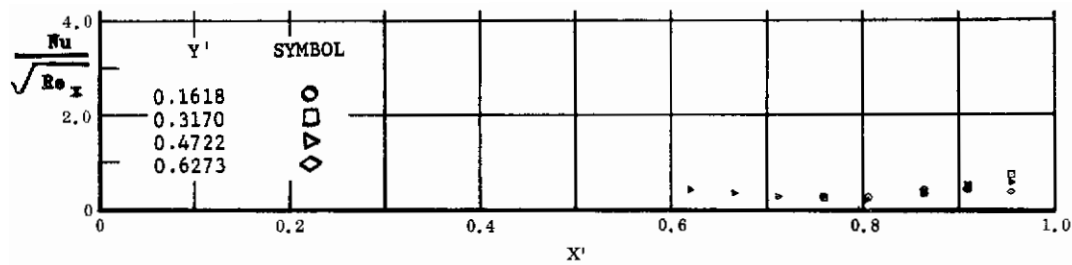
Fig. 62 Streamwise Distributions of Aerodynamic Heating Rates; Basic Configuration, Bottom Flaps Deflected +10°, α = +14.3°, β = 0°, Re_∞/ft = 3,300,000.
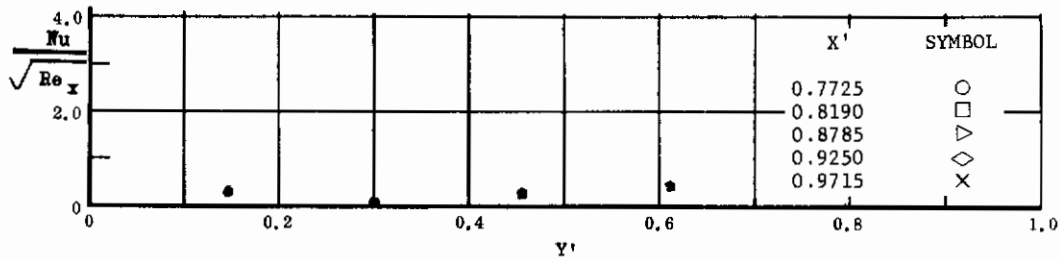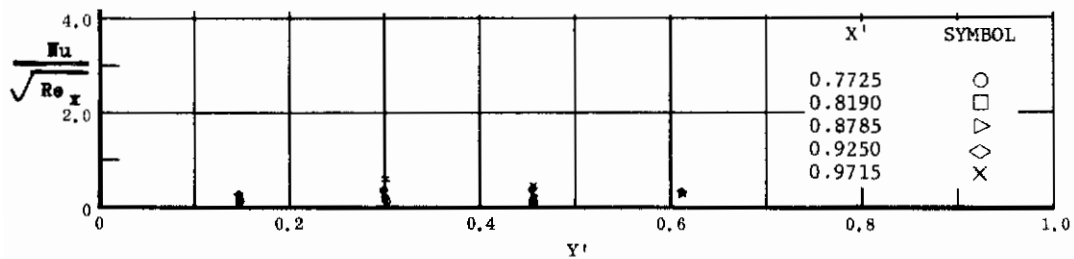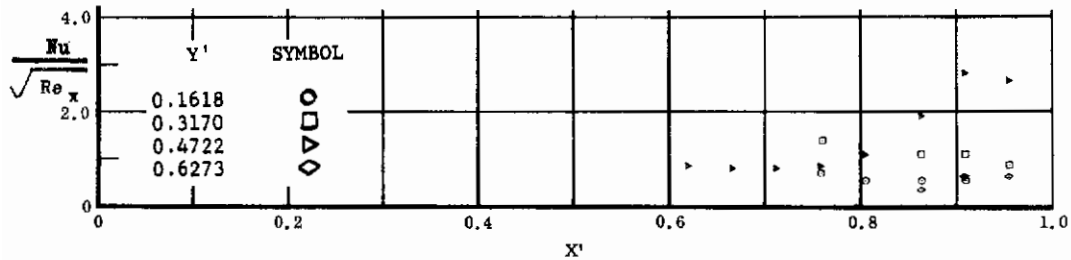

Fig. 62 Spanwise Distributions of Aerodynamic Heating Rates; Basic Configuration, Bottom Flaps Deflected +10°, β = 0°, α = +14.3°, Re_∞/ft = 3,300,000.

Fig. 63 Streamwise Distributions of Aerodynamic Heating Rates; Basic Configuration, Bottom Flaps Deflected +20°, α = +14.3°, β = 0°, Re_∞/ft = 1,100,000.
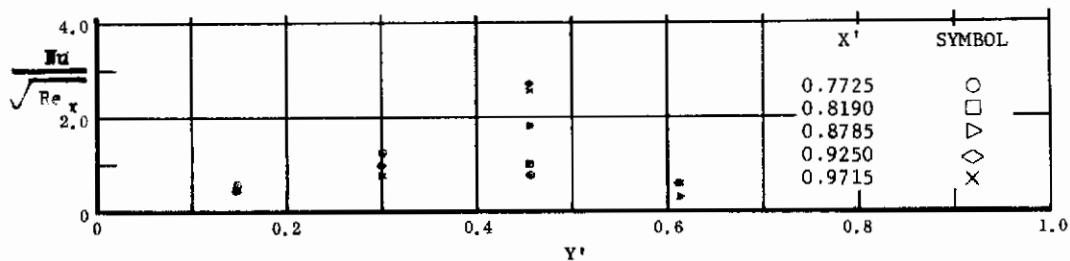

Fig. 63 Spanwise Distributions of Aerodynamic Heating Rates; Basic Configuration, Bottom Flaps Deflected +20°, α = +14.3°, β = 0°, Re_∞/ft = 1,100,000.

110
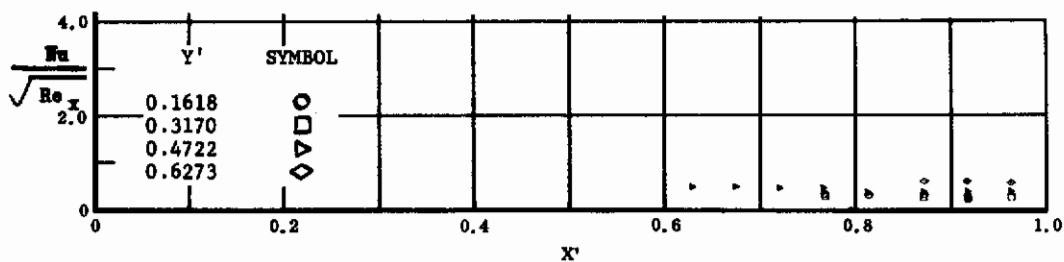
Fig. 64   Streamwise Distributions of Aerodynamic Heating Rates; Basic Configuration, Bottom Flaps Deflected +20°, α = +14.3°, β = 0°, Re_∞/ft = 3,300,000.

Fig. 64   Spanwise Distributions of Aerodynamic Heating Rates; Basic Configuration, Bottom Flaps Deflected +20°, α = +14.3°, β = 0°, Re_∞/ft = 3,300,000.

Fig. 65   Streamwise Distributions of Aerodynamic Heating Rates; Basic Configuration + Canards, Bottom Flaps Deflected +20°, α = +14.3°, β = 0°, Re_∞/ft = 3,300,000.

Fig. 65   Spanwise Distributions of Aerodynamic Heating Rates; Basic Configuration + Canards, Bottom Flaps Deflected +20°, α = +14.3°, β = 0°, Re_∞/ft = 3,300,000.

111

$$\frac{Nu}{\sqrt{Re_x}}$$

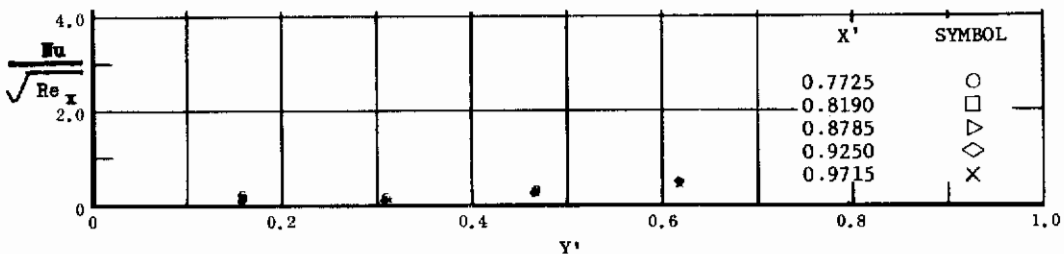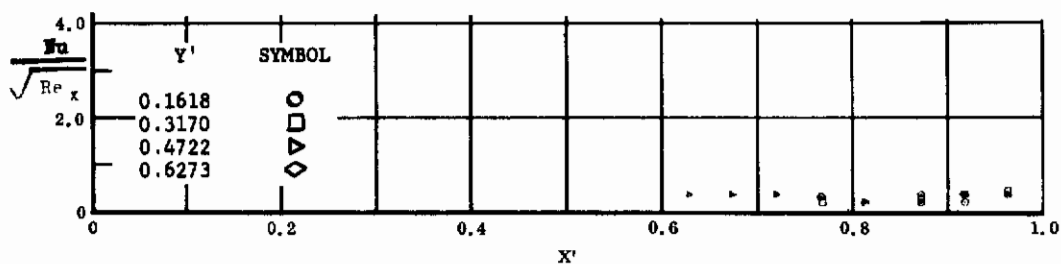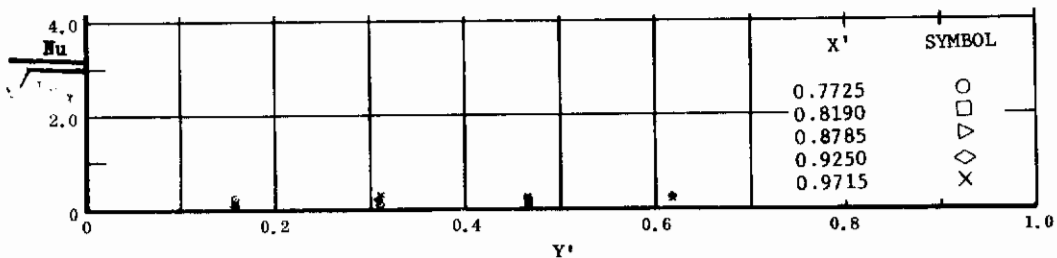| Y'	SYMBOL
0.1618	O
0.3170	□
0.4722	▷
0.6273	◇

Fig. 66 Streamwise Distributions of Aerodynamic Heating Rates; Basic Configuration + Longer Chord Flaps, Bottom Flaps Deflected +20°, α = +14.3°, β = 0°, Re_∞/ft = 1,100,000.
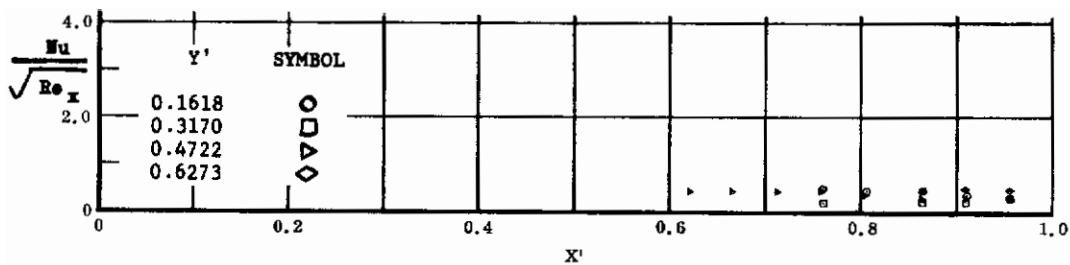

$$\frac{Nu}{\sqrt{Re_x}}$$

X'	SYMBOL
0.7725	O
0.8190	□
0.8785	▷
0.9250	◇
0.9715	X

Fig. 66 Spanwise Distributions of Aerodynamic Heating Rates; Basic Configuration + Longer Chord Flaps, Bottom Flaps Deflected +20°, α = +14.3°, β = 0°, Re_∞/ft = 1,100,000.

$$\frac{Nu}{\sqrt{Re_x}}$$

Y'	SYMBOL
0.1618	O
0.3170	□
0.4722	▷
0.6273	◇

Fig. 67 Streamwise Distributions of Aerodynamic Heating Rates; Basic Configuration + Longer Chord Flaps, Bottom Flaps Deflected +20°, α = +14.3°, β = 0°, Re_∞/ft = 3,300,000.

$$\frac{Nu}{\sqrt{Re_x}}$$

X'	SYMBOL
0.7725	O
0.8190	□
0.8785	▷
0.9250	◇
0.9715	X

Fig. 67 Spanwise Distributions of Aerodynamic Heating Rates; Basic Configuration + Longer Chord Flaps, Bottom Flaps Deflected +20°, α = +14.3°, β = 0° Re_∞/ft = 3,300,000.

Fig. 68 Streamwise Distributions of Aerodynamic Heating Rates; Basic Configuration, Bottom Flaps Deflected +30°, α = +14.3°, β = 0°, Re∞/ft = 3,300,000.
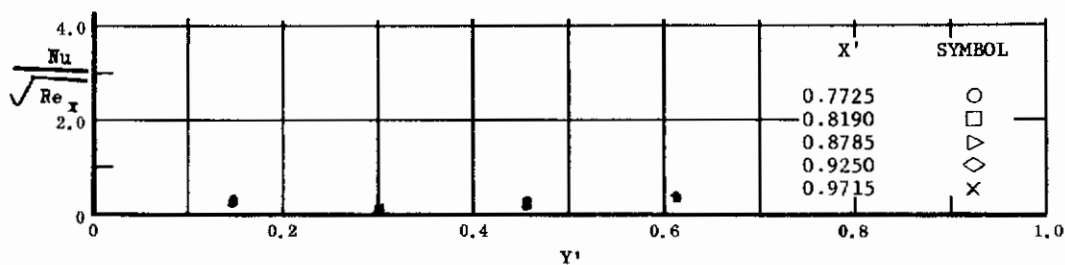
Fig. 68 Spanwise Distributions of Aerodynamic Heating Rates; Basic Configuration, Bottom Flaps Deflected +30°, α = +14.3°, β = 0°, Re∞/ft = 3,300,000.
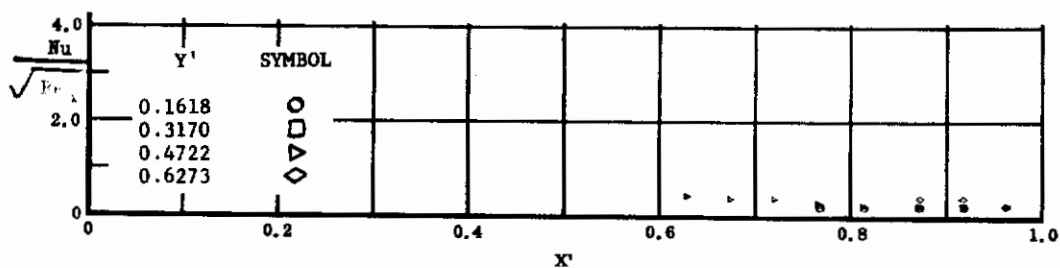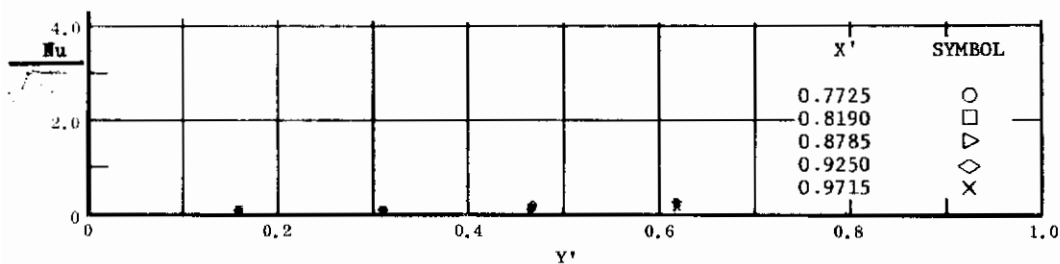

Fig. 69 Streamwise Distributions of Aerodynamic Heating Rates; Basic Configuration, Bottom Flaps Deflected +40°, α = +14.3°, Re∞/ft = 1,100,000, β = 0°.

Fig. 69 Spanwise Distributions of Aerodynamic Heating Rates; Basic Configuration, Bottom Flaps Deflected +40°, α = +14.3°, Re∞/ft = 1,100,000, β = 0°.
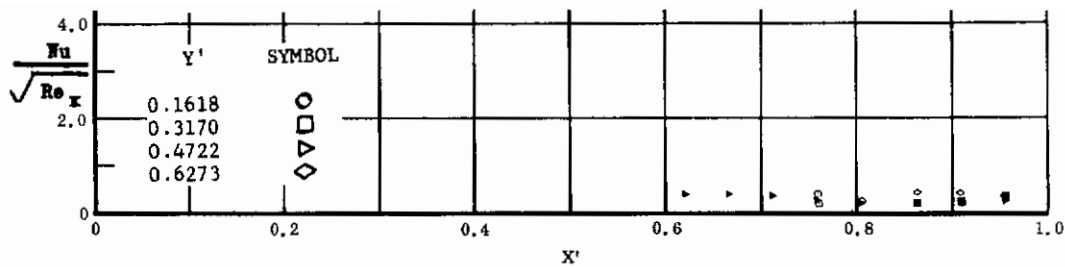
113

Fig. 70 Streamwise Distributions of Aerodynamic Heating Rates; Basic Configuration, Bottom Flaps Deflected +40°, α = +14.3°, β = 0°, Re_∞/ft = 3,300,000.
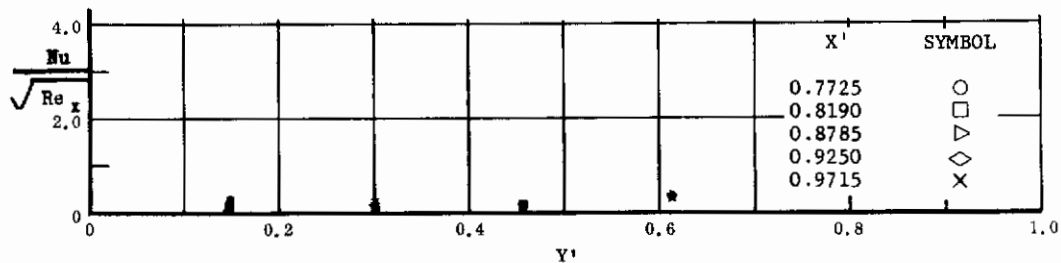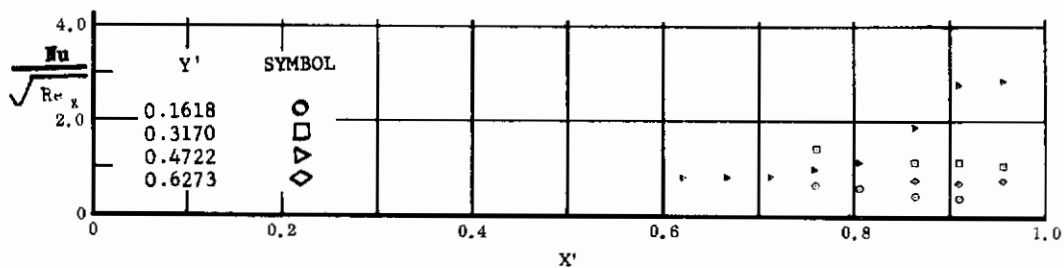

Fig. 70 Spanwise Distributions of Aerodynamic Heating Rates; Basic Configuration, Bottom Flaps Deflected +40°, α = +14.3°, β = 0°, Re_∞/ft = 3,300,000.

Fig. 71 Streamwise Distributions of Aerodynamic Heating Rates; Basic Configuration + Canards, Bottom Flaps Deflected +40°, α = +14.3°, β = 0°, Re_∞/ft = 3,300,000.
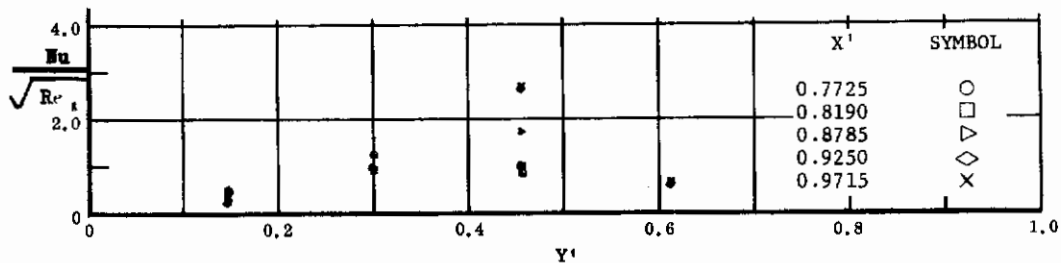

Fig. 71 Spanwise Distributions of Aerodynamic Heating Rates; Basic Configuration + Canards, Bottom Flaps Deflected +40°, α = +14.3°, β = 0°, Re_∞/ft = 3,300,000.
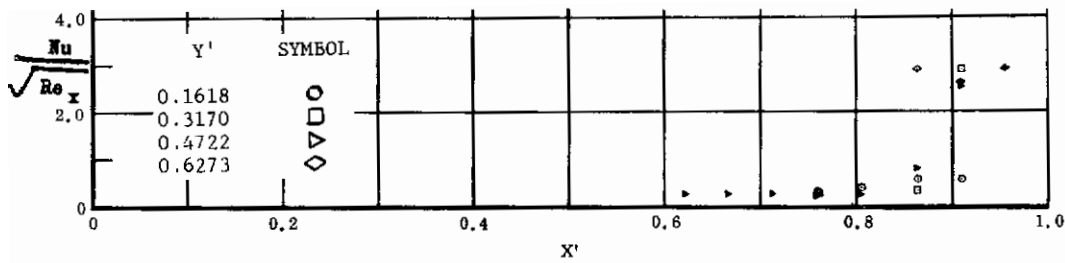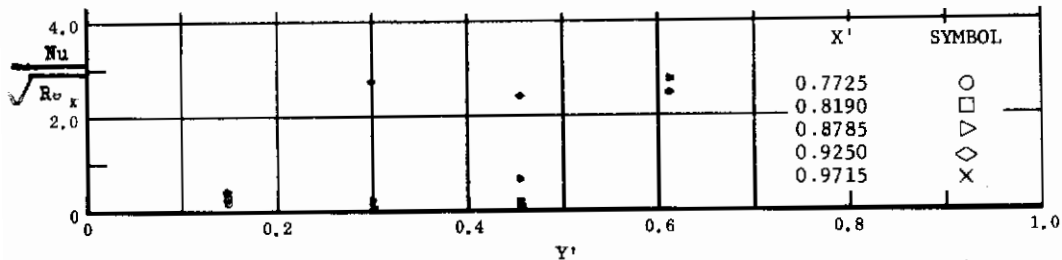
114

Fig. 72 Streamwise Distributions of Aerodynamic Heating Rates; Basic Configuration, Left and Right (Upper) Flaps Deflected -40°, α = +33°, β = 0°, Re_∞/ft = 3,300,000.

Y'	SYMBOL
0.1618	O
0.3170	□
0.4722	▷
0.6273	◇

Fig. 72 Spanwise Distributions of Aerodynamic Heating Rates; Basic Configuration, Left and Right (Upper) Flaps Deflected -40°, α = +33°, β = 0°, Re_∞/ft = 3,300,000.

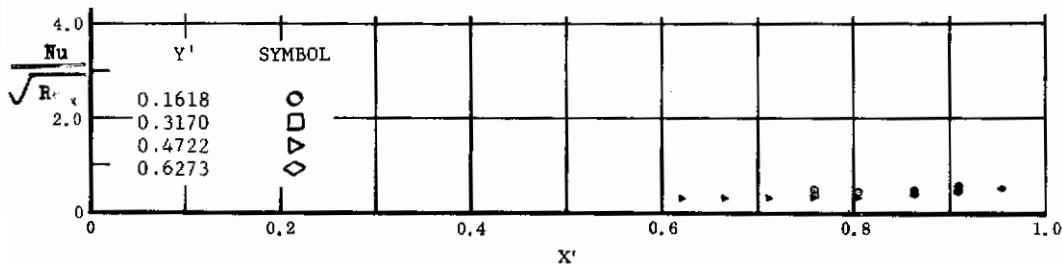| X'	SYMBOL
0.7725	O
0.8190	□
0.8785	▷
0.9250	◇
0.9715	X

Fig. 73 Streamwise Distributions of Aerodynamic Heating Rates; Basic Configuration, No Flap Deflections, α = +33°, β = 0°, Re_∞/ft = 3,300,000.
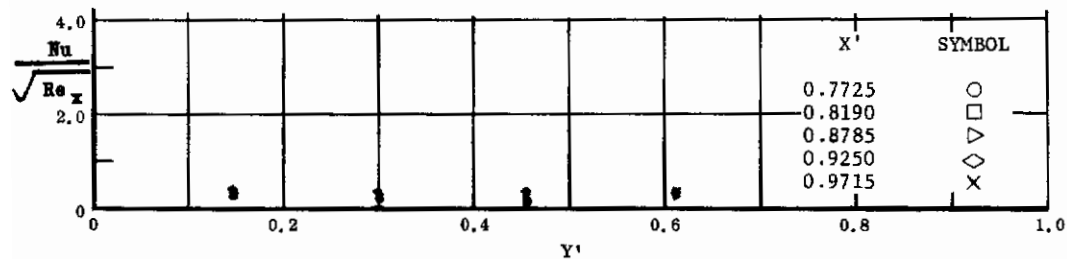
Y'	SYMBOL
0.1618	O
0.3170	□
0.4722	▷
0.6273	◇

Fig. 73 Spanwise Distributions of Aerodynamic Heating Rates; Basic Configuration, No Flap Deflections, α = +33°, β = 0°, Re_∞/ft = 3,300,000.

X'	SYMBOL
0.7725	O
0.8190	□
0.8785	▷
0.9250	◇
0.9715	X

115

$$\frac{Nu}{\sqrt{Re_x}}$$

4.0

2.0

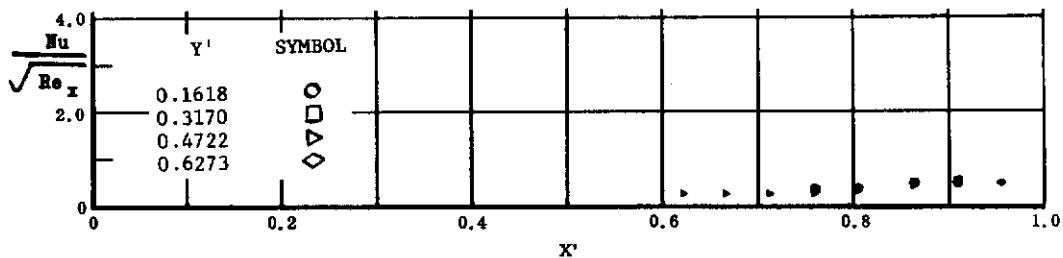| Y'	SYMBOL
0.1618	O
0.3170	□
0.4722	▷
0.6273	◇

0

0   0.2   0.4   0.6   0.8   1.0

X'

Fig. 74   Streamwise Distributions of Aerodynamic Heating Rates; Basic Configuration, Bottom Flaps Deflected +20°, $\alpha = +33°$, $\beta = 0°$, $Re_\infty/ft = 3,300,000$.

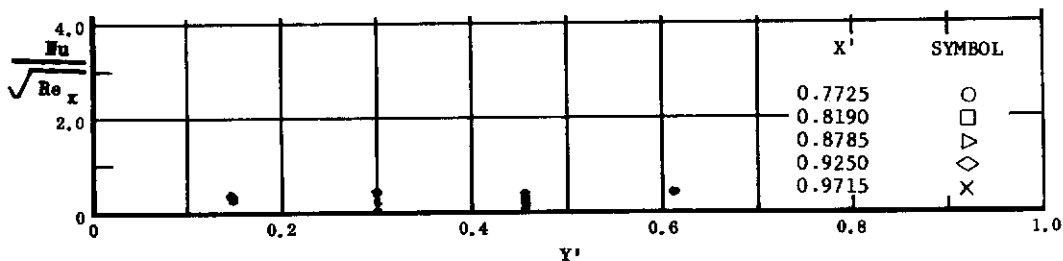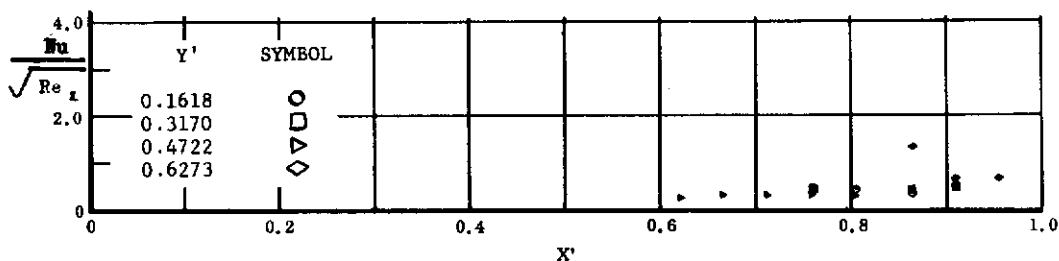$$\frac{Nu}{\sqrt{Re_x}}$$

4.0

2.0

X'	SYMBOL
0.7725	O
0.8190	□
0.8785	▷
0.9250	◇
0.9715	×

0

0   0.2   0.4   0.6   0.8   1.0

Y'

Fig. 74   Spanwise Distributions of Aerodynamic Heating Rates; Basic Configuration, Bottom Flaps Deflected +20°, $\alpha = +33°$, $\beta = 0°$, $Re_\infty/ft = 3,300,000$.

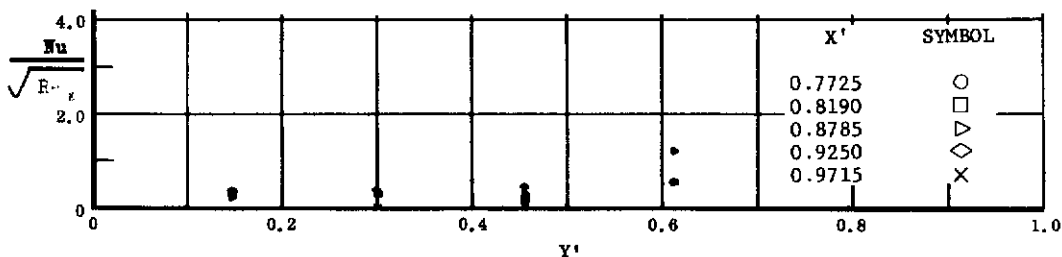$$\frac{Nu}{\sqrt{Re_x}}$$

4.0

2.0

Y'	SYMBOL
0.1618	O
0.3170	□
0.4722	▷
0.6273	◇

0

0   0.2   0.4   0.6   0.8   1.0

X'

Fig. 75   Streamwise Distributions of Aerodynamic Heating Rates; Basic Configuration, Bottom Flaps Deflected +40°, $\alpha = +33°$, $\beta = 0°$, $Re_\infty/ft = 3,300,000$.

$$\frac{Nu}{\sqrt{Re_x}}$$

4.0

2.0

X'	SYMBOL
0.7725	O
0.8190	□
0.8785	▷
0.9250	◇
0.9715	×

0

0   0.2   0.4   0.6   0.8   1.0

Y'

Fig. 75   Spanwise Distributions of Aerodynamic Heating Rates; Basic Configuration, Bottom Flaps Deflected +40°, $\alpha = +33°$, $\beta = 0°$, $Re_\infty/ft = 3,300,000$.
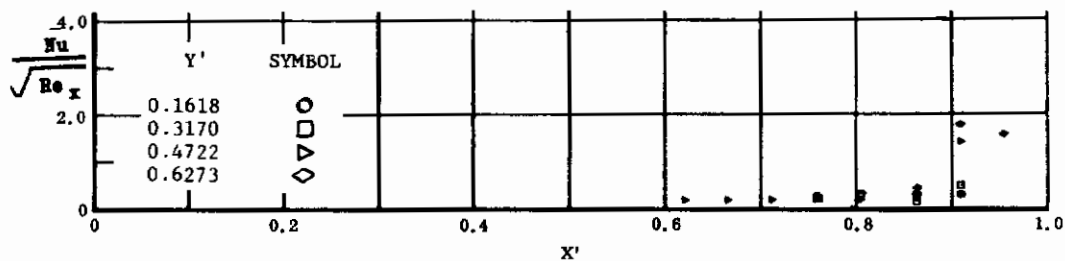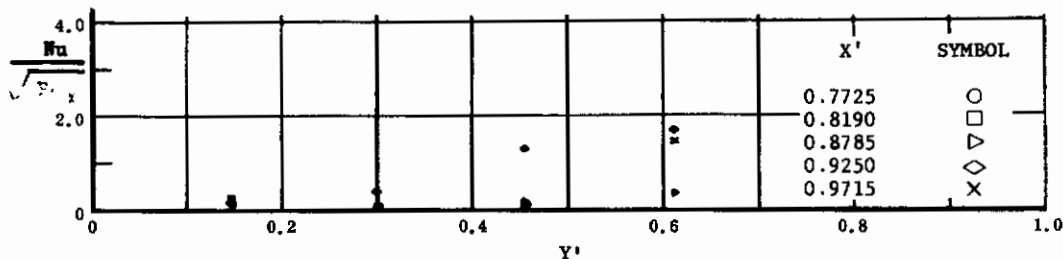
Fig. 76 Streamwise Distributions of Aerodynamic Heating Rates; Basic Configuration, Left and Right (Upper) Flaps Deflected -40°, $\alpha = +45°$, $\beta = 0°$, $Re_\infty/ft = 3,300,000$.

Fig. 76 Spanwise Distributions of aerodynamic Heating Rates; Basic Configuration, Left and Right (Upper) Flaps Deflected -40°, $\alpha = +45°$, $\beta = 0°$, $Re_\infty/ft = 3,300,000$.

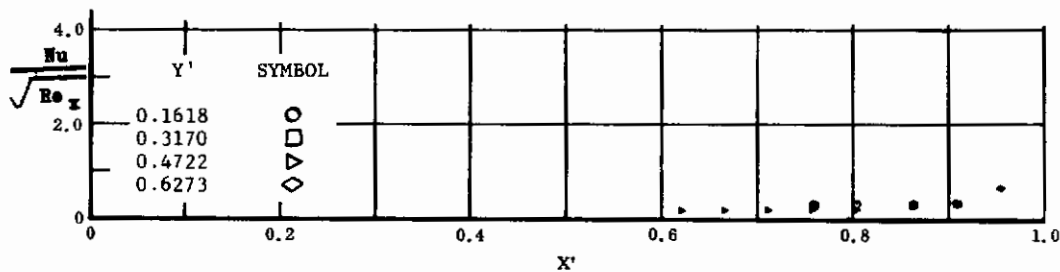Fig. 77 Streamwise Distributions of Aerodynamic Heating Rates; Basic Configuration, No Flap Deflections, $\alpha = +45°$, $\beta = 0°$, $Re_\infty/ft = 3,300,000$.

Fig. 77 Spanwise Distributions of Aerodynamic Heating rates; Basic Configuration, No Flap Deflections, $\alpha = +45°$, $\beta = 0°$, $Re_\infty/ft = 3,300,000$.
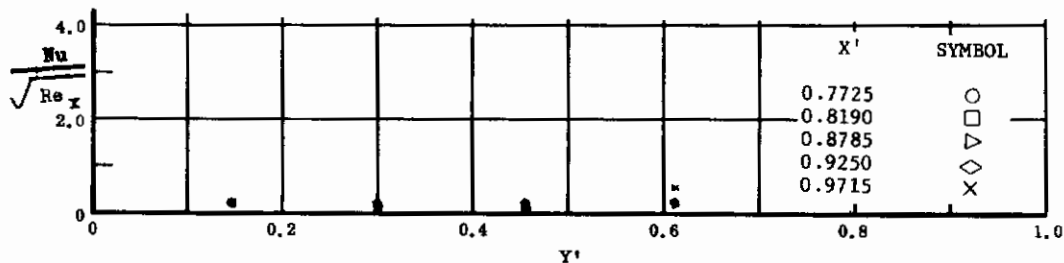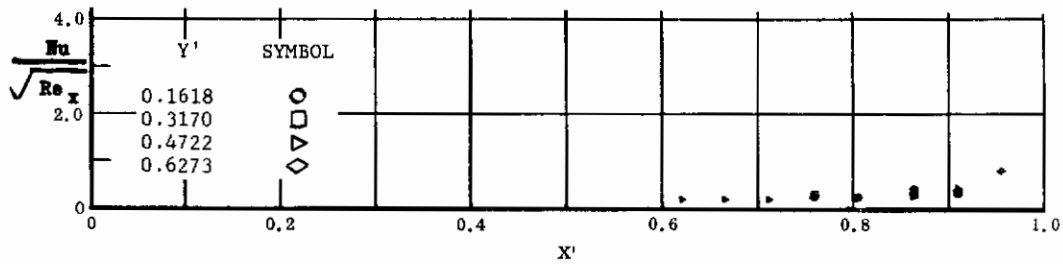
Fig. 78   Streamwise Distributions of Aerodynamic Heating Rates; Basic Configuration, Bottom Flaps Deflected +20°, α = +45°, β = 0°, Re_∞/ft = 3,300,000.
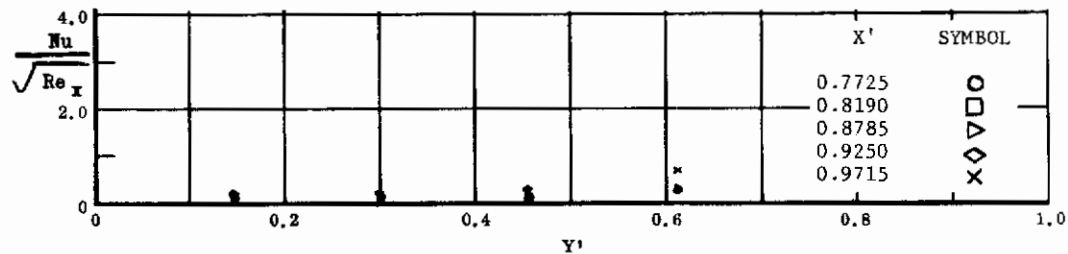

Fig. 78   Spanwise Distributions of Aerodynamic Heating Rates; Basic Configuration, Bottom Flaps Deflected +20°, α = +45°, β = 0°, Re_∞/ft = 3,300,000.
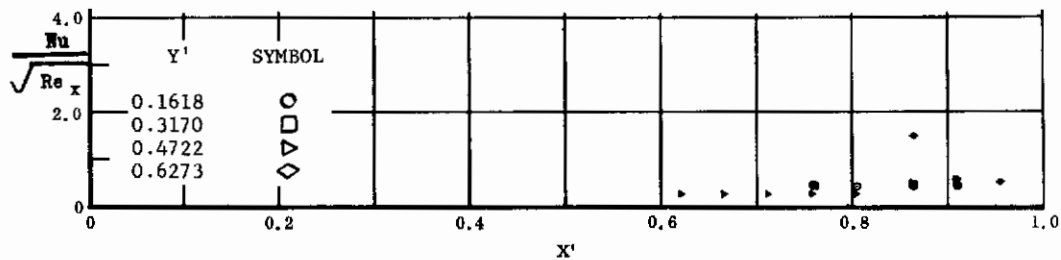

Fig. 79   Streamwise Distributions of Aerodynamic Heating Rates; Basic Configuration, Bottom Flaps Deflected +40°, α = +45°, β = 0°, Re_∞/ft = 3,300,000.

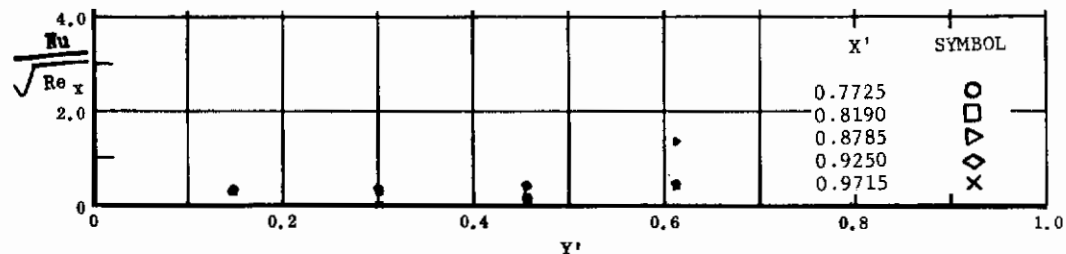
Fig. 79   Spanwise Distributions of Aerodynamic Heating Rates; Basic Configuration, Bottom Flaps Deflected +40°, α = +45°, β = 0°, Re_∞/ft = 3,300,000.

Y'   SYMBOL

0.1618   O
0.3170   □
0.4722   ▷
0.6273   ◇

NOTE

The tunnel flow choked when the cooling shoes were popped open for this set of test conditions. The tunnel shock moved upstream from the diffuser into the test section in the vicinity of the actuator housing and sting support. This caused the model to oscillate violently, with an amplitude of about $\frac{1}{2}$ inch, while the data presented in this figure were being recorded.

$\frac{Nu}{\sqrt{Re}_x}$
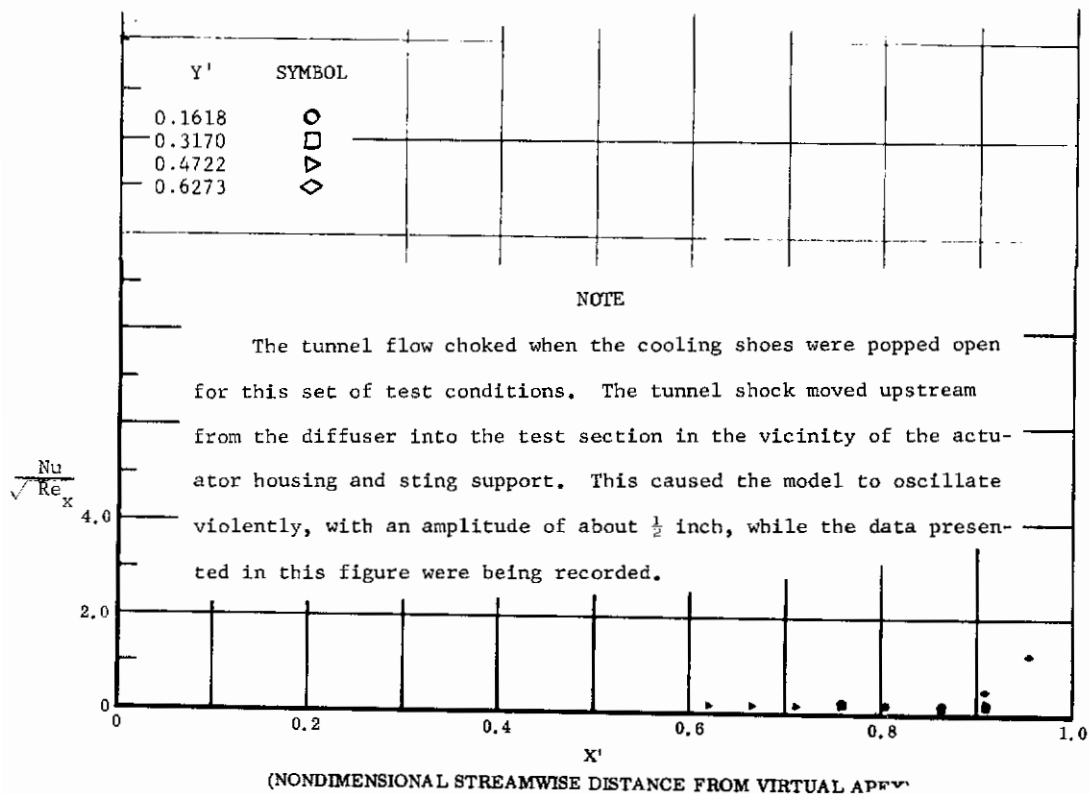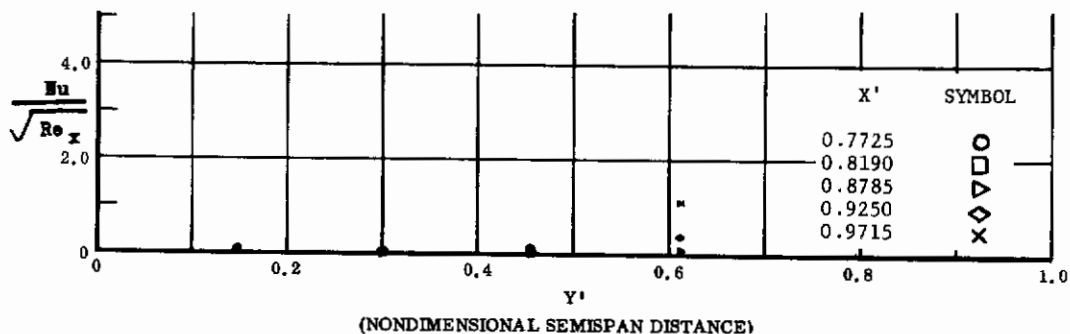
X'

(NONDIMENSIONAL STREAMWISE DISTANCE FROM VIRTUAL APEX)

Fig. 80   Streamwise Distributions of Aerodynamic Heating Rates; Basic Configuration, Left and Right (Upper) Flaps Deflected -40°, α = +54°, β = 0°, Re_∞/ft = ?.

$\frac{Nu}{\sqrt{Re}_x}$

X'   SYMBOL

0.7725   O
0.8190   □
0.8785   ▷
0.9250   ◇
0.9715   ×

Y'

(NONDIMENSIONAL SEMISPAN DISTANCE)

Fig. 80   Spanwise Distributions of Aerodynamic Heating Rates; Basic Configuration, Left and Right (Upper) Flaps Deflected -40°, α = +54°, β = 0°, Re_∞/ft = ?.
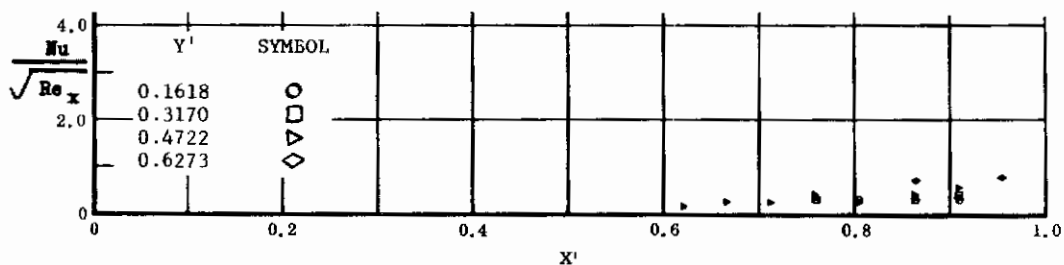
119

Fig. 81   Streamwise Distributions of Aerodynamic Heating Rates; Basic Configuration, Bottom Flaps Deflected +20°, $\alpha = +54°$, $\beta = 0°$, $Re_\infty/ft = 3,300,000$.
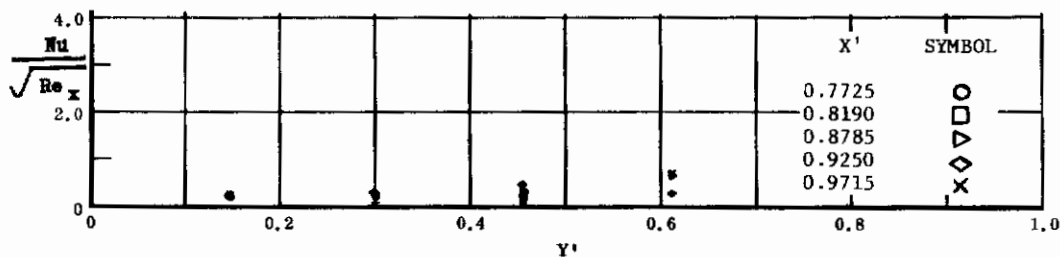

Fig. 81   Spanwise Distributions of Aerodynamic Heating Rates; Basic Configuration, Bottom Flaps Deflected +20°, $\alpha = +54°$, $\beta = 0°$, $Re_\infty/ft = 3,300,000$.

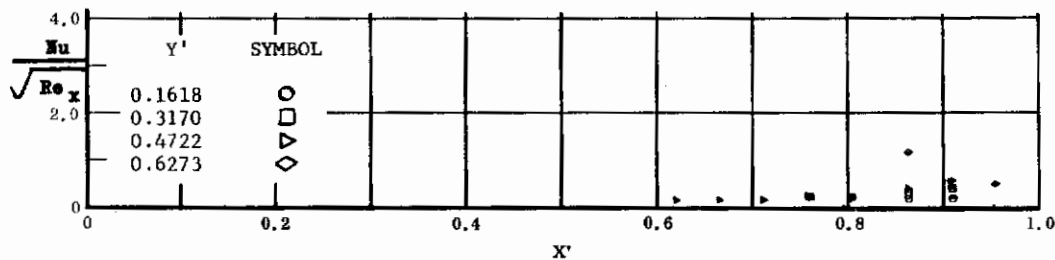
Fig. 82   Streamwise Distributions of Aerodynamic Heating Rates; Basic Configuration, Bottom Flaps Deflected +40°, $\alpha = +54°$, $\beta = 0°$, $Re_\infty/ft = 3,300,000$.
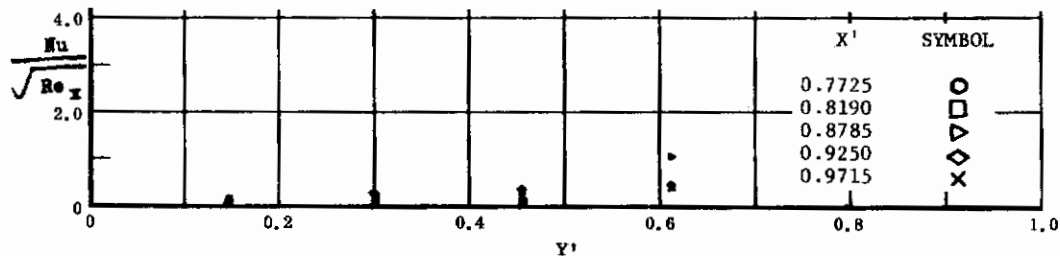

Fig. 82   Spanwise Distributions of Aerodynamic Heating Rates; Basic Configuration, Bottom Flaps Deflected +40°, $\alpha = +54°$, $\beta = 0°$, $Re_\infty/ft = 3,300,000$.

120